Visible Light Positioning using Received Signal Strength for Industrial Environments

Yousef Almadani

PhD 2020

Visible Light Positioning using Received Signal Strength for Industrial Environments

Yousef Almadani

A thesis submitted in partial fulfilment of the requirements of
Manchester Metropolitan University
for the degree of Doctor of Philosophy

Faculty of Science and Engineering
Department of Engineering
Manchester Metropolitan University

2020

To Milo

Abstract

There is a forecast for exceptional digital data traffic growth due to the digitisation of industrial applications using the internet of things. As a result, a great need for high bandwidth and faster transmission data rates for future wireless networks has emerged. One of the considered communication technologies that can assist in satisfying this demand is visible light communications (VLC). VLC is an emerging technology that uses the visible light spectrum by mainly utilising light-emitting diodes (LEDs) for simultaneous indoor lighting and high bandwidth wireless communication. Some of the applications of VLC are to provide high data rate internet in homes, offices, campuses, hospitals, and several other areas. One of these promising areas of application is for industrial wireless communications. The research project will provide a review of VLC applications intended for industrial applications with an emphasis on visible light positioning (VLP). In this research work, a three-dimensional (3D) positioning algorithm for calculating the location of a photodiode (PD) is presented. It solely works on measured powers from different LED sources and does not require any prior knowledge of the receiver's height unlike other works in the literature. The performance of the proposed VLP algorithm in terms of positioning error is evaluated using two different trilateration algorithms, the Cayley–Menger determinant (CMD) and the Linear Least Squares (LLS) trilateration algorithms. The evaluation considers different scenarios, with and without receiver tilt, and with multipath reflections. Simulation results show that the CMD algorithm is more accurate and outperforms the LLS trilateration positioning algorithm. Furthermore, the proposed method has been experimentally assessed under two different LED configurations, with different degrees of receiver tilt, and in the presence of a fully stocked storage rack to examine the effect of multipath reflections on the performance of VLP systems. It was observed from simulations and experimental investigations that the widely used square LED-configuration results in position ambiguities for 3D systems while a non-lattice layout, such as a star-shaped configuration, is much more accurate. An experimental accuracy with a 3D median error of 10.5 cm was achieved using the CMD algorithm in a 4 m $\times$ 4 m $\times$ 4.1 m area with a horizontal receiver. Adding receiver tilt of 5° and 10° increases the median error by an average of 29% and 110%, respectively. The effect of reflections from the

storage rack has also been thoroughly examined using the two mentioned trilateration algorithms and showed to increase the 3D median positioning error by an average of 69% in the experimental testbed for the areas close to the storage rack. These results highlight the degrading effect of multipath reflections on VLP systems and the necessity to consider it when evaluating these systems. As the primary consideration for positioning systems in industrial environments is for mobile robots, the encouraging results in this thesis can be further improved though the use of a sensor fusion method.

Acknowledgements

First and foremost, I would like to thank my family for their support over the last several years. None of this would be possible without them. My gratitude is beyond what can be expressed on this page.

I would like to thank the supervisory team Dr Ijaz and Prof. Bamidele Adebisi. I am in debt to my co-supervisor Dr. Sujan Rajbhandari for his help and guidance throughout my degree from start to finish. A special thank you to Dr. Kirstie Andrews and Dr. David Sawtell for their help with various matters related to the degree.

I would also like to express my gratitude to Prof. David Plets, Sander Bastiaens, and Prof. Wout Joseph from Ghent University and thank them for hosting me during my visit. The collaboration has been very fruitful and the experimental work performed in their labs has been vital to this thesis.

Lastly, I would like to especially thank Milo for always willing to lend a listening ear, and for always being there through the ups and downs.

Contents

List of Figures

List of Tables

List of Algorithms

List of Abbreviations

2D Two-Dimensional.

3D Three-Dimensional.

ACO-OFDM Asymmetrically Clipped Optical Orthogonal Frequency Division Multiplexing.

ADOA Angle-Difference-of-Arrival.

AGV Automated Ground Vehicle.

AOA Angle-of-Arrival.

BER Bit Error Rate.

BLE Bluetooth Low Energy.

CAP Carrierless Amplitude–phase.

CCI Co-channel Interference.

CDF Cumulative Distribution Function.

CF Cost Function.

CIR Channel Impulse Response.

CMD Cayley–Menger Determinant.

CPS Cyber-physical Systems.

CRB Cramer–Rao bound.

CSK Colour Shift Keying.

DCO-OFDM DC-biased Optical Orthogonal Frequency Division Multiplexing.

DD Direct Detection.

DE Differential Evolution.

DFE Decision Feedback Equaliser.

DMT Discrete Multitone.

EKF Extended Kalman filter.

EMI Electromagnetic Interference.

FBMC Filter-Bank Multicarrier.

FET Field-effect Transistor.

FFT Fast Fourier transform.

FLAME Fuzzy Logic Algorithm for Minimising Error.

FOV Field-of-View.

FSO Free-space Optics.

GFDM Generalised Frequency Division Multiplexing.

GPS Global Positioning System.

I2V Infrastructure-to-Vehicle.

ICI Inter-cell Interference.

IEEE Institute of Electrical and Electronics Engineers.

IM Intensity Modulation.

IoT Internet of Things.

IR Infrared.

ISI Intersymbol Interference.

ISO International Organization for Standardization.

ITS Intelligent Transport Systems.

LASM Localization Algorithm Based on a Spring Model.

LED Light Emitting Diode.

Li-Fi Light-Fidelity.

LLS Linear Least Squares.

LOS Line-of-Sight.

MAV Micro Air Vehicle.

MI Modulation Index.

MIMO Multiple-input and Multiple-output.

ML Machine Learning.

MLE Maximum Likelihood Estimation.

MS Median Shift.

NIST National Institute of Standards and Technology.

NLOS Non-Line-of-Sight.

OFDMA Orthogonal Frequency Division Multiplexing.

OOK On-off Keying.

OWC Optical Wireless Communications.

PAM Pulse-amplitude Modulation.

PD Photodiode.

PDOA Phase Difference of Arrival.

PER Packet Error Rate.

PSO Particle Swarm Optimisation.

PWM Pulse-width Modulation.

RE Receiving Element.

RF Radio Frequency.

RFID Radio Frequency Identification.

RGB Red, Green, and Blue.

RMS Root Mean Square.

RSS Received Signal Strength.

RSSI Received Signal Strength Indicator.

RSSR Received Signal Strength Ratio.

SLAM Simultaneous Localisation And Mapping.

SNR Signal-to-Noise Ratio.

SPAO Simultaneous Positioning and Orientating.

SSL Solid State Lighting.

TDM Time-Division Multiplexing.

TDMA Time-Division Multiple Access.

TDOA Time-Difference-of-Arrival.

TOA Time-of-Arrival.

U-OFDM Unipolar Orthogonal Frequency Division Multiplexing.

UAV Unmanned Aerial Vehicle.

UFMC Universal Filtered Multicarrier.

UGV Unmanned Ground Vehicle.

UKF Unscented Kalman filter.

UWB Ultra-Wideband.

V2V Vehicle-to-Vehicle.

VLC Visible Light Communications.

VLP Visible Light Positioning.

VLRC Visible Light Relay Communication.

VPPM Variable Pulse Position Modulation.

List of Symbols

α	Irradiance angle
$\bar{E}_m$	Maintained illuminance level
β	Incidence angle
η	Fixed capacitance of the photodetector per unit area
Γ	The FET channel noise factor
κ	Boltzmann's constant
ψ_{pd}	Field-of-view of the receiver (half angle)
σ_{noise}	Total noise
σ_{shot}	Shot noise
$\sigma_{thermal}$	Thermal noise
θ	Receiver's tilt angle
φ	Azimuthal rotation angle
$\widehat{x}(h)$	Receiver's x position for each of the assumed possible heights
$\widehat{y}(h)$	Receiver's y position for each of the assumed possible heights
$\widehat{z}(h)$	Receiver's z position for each of the assumed possible heights
A_{pd}	Area of the photodiode
B	Bandwidth
c	Speed of light in a vacuum inertial frame
d	Distance between the transmitter and the receiver
D_{error}	Distance error
g_m	The FET transconductance

h	Height of the receiver
h_{LED}	Height of the LED
I_2	Noise-bandwidth factor
I_3	Noise-bandwidth factor
I_{bg}	Photocurrent due to background radiation
m	Lambertian order
n	Refractive index of the concentrator
P_r	Received optical power
P_t	Transmitted optical power
p_{50}	50$^{\text{th}}$ percentile (median)
p_{90}	90$^{\text{th}}$ percentile
p_{95}	95$^{\text{th}}$ percentile
R_r	Receiver's responsivity
t_i	Propagation time from the i^{th} transmitter
t_j	Propagation time from the j^{th} transmitter
T_k	The absolute temperature
x	Receiver's real x position
x_{th}	The x coordinate of the i_{th} transmitter
y	Receiver's real y position
y_{th}	The y coordinate of the i_{th} transmitter
z	Receiver's real z position
z_{th}	The z coordinate of the i_{th} transmitter

Chapter 1

Introduction

1.1 Motivation

The ongoing research in optical wireless communications has opened the door for many uses of the optical spectrum that range from ultra-violet to infrared (IR) spectrum. The use of the visible light spectrum for communications is one of the most promising active areas and is referred to as visible light communications (VLC). VLC systems are envisioned to serve as a complementary technology to the already crowded radio frequency (RF)-based technologies as VLC would help alleviate some of the increasing demand for high-speed data transmission. While there has been a significant amount of research examining the use of VLC in a variety of environments, the use of VLC systems in industrial environments is still considered a relatively new, unexamined area. There has been a growing number of research work characterising VLC and optical channel models in industrial settings but there remains a few gaps and areas that deserves to be further investigated given the unique nature of industrial environments. The scarcity in research work examining the use of VLC systems in industrial environments has led to assertions that the results achieved when testing VLC systems in conventional residential settings can be extended to industrial settings.

These assertions, however, cannot apply to industrial environments because of the harsh characteristics that these environments exhibit. Additionally, utilising VLC for indoor localisation is one of the most promising applications of VLC technology. Visible light positioning (VLP) systems can provide high-accuracy localisation for a variety of applications. Similarly, there is no significant research work examining the use of VLP systems in industrial environments or the challenges and factors that would hinder its performance when adopted in these environments.

As a result, this research work examines how industrial environments differ

from conventional residential and commercial environments. This has led to examining different factors that might impede the adoption of VLC systems in industrial settings, what challenges they might face, and the applicability of VLP system at these types of environments.

Modelling, simulating, and experimentally testing a VLP system also examines the clear results chasm between the simulation and experimental results reported in the literature. A large amount of research work in VLP systems reported results with low centimetre positioning accuracies, but these results were not replicated in experimental work, suggesting that some of the assumptions being made cannot be extended to real-life applications. Moreover, one of the limitations preventing the extension of two-dimensional (2D) VLP systems to three-dimensional (3D) systems is the unknown value of the receiver's height. Due to these reasons, the thesis is largely devoted to investigating the performance of a VLP system in industrial environments.

1.2 Aim and Objectives

The main aim of the research presented in the thesis is to conduct a comprehensive analysis, modelling, and optimisation of a VLP system that is capable of providing a high accuracy for industrial applications.

The objectives are to:

1. Perform a comprehensive review of the current research output for VLC and VLP systems and its corresponding environments.
2. Examine and investigate the factors that differentiate industrial environments from residential and commercial environments. Further, discuss the possibilities and challenges of using VLC for industrial applications.
3. Study the adverse factors that would affect the performance of VLP systems and identify mitigation methods to improve their accuracy.
4. Propose a positioning method that would enable the extension of 2D VLP systems to 3D systems without prior knowledge of the receiver's height.
5. Test and validate the proposed method experimentally in a large setting. Additionally, characterise the effects of different factors such as different transmitters layout, receiver tilt, and the presence of multipath reflections.

1.3 Contributions

The key contributions in the thesis are detailed below. They are also highlighted in Figure 1.1:

- Factors and characteristics that are unique to industrial environments have been extensively reviewed and classified. There has not been any previous work that thoroughly examined what distinguishes these settings, or the challenges that might hinder the adoption of VLC and VLP systems at these types of environments. So this was addressed by also shedding a light on areas and causes that might be problematic for VLC and VLP systems. The major challenges identified were the exaggerated effect of reflections, duplicate position estimates, attenuation, and signal loss. Moreover, the potential of VLC and VLP systems for industrial applications has been discussed along with relevant work from the literature.
  [Chapter 3 – Publications J1, C3, & C5]

- A positioning method that enables the extension of two-dimensional VLP systems to three-dimensional systems is proposed and evaluated. Using a cost function coupled with a trilateration algorithm, the three- dimensional positioning of a receiver can be calculated without prior knowledge of the receiver's height. Moreover, the method has been tested under different sets of circumstances such as receiver tilt and multipath reflections.
  [Chapter 4 - Publications J3 & J4]

- By experimentally testing the proposed positioning method, factors that might degrade the accuracy of the system has been investigated. The system was examined using two different trilateration algorithms. A 3D median accuracy of 10.5 cm has been achieved in a three-dimensional positioning system. The impact of multipath reflections and receiver tilt on the performance of VLP systems has also been examined and their degrading impact has been highlighted. The tilt of the receiver by 5° increased the median error by an average of 29%. Additionally, the impact of multipath reflections from a metal rod increased the median three-dimensional positioning error by an average of 69%.
  [Chapter 5 – Publications J2, J3, & C1]

1.4 Publications

Portions of the work detailed in this thesis have been published in the following conferences and journals:

Journals:

J1. **Y. Almadani**, D. Plets, S. Bastiaens, W. Joseph, M. Ijaz, Z. Ghassemlooy, and S. Rajbhandari, “Visible Light Communications for Industrial Applications—Challenges and Potentials”, *Electronics*, 2020 [Accepted].

J2. **Y. Almadani**, M. Ijaz, B. Adebisi, S. Rajbhandari, S. Bastiaens, W. Joseph, and D. Plets, “An Experimental Evaluation of a 3D Visible Light Positioning System in an Industrial Environment with Receiver Tilt and Multipath Reflections”, *Optics Communications*, 2020 [Accepted].

J3. **Y. Almadani**, M. Ijaz, W. Joseph, S. Bastiaens, S. Rajbhandari, B. Adebisi, and D. Plets, “A novel 3D visible light positioning method using received signal strength for industrial applications”, *Electronics*, 2019.

J4. D. Plets, **Y. Almadani**, S. Bastiaens, M. Ijaz, L. Martens, and W. Joseph, “Efficient 3d trilateration algorithm for visible light positioning”, *Journal of Optics*, 2019.

Conferences:

C1. **Y. Almadani**, M. Ijaz, S. Bastiaens, S. Rajbhandari, W. Joseph and D. Plets, "An Experimental Analysis of the Effect of Reflections on the Performance of Visible Light Positioning Systems in Warehouses", *2019 IEEE 2nd British and Irish Conference on Optics and Photonics (BICOP), London, United Kingdom, 2019.*.

C2. D. Plets, S. Bastiaens, M. Ijaz, **Y. Almadani**, L. Martens, W. Raes, N. Stevens and W. Joseph, "Three-dimensional Visible Light Positioning: an Experimental Assessment of the Importance of the LEDs’ Locations", *2019 International Conference on Indoor Positioning and Indoor Navigation (IPIN)*, Pisa, Italy, 2019.

C3. **Y. Almadani**, M. Ijaz, S. Rajbhandari, U. Raza and B. Adebisi, "Dead-Zones Limitation in Visible Light Positioning Systems for Unmanned Aerial Vehicles," *2019 Eleventh International Conference on Ubiquitous and Future Networks (ICUFN)*, Zagreb, Croatia, 2019.

C4. **Y. Almadani**, M. Ijaz, S. Rajbhandari, U. Raza and B. Adebisi, "Applications of Visible Light Communication for Distance Estimation: a Short Survey," *2019 IEEE Jordan International Joint Conference on Electrical Engineering and Information Technology (JEEIT)*, Amman, Jordan, 2019.

C5. **Y. Almadani**, M. Ijaz, S. Rajbhandari, B. Adebisi and U. Raza, "Application of Visible Light Communication in an Industrial Environment," *2018 11th International Symposium on Communication Systems, Networks & Digital Signal Processing (CSNDSP)*, Budapest, Hungary, 2018.

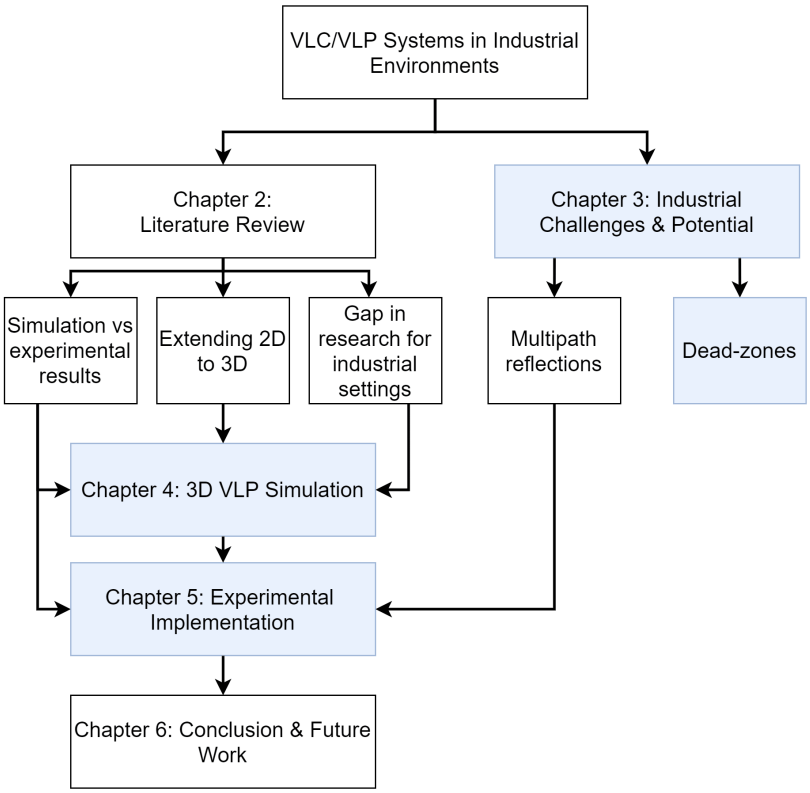

Figure 1.1: Organisation of the thesis.

1.5 Thesis structure

In this section, the outline of the thesis is presented. The organisation of the thesis is shown in Figure 1.1.

Chapter 2 provides a literature review of VLC and VLP systems, in terms of evolution, basic principles, and applications. The system model for VLC is presented and the main methods used for VLP systems are examined and explained. Additionally, distance measurement methods are reviewed.

Chapter 3 examines the potential for VLC in industrial settings and the potential challenges posed by these types of environments. It gathers, reviews, and examines the work and progress that has been made in the literature. It also discusses the challenges VLC and VLP systems might face in these types of settings. Furthermore, the chapter examines two of these challenges through simulation models.

Chapter 4 presents a 3D VLP using the Cayley-Menger Determinant (CMD) trilateration algorithm paired with a cost function to estimate a true 3D positioning without prior knowledge of the receiver's height. The performance of the proposed VLP algorithm is also studied for different tilt angles of the receiver and under the presence of multipath reflections.

Chapter 5 experimentally assesses the performance of the 3D VLP system presented in the previous chapter under different scenarios. The algorithm is evaluated for a system under two different LED configurations with different degrees of receiver tilt, and in the presence of a fully stocked storage rack to examine the effect of multipath reflections.

Chapter 6 concludes the thesis and discusses future research directions that might add value to the literature. As well as discussing some promising extensions to the work presented in the thesis.

Chapter 2

Literature Review

This chapter provides a background review for VLC and VLP systems. A history of VLC is briefly introduced and then the basic channel principles are presented. Followed by examining the different environments for VLC uses that have been proposed and researched. An examination of different VLP methods is also discussed. Given that a majority of VLP research is based on trilateration, which relies on distances, the methods used to obtain distance measurements in VLC systems are examined.

2.1 Visible Light Communication

VLC is an optical wireless communication system that offers an efficient alternative to the crowded wireless spectrum by using an optical light source for communications. The used light sources are generally light-emitting diodes (LEDs) that operate in the visible light spectrum between 400 and 800 THz (380-780 nm), which is mainly used for illumination. The visible light spectrum is around 10,000 times larger than the RF spectrum (Burchardt et al., 2014). The vision of having VLC complementing existing technologies is promising given that the lighting infrastructure is already in place. Employing LEDs allows its use for illumination and communicational purposes without emitting any RF, making it safe for use in environments that prohibit the use of RF equipment such as hospitals and chemical plants (Burchardt et al., 2014). The use of LEDs for both illumination and data communication simultaneously is an appealing notion for several reasons. It is low-cost, capable of achieving high-speed data rates, secure (as light does not penetrate walls), does not cause electromagnetic interference, and it is power efficient. VLC systems are also showing great potential for indoor po-

sitioning applications. As lighting systems are already distributed throughout a floor plan, this means that each transmitting LED would serve as a cell covering a small area. Leading to a highly accurate estimation of the user's position. Positioning applications would be particularly helpful for consumers, autonomous vehicles in industrial settings, and in health facilities for visually impaired people (Nakajima and Haruyama, 2012).

The use of VLC also extends to outdoor applications. Modern-day traffic lights already use LEDs for better visibility and energy savings. Future applications envision vehicles receiving information sent by the traffic lights instructing vehicles to slow down and stop when the light is red. While other vehicle-related applications proposed utilising the cars' headlights to communicate between them.

2.1.1 Background

The history of optical wireless communications predates RF communications. The photophone is considered as the first VLC system as it was the first device that was used to transmit and receive a signal using only light. This innovation by Alexander Graham Bell in 1880 successfully carried sound over a distance of 213 meters. Modern uses in 20th century of optical communications were mainly restricted to lasers until some modern advancements in solid-state lighting (SSL), which led to the development of LEDs and generated renewed interest in optical wireless communications (OWC). The early uses of LEDs for optical communications used the infrared spectrum and significant research work was made in IR communications with a promising future envisaged for it. This has led to IR communications being adopted and integrated into many consumer devices such as mobile devices, laptops, and some desktop computers from the late 1990s through the early 2000s (Ramirez-Iniguez et al., 2008). It was also being proposed for many applications not too dissimilar to the ones currently being proposed to be used with VLC systems. However, IR communications did not take off as predicted and was displaced by other wireless technologies such as Bluetooth and Wi-Fi as they do not require line of sight and do not pose a health risk for some types of applications. Nevertheless, the use of IR communications still exists today through consumer remote controllers. Interestingly, the use of the visible spectrum for communications is not exclusive to using LEDs. The idea of utilising the ubiquitous lighting infrastructure for communications and localisation purposes can be traced back to 1998 by researchers at MIT through the use of fluorescent lights (Leeb et al., 2004; Jackson et al., 1998). This ac-

complishment is overlooked when discussing the history of VLC but deserves to be noted as many of the arguments presented back then advocating for the adoption of smart lights are essentially the same ones presented now when advocating for VLC. The first prototype using fluorescent lights was successfully built by researchers in 2000 and was experimentally used for tracking and guiding patients in healthcare facilities (Leeb et al., 2000; Hinman et al., 2003; Burke et al., 2001; Hinman et al., 2004).

Research output continued through the early 2000s and increased significantly in the last decade. VLC has gained renewed popularity in 2011 after a demonstration a video transmission using a desk lamp Light Fidelity (Li-Fi) was demonstrated, and as a result, an increase in interest by the public raised the profile of VLC/Li-Fi.

2.1.2 VLC/Li-Fi Terminology

The terms VLC and Li-Fi have been used interchangeably ever since the term Li-Fi has been introduced. Haas et al. (2016) explained the differences between VLC and Li-Fi by stating that "VLC has been conceived as a point-to-point data communication technique – essentially as a cable replacement". This was adopted the early standardisation of VLC as part of the Institute of Electrical and Electronics Engineers (IEEE) 802.15.7 standard when it was first introduced in 2011 (Rajagopal et al., 2012). At that point, VLC was considered then as a point-to-point system for data communication and the idea of having a multi-user bidirectional VLC network was not incorporated in the standard. Whereas Li-Fi is considered to be a complete wireless network that supports multiuser bidirectional data communication that includes multiple access points that share the Wi-Fi concept of having different routers. The use of VLC instead of Li-Fi is still prevalent in the literature by researchers that generally consider the term VLC to be sufficient.

2.1.3 Basic Principles

The fundamental design of VLC systems commonly uses an LED as a transmitter and a photodetector as a receiver. Data transmission is performed by modulating the light intensity in such high rates that are undetectable to the human eye without appearing to flicker. The receiver then demodulates the received signal. Optical filters are generally used to filter out ambient light from sunlight

and other light sources such as incandescence and fluorescent lights.

Different types of LEDs can be used in VLC systems, the two most commonly used ones are discussed here. The most widely used type of LED is the phosphor-based white LEDs owing to its simplicity and low manufacturing cost. It compromises of a blue LED coated with phosphor, specifically, a luminophore called YAG (Yttrium, Aluminium, and Garnet) doped with Cerium (chemical symbol Ce), resulting in YAG:Ce. The white light is generated when the blue light is emitted is then absorbed by the yellow phosphor coating, the two wavelengths then produced that are viewed as white light. Varying the thickness of the phosphor produces different temperatures of white light. The phosphor, however, limits the modulation bandwidth of LEDs to a few MHz (Pathak et al., 2015). This is one of the major limitations to achieving higher speeds in VLC systems.

The second most widely used method in producing white LEDs is by combining the red, green, and blue (RGB) wavelengths. The use of three wavelength means that three channels can be modulated separately. Using RGB LEDs in VLC systems have produced high-speed transmission rates. The challenge, however, is that a balance between these three wavelengths is needed to ensure that white light is being emitted. Other methods in producing white LEDs that do not require the use phosphor is based on the homoepitaxially grown zinc selenide (ZnSe) on a ZnSe substrate that simultaneously emits blue light from its active region and yellow light from the substrate. Using this type of LED in VLC systems has yet to be properly examined in the literature but work performed by Binh and Hung (2016) has shown great potential.

2.1.3.1 Channel Model

Typical indoor environments have light luminaires placed on the ceiling while the receiver is placed at desk height. Most of the light received by the photodiode (PD) is through the direct path between the LED and the PD and is referred to as line-of-sight (LOS) signal, shown in Figure 2.1 (a). Other signals can still reach the PD from reflections that are caused by the light rays bouncing off walls and objects before being received by the PD. These reflections can degrade the performance of VLC and VLP systems but the vast majority of the research in the literature neglect reflections as the LOS signal will be dominant. As such, this subsection presents a characterisation of the LOS channel model.

Light emissions from LEDs can be modelled with generalised Lambertian emission characteristics (Gfeller and Bapst, 1979). The Lambertian model is

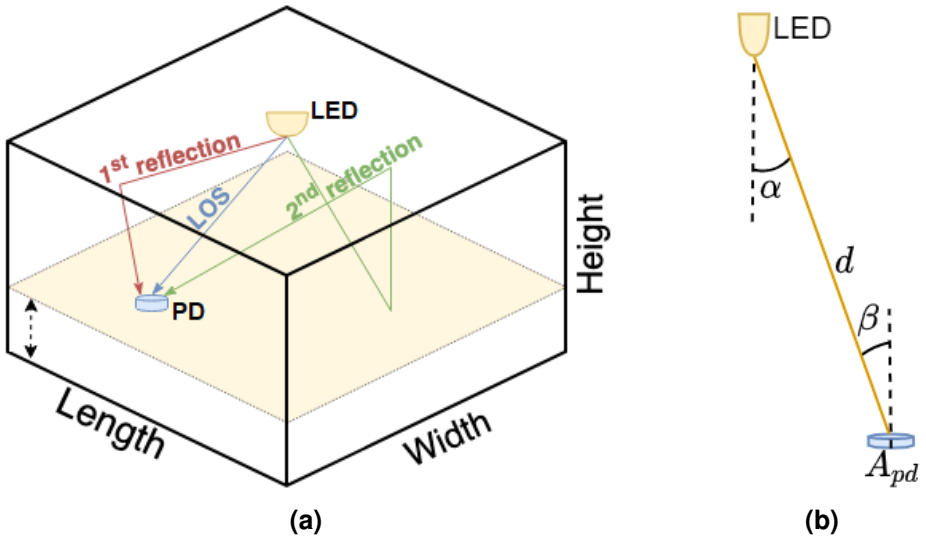

Figure 2.1: (a) VLC channel in a room with reflections in an indoor environment. (b) Line-of-sight VLC channel parameters.

dependent on the transmitter and specifies the radiation pattern of the LED. The Lambertian order m is related to the semi-angle of the LED, $\Theta_{1/2}$, that is defined by (Kahn and Barry, 1997):

$$m = -\frac{\ln(2)}{\ln(\cos(\Theta_{1/2}))} \tag{2.1}$$

Figure 2.2 shows a polar plot of the normalised radiation patterns of Lambertian LEDs with m orders of 1, 2 and 4.8, which correspond to semi-angles of 30°, 45°, 60°. The figure also demonstrates the photometric diagram of the LED chip (BXRE-50C3001-D-24) used in Chapter 5. A small deviation can be from their advertised 60° semi-angle divergence with a Lambertian order of m=1.138 (Bastiaens et al., 2020). Figure 2.1 (b) shows a receiver placed at a distance, d, away from the LED transmitter. In this case, the optical LOS channel path loss depends on the inverse of the square of the distance between the LED and the PD, with the LOS received power given as (Kahn and Barry, 1997):

$$P_r = \begin{cases} P_t \frac{(m+1)A_{pd}}{2\pi d_i^2} \cos^m(\alpha) \cos(\beta) T_{pd}(\beta) G_{pd}(\beta), & 0 \leq \beta \leq \psi_{pd} \\ 0, & \beta > \psi_{pd} \end{cases} \tag{2.2}$$

where P_t is the transmitted power, A_{pd} is the area of the photodiode, d is the distance between the transmitter and the receiver, α is the angle of irradiance, β is the angle of incidence, and ψ_{pd} is the field-of-view (FOV) of the receiver.

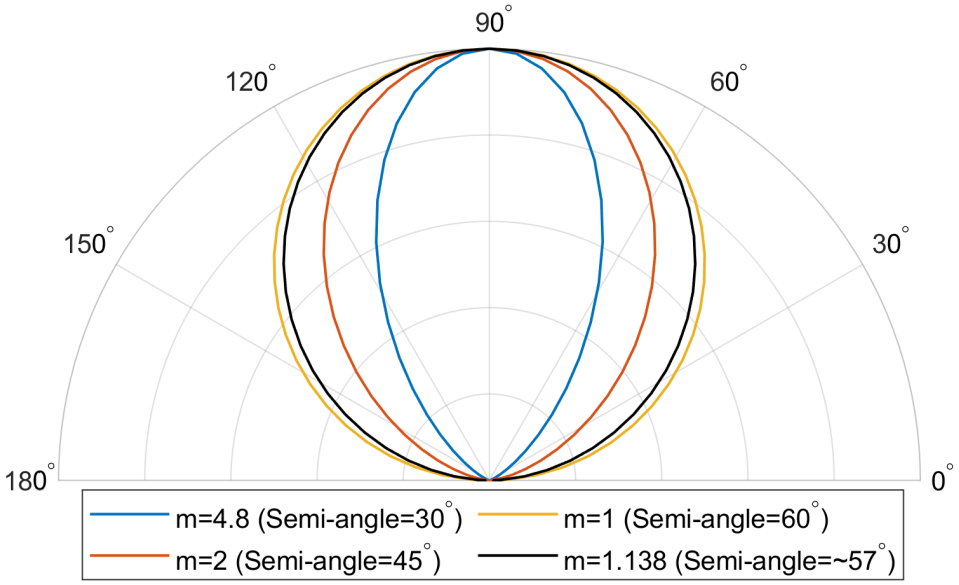

Figure 2.2: Polar plot of Lambertian radiation patterns for m = 1, 1.38, 2, 4.8.

The optical filter's gain $T_{pd}(\beta)$, and the optical concentrate's gain, $G_{pd}(\beta)$, are generally assumed in the literature to be equal to 1 (Shi et al., 2019; Peng et al., 2018). However, if an optical concentrator is used then the optical gain of a concentrator with an internal refractive index n is given by:

$$g(\beta) = \begin{cases} \frac{n^2}{\sin(\psi_{pd}{}^2)}, & 0 \leq \beta \leq \psi_{pd} \\ 0, & \beta > \psi_{pd} \end{cases} \tag{2.3}$$

The PD current in VLC systems is usually affected by two types of noise. Shot noise, the fluctuations in the electric current due to received optical powers from the desired signal in additional to other ambient light sources (Zhuang et al., 2018). The second source of noise is thermal noise, which is the current fluctuations caused by the temperature of the electrical circuit. In outdoor and most indoor environments, the prevalence of ambient light sources from fluorescent and incandescent lamps, as well as sunlight, affects the VLC systems through shot noise. While this effect can be minimised through optical filters. Shot noise is still the most dominant noise source except in dark environments, where the thermal noise becomes the dominant noise. The shot noise model is given by (Kahn and Barry, 1997):

$$\sigma^2_{shot} = 2qR_rP_rB + 2qI_{bg}I_2B \tag{2.4}$$

where q is the electronic charge, R_r is the receiver's responsivity, B is the elec-

Table 2.1: Noise model parameters.

Parameter	Symbol	Value
Electronic charge	q	1.6 × 10^{-19} (C)
Noise bandwidth factor	I_2	0.562
Boltzmann's constant	κ	1.38 x 10^{-23} (J/K)
Absolute Temprature	T_k	300 (K)
Fixed capacitance of PD per unit area	η	112 (pF/cm^2)
Open-loop voltage gain	G	10
FET channel noise factor	Γ	1.5
FET transconductance	g_m	30 (ms)

trical bandwidth, I_{bg} is the background radiation, and I_2 is the noise bandwidth factor. The effect of ambient light is taken into account by I_{bg}, which varies depending on the light source. Table 2.2 lists the values of the background current from sunlight and different light sources. The thermal variance is given by:

$$\sigma^2_{thermal} = \frac{8\pi\kappa T_k}{G}\eta A_{pd} I_2 B^2 + \frac{16\pi\kappa T_k \Gamma}{g_m}\eta^2 A^2_{pd} I_3 B^3 \tag{2.5}$$

where κ is Boltzmann's constant, T_k is the absolute temperature, G is the open-loop voltage gain, η is the fixed capacitance of the photodetector per unit area, A_{pd} is the effective area of the PD, Γ is the field-effect transistor (FET) channel noise factor, g_m is the FET transconductance, and I_3 is the noise bandwidth factor. The total noise variance is calculated through the sum of the noises by:

$$\sigma^2_{noise} = \sigma^2_{shot} + \sigma^2_{thermal} \tag{2.6}$$

Table 2.1 lists the values of the most commonly used noise model parameters (Luo et al., 2014). An important metric in evaluating the performance of VLC system is through the signal-to-noise ratio (SNR). The effect of SNR in the electric current from the LOS signal can be calculated by (Ghassemlooy et al., 2012):

$$SNR_i\,(dB) = 10log_{10}\frac{(R_r P_{ri})^2}{\sigma^2_{noise}} \tag{2.7}$$

2.1.4 Applications

Given the unique characteristics and advantages of VLC systems, it has been proposed to be used for different applications and environments beyond residential and commercial settings. These environments range from hospitals,

Table 2.2: Background current from different light sources. Adopted from Moreira et al. (1997).

Source	Without optical filter [μA]
Direct sunlight	5100
Indirect sunlight	740
Incandescent light	84
Fluorescent light	40

underwater, outdoor, and industrial settings.

2.1.4.1 Underwater Communications

There has been active research investigating the use of VLC for underwater applications as light offer higher data capacities than acoustic communications that have limited bandwidth with high latency. Underwater communication systems are typically used to support human exploratory activities in underwater environments which includes scientific data collection, maritime archaeology, and port security amongst a few (Gussen et al., 2016).

Performance characterisation of an underwater VLC system was carried out by Elamassie et al. (2019). The authors developed a closed-form path loss expression and then used it to determine the maximum achievable distance for different water types, which is usually limited to a few tens of meters. They proposed and investigated a multi-hop system to extend the transmission range. Miramirkhani and Uysal (2018) carried out channel characterisation and took into account the presence of human and man-made objects to analyse the effects of shadowing and blockage. While VLC largely relies on LOS, ray-tracing simulations found that transmission is possible even where there is LOS blockage due to scattering. The feasibility of an underwater water VLC system was carried out by Hessien et al. (2018). Asymmetrically clipped optical-orthogonal frequency-division multiplexing (ACO-OFDM) was used with a white-LED over 4 meters and demonstrated that it can support up to 15.36 Mbps data rate when the bandwidth of the LED is 10 MHz. The work in (Cossu et al., 2013) also experimentally validated a high-speed underwater transmission over 2.5-meter distance. Achieved transmission rates were 6.25 Mbit/s using Manchester coding and 58 Mbits/s with discrete multitone (DMT). Based on these preliminary results, the authors estimate that a maximum transmission distance of more than 60 meters is achievable in clear water. The work in (Wang et al., 2016) claimed that the communication distance could be further extended by using an LED with a narrow design and a single-photon avalanche diode for a receiver.

Simulation results showed that the distance could be extended to 500 meters.

2.1.4.2 Medical Facilities

One of the popular areas VLC is poised to have a future in is in hospitals and medical facilities. The use of conventional technologies is generally prohibited in these areas as electromagnetic interference (EMI) would interfere with sensitive hospital equipment. As such, this has created a potential for VLC systems (Simona Mirela et al., 2019). The uses are generally for patient monitoring systems with some research looking into the applicability of an optical back-haul system for hospital uses.

An integrated hybrid hospital communication system was presented by Song et al. (2014). The system is based on the use of power line communications and VLC in order to support e-health services at high capacities while being radiation free. The work in (Cahyadi et al., 2015) examined the use of VLC for static patient monitoring scheme suitable for hospital environments. The method proposed the use of VLC for uplink data transmission for patient monitoring with the signal being received by photodetectors mounted on the ceiling. Experimental tests were performed and validated the proposed system. A VLC system for electromagnetic wave free indoor healthcare facilities was presented by An and Chung (2016). The study experimentally tested a time-hopping VLC system and achieved a packet error rate of 5×10^{-3} over a distance of 1 meter. Le Bas et al. (2017) evaluated the use of a bidirectional infrared and visible light communication for health monitoring purposes and shown that low VLC powers for downlink are needed. Lebas et al. (2018) carried out using ray-tracing simulations the statistical behaviour of both an IR and VLC channel. The results highlighted the importance of modelling the presence of a person and the orientation and movement of the body. The authors also stated that the system can be used for indoor positioning. Moreover, experimental tests were performed in a laboratory setting and demonstrated the capability to support over 48 Mbps data rate. The work by Murai et al. (2012) presented an autonomous mobile delivery robot that relies on VLC for navigation in a hospital. It was also equipped with additional sensors for obstacle detection. The robot was successfully tested in an actual hospital environment and carried out real operations.

2.1.4.3 Intelligent Transport Systems / V2V Communication

Intelligent transport systems (ITS) is another area where the use of LEDs have paved the way for the use of VLC systems. The use of LEDs in traffic lights resulted in one of the earliest proposals for VLC applications in the research (Akanegawa et al., 2001). Communication between traffic light, or other infrastructure, and vehicles are referred to as infrastructure-to-vehicle (I2V) while communication between vehicles is referred to as vehicle-to-vehicle (V2V). The communication between vehicles allows them to share information relating to their position, velocity, etc. They can also share information about the traffic. This is especially important for vehicle platooning, which is when vehicles are organised into groups that closely follow each other (Ucar et al., 2016).

The LEDs in traffic lights can be used in order to transmit signals that are received by the vehicle containing commands signalling it to stop, or to transmit any type of communication relevant to transportation at the time. Zhao and Lin (2016) analysed the performance of a camera sensor-based vehicle positioning systems that use the information transmitted from traffic lights. Simulation results show that a positioning accuracy in the order of centimetres is achievable for distances up to 30 meters between the traffic light's LED arrays and the camera receiver. The authors also noted that the number of LEDs used and the focal length of the receiver, as well as the distance, all affect the accuracy. An analytical feasibility study for using VLC for platooning control was performed by Abualhoul et al. (2013). The authors investigated the use of the vehicle's rear lights for robust communications and simulation results showed that a bit-error-rate (BER) of 10^{-6} is achievable for distances up to 7 meters. Cailean et al. (2012) developed a data transmission system for vehicle cooperation between vehicles and road infrastructures that is capable of providing a robust connection for distances up to 15 meters. Experimental results by Cailean et al. (2013) presented a system that integrates I2V and V2V prototypes. The tests demonstrated the possibility of extending the communication range by having vehicles act as a relay point between the traffic light and the vehicles behind it. An experimental implementation of a V2V communication system with LED headlamps was demonstrated by Yoo et al. (2016). Experimental tests were capable of transmitting 10 kbps data rate over 30 meters in daytime conditions.

The growing research into using VLC for V2V and ITS applications is emerging as a solution with great potential in enhancing safety for road transportation applications. A detailed discussion of the challenges for VLC usage in vehicle-related applications is discussed by Căilean and Dimian (2017).

2.1.4.4 Industrial Environments

The use of optical communications and VLC in industrial environments is gaining some attention in the literature. Industrial environments are historically slow when adopting newer technologies for a number of reasons. It can mainly be attributed to stability and reliability concerns. As any downtime would prove costly in both time and monetary aspects. The newly developing industrial trend referred to as Industry 4.0 require high speeds with low latency that optical communication systems can provide. The use of VLC for communicational and localisation purposes is already showing great promise for adoption in industrial environments. Applications utilising VLC would allow for high data-rate data exchange within the framework of modern factories. A full discussion of the potential for VLC systems in industrial applications and the challenges they might face is provided in the following chapter.

2.1.5 Standardisation

A widely accepted standard offers great benefits for researchers, the industry, and consumers. Efforts by the IEEE are seen as the most serious attempt for international standardisation. The first standard, 802.15.7 standard for *Local and Metropolitan Area Networks–Part 15.7: Short-Range Wireless Optical Communication Using Visible Light*, critically needed an update to include the advances made since it was first published in 2011 (IEEE, 2011). For instance, the first standard only supported on-off keying (OOK), variable pulse position modulation (VPPM), and colour shift keying (CSK). Also, the standard was not widely adopted as most developers are focused on decreasing the system's cost complexity instead of complying with the standard's requirements (Cailean and Dimian, 2017). Since then, the standard has been extensively revised to incorporate the latest advancements in the field. The new revised standard has only been published in 2019 So its adoptability is still in its early stages (IEEE, 2019). Moreover, the standard now encompasses OWC instead of just VLC.

For indoor VLP systems, the lack of a standard benchmark introduces some difficulties. Within the research, there is no agreed-upon metric or procedure to evaluate the performance of VLP systems. This makes it difficult to fairly compare them and leads to unfair comparisons between their respective performances. The metrics used when reporting the accuracy of VLP systems lacks any guidelines or even unified definitions of the metrics itself. The positioning error, which is the Euclidean difference between the estimated point and the

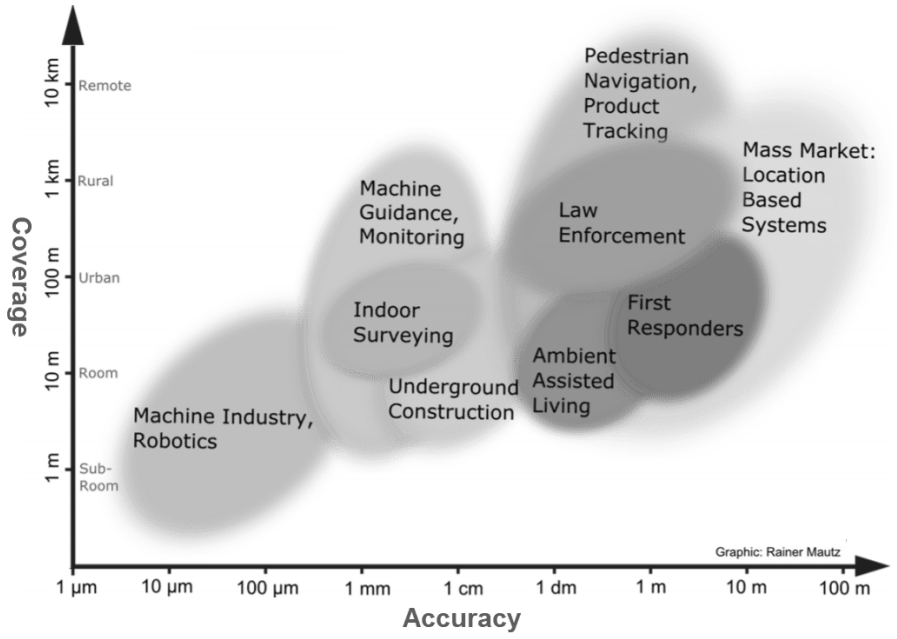

Figure 2.3: Overview of positioning requirements in terms of accuracy and area coverage. Adopted from Mautz (2012).

real position, is usually used to reflect the accuracy of these systems. This particular metric, however, often varies. Sometimes the median, mean, RMS error or a chosen percentile is reported to reflect the performance of the system. Some papers even report the lowest positioning error as proof of the system's high accuracy. Moreover, there should be clear differentiation between the *accuracy* and *precision* (Hightower and Borriello, 2001). This has affected survey papers as well. Review papers generally resort to classifying the work of other researchers based on the *stated* accuracy of VLP systems, which sometimes results in pitting median against mean values. The use of the mean should not be relied on as the presence of outliers may not accurately reflect the performance of the system. An example of the disparity between the mean and median values can be seen in the work by Potortì et al. (2015). By using quantiles, it reflects how often does the system give an accuracy below, or above, a reported error. The EvAAL (Evaluation of Ambient Assisted Living) framework aims to establish benchmarks and evaluation metrics to provide a consistent way for evaluating the performance of an indoor positioning system. The EVAAL framework recommends the use of the 75^{th} percentile to report the system's performance along with other criteria (Barsocchi et al., 2013). In this thesis, the 50^{th} (median), 90^{th}, and 95^{th} percentile errors are used. Another standard is the ISO/IEC 18305 international standard for testing localisation and tracking systems. The standard mentions the use of the median and the 95^{th}, but using a high percentile such as the 95% to report the system's performance is more suitable for consumer-ready

products as opposed to experimental research work (ISO, 2016).

In addition, it is important to check whether the designed system is fit for purpose for the intended application. Again, this has been largely absent when evaluating VLP systems with no references being made to specified requirements. Each intended application would require a different accuracy depending on the task. Figure 2.3 demonstrates the required accuracies for a variety of applications (Mautz, 2012). The work in this thesis can be classified under 'product tracking'. As can be seen from the figure, the range is usually around 10 cm for a room-sized area.

2.1.6 Illumination Levels

The main task of artificial lighting in indoor settings is to provide sufficient illumination for performing visual tasks efficiently without experiencing discomfort (Korolija et al., 2013). The unit of illuminance and luminous emittance is defined as Lux (lx). The International Organisation for Standardization (ISO) recommends an illuminance range of 300 to 1500 lx for work environments (Komine and Nakagawa, 2004). This value range is what is generally referenced in the literature when a VLC/VLP system is tested. However, the European Standard EN 12464-1:2002 provides more detailed recommendations of the illuminance levels ($\bar{E}_m$), that is defined as "the value below which the average illuminance on the specified area should not fall" (de Normalisation, Comité Européen, 2002). The standard lists the minimum illumination levels for the type of activity and the areas related to the activity. For example, the minimum illumination levels for office environments where work is carried out generally range from 300 to 500 lx, but it differs for areas where technical drawings are performed, which has a minimum illumination level of 750 lx.

For industrial environments, the standard details a more encompassing list that range from work related to chemical, plastics and rubber industry to vehicle construction. A selection of illumination levels for different tasks and areas is shown in Table 2.3.

In order to check that the illumination levels meet European standards, light planning software applications are generally used to generate a visual presentation. DIALux® (DIAL) is a 3D commercially available professional light planning software that has a catalogue of a wide variety of luminaires from different manufacturers. It also allows the inclusion of different objects within their environment. The software also has the European standard integrated within it to verify if the

Table 2.3: Minimum maintained average illuminance levels for different settings. Adapted from de Normalisation, Comité Européen (2002).

Type of interior, task or activity	Area	($\bar{\mathrm{E}}_{\mathrm{m}}$) lx
Offices	Filing, copying, etc.	300
	Writing, typing, reading, data processing	500
	Conference and meeting rooms	500
Storage rack areas	Gangways: unmanned	20
	Gangways: manned	150
	Control stations	150
Metal working and processing	Welding	300
	Plate machining: thickness $\geq$ 5 mm	200
	Sheet metalwork: thickness $<$ 5 mm	300
Vehicle construction	Body work and assembly	500
	Painting, spraying chamber, polishing chamber	750
	Final inspection	1000
Rolling mills, iron and steel works	Mill train; coiler; shear line	300
	Furnaces	200
	Test, measurement and inspection	500

designed layout meets the minimum illumination requirements.

2.2 Visible Light Positioning Methods

Using VLC for indoor positioning is one of the most promising uses for this technology, and is generally referred to as VLP. The research work in indoor positioning systems is an active area in the literature as it has great promises for real-life applications. This is largely due to the wide range of potential applications accelerated by leveraging the internet of things (IoT) and the demand for a more customised experience in indoor spaces. Additionally, the wide adoption of smartphones and wearable devices by the public meant that indoor navigation can be provided to any user for localisation and guiding purposes. Indoor navigation has been extensively researched in the last few decades using different technologies for a range of applications such as surveillance, building management, and for use in the health sector. Conventional positioning methods that rely on satellites such as global positioning system (GPS) are unreliable for indoor positioning due to the high penetration loss of walls and building materials. To counter this, complementary methods such as assisted-GPS and pseudo-satellite have been proposed to address the shortcomings of conventional satellite-based systems in indoor settings. The accuracy, however, is still inadequate, not to mention the added complexity of integrating two different systems (Xu et al., 2015). The majority of the technologies used for localisation systems are RF-based, which are

prone to EMI. There are also a number of vision-based and acoustic-based localisation methods but they will not be discussed here as it is beyond the scope of this section, the reader is instead referred to Zafari et al. (2019) and Mautz and Tilch (2011) for a more detailed discussion of these methods. Technologies that have been proposed for indoor positioning and navigation use employ Bluetooth, infrared, ultrasound, ultra-wide-band (UWB), and other RF-based technologies (Zafari et al., 2019). The use of WiFi was expected to gain popularity and wide adoption due to its prevalence and because most consumer devices have WiFi capabilities, rendering it an ideal candidate. However, the current use of WiFi remains for communicational purposes instead of localisation purposes. Radio frequency identification (RFID) has been used for localisation as well. The system requires an RFID reader and tags. The work by Shirehjini et al. (2012) proposed an RFID-based system that achieved a localisation accuracy of 6.5 cm. However, the system design requires a carpet of RFID tags. Also, the typical reading range in RFID systems is 1-2 meters for passive tags. Sadowski and Spachos (2018) compared the performances of WiFi, Bluetooth low energy (BLE), ZigBee and long-range wide area network (WAN) for indoor localisation for IoT devices. Experimental results showed that WiFi proved to be the most accurate with positioning errors of 0.66 meters on average. The second most accurate was BLE with a positioning error of 0.75 meters. The authors also compared the power consumption of the systems and found that BLE used the lowest amount of power.

However, there is an alternative cost-effective and interference-free technology. VLP is one of the most promising technologies being proposed for indoor positioning given the readily available infrastructure and its many advantages such as increased security and low relative complexity when compared with RF-based positioning. While most of the technologies being researched and proposed for indoor localisation are based on the highly congested RF spectrum, VLP systems are not sensitive to electromagnetic interference, which enables it to be used in areas that are sensitive to electromagnetic waves such as hospitals and certain power plants.

This section discusses the research work in VLP systems. They vary based on the type of receiver and methods of implementation. The most widely used ones in the literature are discussed here. Additional works in the literature are discussed in chapters 4 and 5. The main methods of trilateration or multilateration are methods used in determining the position through distance measurements. Another method uses triangulation or multiangulation, which utilises the angle-of-arrival (AOA) of the signals in order to determine the position of the receiver. These positioning methods are not unique to VLP systems and are

used in different technologies, but the discussion here will be limited to its use in VLP systems. In the literature, there is a somewhat inaccurate classification of positioning methods as it is often being conflated with distance estimation methods. Ideally, there would be a distinction solely discussing positioning algorithms. Nevertheless, the categorisation of positioning methods here follows the majority of published work, but it is then accompanied by a separate discussion on distance estimation methods. Figure 2.4 shows a classification of the positioning methods discussed here.

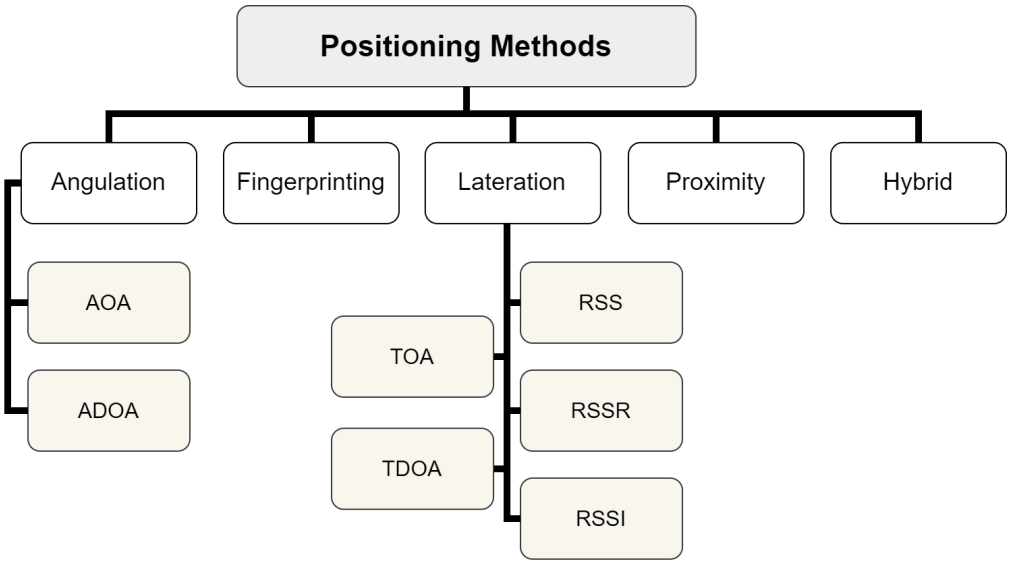

Figure 2.4: General VLP methods.

2.2.1 Lateration

Multilateration is a technique that estimates the location of a target based on distance measurements from multiple sources. When three sources are used, it is then referred to trilateration. Trilateration or multilateration are used in time-of-arrival (TOA), time-difference-of-arrival (TDOA), and received signal strength (RSS) positioning methods and generally require at least three base stations to determine the position of a receiver. The most common trilateration algorithm is based on the least squares algorithm. The algorithm requires a minimum of three distances to determine a location but is capable of including additional distances in the algorithm. The use of additional distances would improve the positioning accuracy. However, if the additional included distances are not precisely accurate, then the inaccurate distances would decrease the overall accuracy of the system. Distance estimation methods in VLC are discussed in a separate upcoming section.

2.2.1.1 Time-of-Arrival / Time-Difference-of-Arrival

TOA calculates the position of the receiver based on the distances between the transmitters and receiver that are derived from the absolute arrival time of the signal. However, it is extremely difficult to use it in indoor settings where the signal (light) only travel a few meters. This also means that all the transmitters and receivers are synchronised with each other to accurately measure the time. This resulted in having limited work examining the use of TOA in VLP systems. Zhao and Wang (2019) used TOA and proposed the use of a novel positioning method that takes into consideration the shapes of the transmitters to ensure high indoor accuracy. They reported results of around 4 cm when the light sources with a length 10 cm were used. The works by Wang et al. (2013) and Amini et al. (2016) assumed perfect synchronisation between the transmitter and receiver to present an analysis of the Cramer–Rao bound (CRB) of a TOA-based ranging for an indoor positioning system.

The time synchronisation requirement between the transmitter and receiver can be avoided by using the TDOA method. The use of the TDOA only requires synchronisation between the transmitter nodes, as a result, it is more researched than the TOA method. The work by Jung et al. (2011) simulated a TDOA-based optical wireless positioning system and reported simulation results of less than 1 cm. Naz et al. (2018b) proposed the use of a single LED with multiple PDs and the system was tested with different photodiode arrangements. The reported simulation results were the lowest when the photodiodes were in a circular arrangement with a reported accuracy of 0.13 mm, and accuracies of 0.441 mm and 0.58 mm for the square and hexagonal arrangements, respectively. The effects of the shot, thermal, as well as reflected light noises from the wall were considered by Trong-Hop Do et al. (2013) and reported simulation results of 3.59 cm. Two error minimisation methods were used by Nah et al. (2013) in a TDOA-based positioning system. Their reported simulation results were 3.89 cm after the fuzzy logic algorithm for minimising error (FLAME) was used, and 6.67 cm when the localisation algorithm based on a spring model (LASM) was used (Parthiban and Menon, 2009; Chen et al., 2008). Li et al. (2018) proposed the use of a neural network-based machine learning (ML) method with reference points obtained through TDOA, and a positioning error of 1.66 cm was achieved. A low-complexity TDOA-based VLP system was demonstrated by Du et al. (2018). The authors proposed the use of cross-correlation and experimentally tested their systems, achieving an average positioning accuracy of 9.2 cm in an area measuring 1.2×1.2 m^2. The method has also been adopted for outdoor uses. An outdoor vehicle positioning model was presented by Bai et al. (2011).

The authors proposed that the vehicle position could be determined based on the received position information of the traffic light and the TDOA from the LED signal to the two photodiodes placed on the vehicle. Kim et al. (2013b) simulated a TDOA-based system and suggests that the use of a sinusoidal pilot signal for TDOA-based systems achieves better accuracy than using square waves.

There has been some work that utilises the phase-difference-of-arrival PDOA in indoor VLP systems (Naz et al., 2018a; Zhang et al., 2018). PDOA is similar to the TDOA-based method in concept but uses continuous sine waves instead of short pulses. Because PDOA can be used to calculate the TDOA, this has led to PDOA work being discussed and listed under TDOA (Du et al., 2018; Maheepala et al., 2020).

While TDOA does not require synchronisation between the transmitters and receiver. All of the transmitters need to be perfectly synchronised.

2.2.1.2 Received Signal Strength

Using the received signal for positioning is less complex than the previous methods. Typically, the distances are derived from the received signals and are then used by a trilateration-based positioning algorithm.

The work performed by Gu et al. (2016) presented an RSS-based positioning system and analysed the impact of reflections. The authors reported that most of the simulated positioning errors were within 0.5 cm when taking into account thermal noise and shot noise in a LOS scenario. The inclusion of reflections increased errors to within 1 meter for some locations and 1.7 m near the corners. Lin et al. (2017) presented a demonstration of an RSS-based positioning system that employs the orthogonal frequency division multiplexing access (OFDMA) and reported a mean positioning error of 1.68 cm over an area measuring 20 cm $\times$ 20 cm $\times$ 15 cm. The algorithm proposed by Zhang et al. (2018) uses RSS and combines the use of the chaos algorithm and particle swarm optimisation (PSO) to achieve a 3D VLP system. Their reported simulation accuracy achieved less than 3.55 cm for the majority of locations with an average error of 1.4 cm. Further experimental test performed in an area measuring 1 m $\times$ 2 m $\times$ 2 m with the receiver being placed at two different heights achieved positioning errors within 10 cm. Wu et al. (2018) used an RSS-based indoor positioning system to calculate the 2D position of the receiver and then used a modified differential evolution algorithm (DE) to calculate the height of the receiver, achieving an average positioning error of 0.69 cm. Other work proposed

localisation methods based on the received signal strength ratio (RSSR). The work by Jung et al. (2013) proposed the use of RSSR for localisation by utilising the ratio difference between the received powers. Simulation results reported a maximum simulated positioning error of 3.65 cm and a mean location error of 1.12 cm. Zhang et al. (2014) derived the CRB model of a VLP based on RSS indicator (RSSI). The results reported an accuracy below 5 cm and showed that the positioning accuracy with triangle LEDs is higher than the ones with square LEDs.

Using the RSS in positioning systems is the most popular and widely adopted method as it offers a simple low-complex alternative to other methods that require synchronisation or additional receivers.

2.2.2 Angulation

Using the signal's AOA to determine the position of the receiver is a popular method for indoor and outdoor positioning applications, but the method requires the use of multiple photodiodes in VLC positioning implementations. Triangulation algorithms are generally adapted depending on the receiver's design. There are also methods that make use of the angle-difference-of-arrival (ADOA) to estimate the receiver's position (Bergen et al., 2018).

2.2.2.1 Angle-of-Arrival

The use of arrival signals from multiple LEDs can be used to determine the receiver's position. AOA-based algorithms rely on the measured angles relative to multiple base stations to find the position of a receiver. The arrival angle of the signal can be obtained through a PD array or an image sensor. There have been different design layouts proposed in the literature that range from circular to a corner-cube shaped design.

The work by Seongsu Lee and Sung-Yoon Jung (2012) proposed an AOA estimation algorithm that uses a circular PD array design to determine the angle of the arriving signal. The irradiance angle of the signal is determined using a truncated-weighting algorithm, which is a weighted sum of angles of PDs in the PD array, that is used to increase the accuracy of the estimated AOA. Reported simulation results showed that the distance errors are between 5-30 cm with the accuracy increasing if additional numbers of PDs are used. Arafa et al. (2015)

proposed the use of three orthogonal PDs to receive the signal from multiple LEDs. Each Led was modulated with distinct frequency channels, to allow the PD to separately process each channel and calculate the AOAs from all observable transmitters. The authors reported a mean 3D positioning error of 5 cm. Sun et al. (2015) derived the CRB of an AOA-based VLP system and discussed the impact of the room's height and the elevation angle. They concluded that the system is able to achieve an accuracy of under 8 cm with high SNR values. Estimating the AOA based on the relative differences in the received signal strength was also used by Steendam (2018). The author proposed the use of an aperture-based receiver with 8 receiving elements (RE) in order to have angular diversity that allows the receiver to detect the direction of the light signal and find the AOA based on the maximum likelihood estimation (MLE) principle. The proposed algorithm achieved an accuracy of 10 cm or better in an area measuring 5 m $\times$ 5 m.

Yasir et al. (2013) used the accelerometer in mobile devices to determine the AOA of the signal. The proposed method does not require prior knowledge of the receiver's height unlike many of the proposed methods in the literature. However, a pre-calibration step is needed, so two measurements were made by having the receiver's location fixed and then rotating the mobile device by small angles. This means that two received powers from each transmitter are recorded at different incident angles. If the method is to be used in a three-dimensional system, then at least three measurements using three distinct orientations of the receiver are need. The locations of the LED transmitters are transmitted and the receiver is assumed to be able to distinguish the signals from each transmitter using time division multiple access (TDMA). Simulation results show that positioning errors of less than 50 cm are achievable when the SNR values of the accelerometer and the received signal are both over 30 dB. The work was experimentally verified with results showing that the system can deliver an average positioning error of less than 25 cm (Yasir et al., 2014).

Compared with other VLP methods such as RSS and TDOA, AOA-based positioning offers many advantages such as avoiding the need for any synchronisation and the fact that it doesn't require the need to consider the path loss model used in RSS-based positioning.

2.2.3 Fingerprinting

The general working principle of fingerprinting for indoor positioning is to gather measurements, referred to as fingerprints. from an indoor environment such as an office in advance and then create a fingerprint map consisting of all the measurements. These measurements can be any signal characteristics but usually, RSS is considered in most cases. The map is then used to estimate the receiver's location. Most fingerprint methods are map-based ones that consist of two stages: offline and an online stage. The offline stage consists of performing a site survey of the indoor environment in order to generate a fingerprint map and the online stage is where the position of the receiver is matched to the map location that holds the closest measurement reading. This method was used and experimentally tested by Qiu et al. (2016). A correlation-based technique was used to decompose lights signal and obtain fingerprints from 12 different LED light tube sources in a 4.7 m $\times$ 8.6 m indoor environment. Experimental results achieved an accuracy of 0.56 m in their experiments. The work by Vongkulbhisal et al. (2012) proposed a 2D indoor localisation system that uses fingerprinting of received optical signals emitted from the LEDs. Each LED is assigned a different frequency and then the power spectral density of the received signal is calculated by the receiver to estimate the location based on the fingerprint map. Simulation results achieved positioning accuracies ranging from 4 to 16 cm and the system was also experimentally tested in a testbed measuring 1.8 $\times$ 1.2 $\times$ 1 m^3. Measurements every 10 cm was recorded at 160 uniformly distributed fingerprint locations and the average positioning error was 14.86 cm in a free space scenario and 22 cm with the inclusion of obstacles. Jung et al. (2012); Gao et al. (2017) used four LEDs each assigned a unique address with a correlation method in order to determine the receiver's location. The correlation between the predetermined addresses and received data was used to locate the target position and the proposed positioning system was experimentally tested in a 1 $\times$ 1 $\times$ 1.2 m^3 area. Experimental results reported a mean of 4.38 cm and a maximum of 12.46 cm. The use of the extinction ratio, which is the ratio between the received powers when bits of 1 and 0 are transmitted, for fingerprinting was proposed in (Yang et al., 2013; Yang et al., 2012). The signals from the LEDs were sent using time-division multiplexing (TDM) to mitigate interference and achieved an average positioning error of 1.58 cm.

While fingerprinting can produce high accuracies, fingerprint measurements need to be entirely re-created if new transmitters were added or removed. The measurements map would also need to be recreated if the layout of the room is changed and/or furniture is moved (Jang and Kim, 2019).

2.2.4 Proximity

Proximity-based localisation is one of the less complex methods used for positioning. The receiver's location is estimated based on its closeness to the transmitter and gives a rough location estimation in that vicinity. To improve the performance of proximity-based localisation, the work by Sertthin et al. (2009) proposed the use of a six-axes sensor paired with the proximity-based information. The sensor provides azimuth and tilt angles to enhance the performance using wide FOV receivers and the authors reported an improvement of more than 30% when this method is used compared with the conventional position estimation scheme.

del Campo-Jimenez et al. (2013) presented a low-complexity, cost-effective indoor localisation system was presented. The system consists of the LEDs with each one continuously transmitting an identification code indicating its position within the building and two system designs were presented. The first one is a passive beacon that continuously sends a location identifier intended for use in airports or hospitals, and an active beacon for use in highway tunnels that sends additional information such as accident alerts or traffic jam information. An experimental verification showed error-free communication for up to 4.5 meter range.

The work by Nakajima and Haruyama (2013) presented an indoor navigation system for visually impaired people and built a prototype for testing. The method makes use of the LED lights with a geomagnetic sensor as a correction method. The geomagnetic information beneath each LED was taken in advance due to the unreliability of geomagnetic sensors in the presence of obstacles. When paired with visible light communication, the user's position estimation was within a range of 1–2 meters.

While this method is easily implemented. Its accuracy is heavily based on the density of transmitters used in an area. For indoor settings, this means that LED lamps are positioned every 2 or 3 meters, while this is sufficient for some applications it may not be for applications that require high accuracy.

2.2.5 Hybrid Methods

There are also additional methods that combine the use of different technologies and/or methods to determine the location of a receiver. Which results in it being

more complex than other methods.

Torres-Zapata et al. (2019) designed and implemented a VLC-based indoor positioning system that combines the use of VLC for down-link with an ultrasonic system for up-link. The experimental results achieved an average localisation accuracy of 4 cm for direct links and 10 cm for indirect links. However, the system was sensitive to the alignment of ultrasound sensors as well as being affected by ambient light. Akiyama et al. (2017) proposed a similar concept with the use of sound waves along with VLC for smartphones. Experiments conducted using a TOA-based 3D positioning reported accuracies of 1-2 cm when the smartphone was placed 1 meter away from the LED. Two hybrid system design techniques with VLC and ad-hoc wireless network were proposed by Lee and Kavehrad (2012). The first design uses a non-carrier VLC for low data rate applications and reported an error-free communication range between 0.33-0.403 m. The second design uses a 4 MHz carrier VLC-based hybrid positioning technique for high data rate optical sensing with results reporting error-free transmission within the range of 0.0057-0.479 m. Amsters et al. (2019) presented a proof-of-concept by using a mobile robot. The system design utilises a simultaneous localisation and mapping (SLAM) algorithm with rolling shutter based frequency detection. The source map generated is then used by VLP systems in order to enhance the positioning accuracy.

Given that most of VLP algorithms assume a fixed height for the receiver, Lam and Little (2018) proposed an indoor VLP system that solves the receiver's height uncertainty through a steerable laser. The method combines angular information from the steerable laser with RSS-based signals to estimate the receiver's position. The authors reported that the information from the laser can reduce the positioning errors to near zero when the height of the receiver is known (2D) and can achieve a 3D mean square error of less than 12.89 cm.

2.3 Distance Estimation

As mentioned before, a large number of localisation algorithms are trilateration-based methods, which require distance measurements from multiple reference points to determine the coordinates of an unknown position. Hence, the accuracy of the distance estimate directly affects the positioning accuracy (Luo et al., 2017). A different application for distance estimations can be found in ITS. By utilising the vehicle's headlights and taillights, the distance between vehicles or a vehicle and an infrastructure (e.g. a traffic light) can be calculated and used for

automatic vehicle driving systems, vehicle collision avoidance, and platooning applications (Abualhoul et al., 2013; Béchadergue et al., 2017, 2018). Distance estimation using VLC has also found applications in underwater environments (Schill et al., 2004).

Distance estimation is usually performed at the receiver's side to calculate the distance from the transmitter. This subsection is devoted to discussing distance estimation methods in VLC systems. A specific discussion is provided on distance estimation as some applications only utilise distance information without requiring a communicational aspect. In addition, distances estimation is often a precursor to utilising some positioning algorithms (Almadani et al., 2019a). This is also especially relevant as the positioning method presented in this thesis relies on distance measurements.

Distance estimation methods generally fall within the following groups: (i) time-based methods, (ii) angle-based methods, (iii) image sensor, (iv) signal-based methods, (v) phase difference methods, and (vi) hybrid systems (a combination of different technologies). Time-based methods rely on measuring the signal propagation time between the transmitter and the receiver. The main drawback of time-based methods is that synchronisation is required. Angle-based methods measure the propagation direction, resulting in more accurate positioning. However, it is more complex to implement as it requires an array of receivers or image sensors. The signal-based method is a simple and cost-effective algorithm that determines the distance based on the received signal strength.

2.3.1 Time-based Methods

The main two time-based methods uses are TOA and TDOA. In TOA, the distance between the transmitter and the receiver d is calculated from the delay using (Wang et al., 2013):

$$d = c\,t \tag{2.8}$$

where c is the speed of light, and t is the propagation time. TOA requires perfect time synchronisation between the transmitters and receivers. While it is possible to achieve synchronisation using a clock, it is problematic at short distances, as with indoor environments. This is due to the reason that a small deviation in the clock increases the positioning error exponentially. For example, a deviation of 1 ns in clock results in a 0.3 m error (Do and Yoo, 2015). Even if it is assumed that the system has a fine resolution clock, the accuracy of time measurement

depends on the response time of photodiode as well as the frame rate of image sensors (Do and Yoo, 2015).

The time synchronisation requirement between the transmitter and receiver can be avoided by using TDOA. TDOA exploits the time difference between the arrival times of the optical signals from different transmitters to find the distance between the transmitters and the receiver and is given by:

$$d_{ij} = c\,(t_i - t_j) \tag{2.9}$$

where d_{ij} is the distance between the transmitter and receiver, t_i is the propagation time from the i^{th} transmitter, and t_j is the propagation time from the j_{th} transmitter.

Unlike TOA, this method only requires time synchronisation between the transmitters without the need for synchronisation with the receiver. The propagation time difference is then converted into the distance by multiplying it with the speed of propagation. This technique is more widely used than the TOA due to its low complexity since the transmitter can share the same clock within the same room (Du et al., 2018).

2.3.2 Angle-based Method

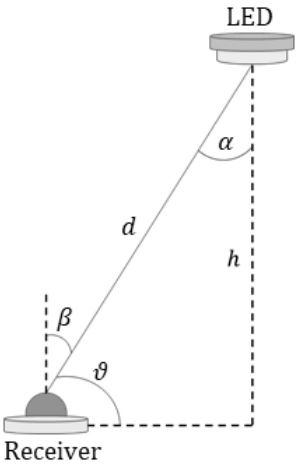

Figure 2.5: Parameters for distance calculation using the elevation angle.

Using basic trigonometric functions, the distance can be used to calculate the distance between the transmitter and the receiver using (Seongsu Lee and Sung-

Yoon Jung, 2012; Sun et al., 2015):

$$d = h \ \sin \vartheta \tag{2.10}$$

where h is the vertical height difference between the transmitter and receiver, and ϑ is the elevation angle, which is the angle between the horizontal plane and the line of sight, as shown in Figure 2.5.

In order to calculate the distance d, the vertical height h between the transmitter and receiver must be known, along with the elevation angle, which is impractical.

2.3.3 Image Sensor

Estimating the distance using image sensors is mainly employed in V2V applications. The image sensor is used to capture images of the transmitters (LEDs), and then the location of the receiver is calculated based on the correlation between the 3D coordinates of the LEDs and the 2D coordinates of the LEDs that have been captured.

Using two image sensors and two lenses have been proposed by Rahman et al. (2011) to estimate the distance between the LEDs and a receiver. The receiver coordinates are assumed to be a point located between the lenses. The distance between the LEDs and the difference in their positions on the imaging sensor can provide the unknown location of the receiver. The distances can be calculated from the geometric structure between the distance and the position difference of the LED images on the two image sensors. The distance between the centres of the lenses L, and the focal length of the lenses f, are known. The distances of the image centres from the centre of the image sensors are i_1, and i_2, and their projection on the axis of the image sensors are Pi_1 and Pi_2, the distance d_1 can be calculated using the following equations (Rahman et al., 2011):

$$d_i = |Pi_1 - Pi_2|, h = \frac{fL}{d_i}, c = \sqrt{f^2 + i^2}, d = \sqrt{f^2 + i_2^2}, a = \frac{hc}{f}, b = \frac{hd}{f} \tag{2.11}$$

$$\theta = \cos^{-1}(\frac{a^2 + L^2 - b^2}{2aL}) \tag{2.12}$$

$$d_1 = \sqrt{a^2 + (\frac{L}{2}) + 2a\frac{L}{2}\cos\theta} \tag{2.13}$$

where the distances d_2 and d_3 can be obtained similarly from the other two LEDs.

The concept has also been used by other researchers Tram and Yoo (2018); Myoung-geun et al. (2015). The work by Tram and Yoo (2018) proposed a camera-based ITS positioning technique that estimates the distance between vehicles using image sensor-based VLC. The method uses two image sensors but only requires one LED to calculate the distance. This method, however, has strict requirements that need to be exact. The lenses should have identical properties and all the distances should be maintained strictly (Rahman et al., 2011).

2.3.4 Signal-based Methods

Using the received signal for distance estimation is the most widely utilised method as it is cost-effective and does not require complex time synchronisation (Zhuang et al., 2018; Kim et al., 2013a). Estimating the distance using the received power uses the attenuation property of the emitted signal strength. The signal strength decreases as the distance increases. Hence, the distance can be obtained using the inverse of the received power strength (equation 2.2) Zhang et al. (2014):

$$d = \sqrt{\frac{(m+1)A_{pd}P_t \cos(\alpha)^m \cos(\beta)}{2\pi P_r}} \tag{2.14}$$

This equation, however, would mean that the receiver is capable of knowing the irradiance and incidence angles. If it is assumed that the transmitting and receiving planes are parallel to each other (i.e. $\cos(\alpha) = \cos(\beta) = h/d$). After substituting, the equation becomes:

$$d = \sqrt[m+3]{\frac{(m+1)\,A_{pd}P_t h^{m+1}}{2\pi P_r}} \tag{2.15}$$

The distance can be calculated using this equation but would still require knowledge of the receiver's height. Nevertheless, it is widely used in VLC-based positioning systems.

2.3.5 Phase Difference

The distance can also be obtained by measuring the phase change of an emitted signal (Béchadergue et al., 2018; Wu et al., 2016). Wu et al. (2016) proposed a differential phase-shift measurement scheme for range estimation. In the proposed scheme, an RF signal at a frequency f_0 with an initial phase is used to modulate the LED, and then the flight time of the reflected rays from the targeted area is converted into a phase shift. The distance d between the transceiver and the target can be given by:

$$d = \frac{1}{2}\,\tau_d\,c \tag{2.16}$$

where τ_d is the propagation time given by:

$$\tau_d = \frac{\Delta\varphi}{2\pi f_0} \tag{2.17}$$

where $\Delta\varphi$ is the phase shift of the modulated RF signal at a frequency of f_0.

The system, however, requires the emitter to be a transceiver and it needs to be directed at the required object in order to measure the distance. The results show a detection range of up to ≈6 m with an accuracy of up to ≈5 cm. A proof of concept of a phase shift visible light rangefinder for V2V applications was presented by Béchadergue et al. (2018) and was able to measure distances up to 25 m with a resolution under 10 cm, and up to 30 m with a 30 cm resolution.

2.3.6 Hybrid Systems

Various hybrid methods can estimate the distance by incorporating different technologies such as lasers or ultrasound. Researchers Rabadan et al. (2017) proposed a TDOA-based distance measurement method that adapts the Cricket system with an optical signal (Priyantha et al., 2000). The transmitter node consists of an optical driver, an optical receiver, and an ultrasound emitter. The receiver node consists of an optical and an ultrasound receiver, as well as an optical driver. The transmitter sends an optical and an ultrasound pulse at the same time. The receiver receives the optical pulse first, and then the ultrasound signal. After the ultrasound signal is detected, the receiver sends back a light pulse to the transmitter indicating that the ultrasound signal has been received. The base station is then able to measure the distance by measuring the time difference between when the ultrasound was transmitted, and when the optical signal from the mobile node has been received. Cox et al. (2016) proposed a

distance measurement method using an LED as a light source and a piezotransducer as a sound source. The receiver calculates the TDOA of the ultrasound and the receiver. While the LED used by the authors is infrared, other LEDs can be used. A ranging method by Sasaki et al. (2015) uses a camera system and an image sensor, with VLC being used to provide additional data such as the size of the vehicle. While Suzuki and Mizui (2015) proposed a ranging system using a laser and visible light bidirectional communication system. Hybrid systems are often complex and require transceivers or hardware alterations.

2.4 Summary

This chapter presented the background on VLC and VLP systems. The basic principles of VLC were discussed and presented. The VLC system's applicability in different environments was demonstrated by discussing the relevant research for each of the areas. The importance of maintaining adequate illuminations level and the specified level for a selection of the environments were presented. Then, common methods used for VLP systems and their respective algorithms were presented. The two main categories are trilateration and triangulation. The positioning methods were discussed in term of complexity and accuracy. The TOA and TDOA methods are challenging as they require perfect clock synchronisation, rendering it complex for indoor applications. Fingerprinting generally requires a survey of the room to be implemented beforehand and proximity methods are not deemed highly accurate. Using the received signal strength with a trilateration algorithm, on the other hand, is relatively easier than the rest of the methods as well as cost-effective.

Several distance estimation methods were then presented and discussed. The methods differ from one another due to the requirements of synchronisation and complexity. While there is an overlap in the discussion between positioning algorithms and distance measurement methods, the discussion is important as distance measurements in VLC/VLP systems is usually glossed over. Distance estimation is also a precursor to using any trilateration-based algorithm. Additionally, some applications use distance measurements without using it for positioning.

As such, a trilateration based method that uses RSS was adopted for the work performed in the thesis in chapters 4 and 5. The following chapter demonstrated the potential for VLC and VLP methods in industrial environments as well as the relevant challenges.

Chapter 3

Visible Light Communications for Industrial Applications: Challenges and Potential

3.1 Introduction

In the last decade, a great amount of research has been focused on developing and optimising the performance of VLC systems. Most of the research focuses on VLC applications in home and office environments, underwater applications, and V2V communications (Matheus et al., 2019; Ghassemlooy et al., 2015; Căilean and Dimian, 2017). However, there has been limited work in the literature examining the application of VLC systems in industrial environments. The developing trend in an industry known as the fourth industrial revolution (Industry 4.0) envisages a substantial increase in operational effectiveness along with the development of new products and business models (Kannan et al., 2017). Several similar initiatives are taking place globally, such as 'Factories of the Future', 'Made in China 2025', and work performed by institutions such as the Fraunhofer Institute and the National Institute of Standards and Technology (NIST) (Lu et al., 2016). The fourth industrial revolution is still in its early stages and researching the applicability of VLC systems would help and promote its use in the industry.

The integration of cyber-physical systems (CPS) in the value chain serves as the foundation of Industry 4.0 and would enable the interconnectedness of the supply, manufacturing, maintenance, and delivery processes all through the internet (Kagermann et al., 2016). This will allow data to be exchanged in real-

time to optimise the production processes. A key element to achieving this is high-speed data exchange that requires a low-latency and reliable data transmissions to ensure smooth operations (Wilke Berenguer et al., 2018). Current RF systems can be used to meet these requirements but suffer from drawbacks, and are prone to interference due to multipath reflections from metal installations that can impair the signal for applications such as the controllers on the production floor (Remley et al., 2008). Moreover, some industries and areas (e.g. petrochemical and nuclear power plants) restrict the use of RF-based wireless technologies (Ye et al., 2015; Keebler and Berger, 2011). OWC technologies, including VLC, can be used in Industry 4.0 applications offering a wide bandwidth using a license-free spectrum. VLC can provide high bandwidth and low latency data communication with no EMI. Furthermore, the lighting infrastructure in modern industries already utilises LEDs for their power efficiency. These light fixtures can be used for dual functionality for illumination and communication, which also has the potential to reduce operational costs.

Adopting VLC in industrial environments can be also be used for indoor positioning of forklifts and aerial drones to carry out autonomous tasks. For example, unmanned aerial vehicles (UAVs), also known as drones, offer a safe and cost-effective way in performing inspections, especially for hard-to-reach areas. Currently, their use in warehouses for conducting physical inventory is gaining increasing attention and current implementations rely on RF-based communications. Which exhibits unreliability issues in industrial environments.

Though significant development has been achieved in VLC for many applications, there has been limited research in VLC for industrial applications. These applications range in their intended use in different types of environments. While the use of smart lighting systems in industrial settings did not attract much attention in the literature, it can lead to increased quality, lower long-term cost, higher productivity, and reduce accidents (Füchtenhans et al., 2019). Moreover, the illumination requirements set by governing bodies ensuring that work areas should be well-lit means that the coverage area of VLC systems is almost always present (de Normalisation, Comité Européen, 2002).

Given the sparse work being researched in VLC for industrial applications, this chapter reviews and examines the potential for VLC in industrial settings. VLC/VLP systems can contribute to different industrial settings such as warehouses, mines, and factories. There has been some experimental work demonstrating the potential for VLC in manufacturing cells and for VLP systems in mines, but the potential for VLP uses with autonomous aerial and ground vehicles is highlighted here. The chapter also discusses the possible challenges

posed by these types of environments. These challenges include greater link distances, indoor attenuation, severe multipath reflections, duplicate position estimates, and LOS signal loss. While there has been some work examining a few of these challenges, the effect of some of the discussed challenges on VLC and VLP systems is still absent in the literature.

3.2 Communication Technologies for Industrial Environments

Until a few years prior, industrial communications were a mixture of Fieldbus systems and Ethernet cables with some wireless communications (Wollschlaeger et al., 2017). Ethernet-based networks followed when internet technology became popular. However, the lack of real-time capabilities in standard Ethernet prevented the development of one single Ethernet solution for automation purposes and resulted in the proposal of dedicated solutions (Danielis et al., 2014). The evolution of wireless networks for industrial automation meant that devices can be moved and connected without restrictions caused by cable connections. The adoption of wireless networks for industrial applications did not take hold as the most critical issue in industrial systems is the system's reliability in order to provide efficient, safe, and productive operation (Tsang et al., 2016).

Due to the dynamic nature of modern industrial applications, traditional technologies are not adequate in fulfilling the requirements of these applications in these harsh environments. Existing wireless industrial standards usually have a centralised network management scheme that has difficulty in coping with large and dynamic large-scale networks (Zand et al., 2012). Also, industrial wireless communication systems usually use the 2.4 GHz frequency band which has relatively low data rates with an upper cap of 250 kbps, causing a bottleneck for some industrial applications. RF-based industrial wireless systems face several challenges that contributed to their lack of mass adoption in industrial environments. These challenges mainly come from a large number of connected devices with data transmission at extreme conditions such as dust, electromagnetic interference, and heat, causing uncertainty in industrial environments (Tsang et al., 2016). A major limitation is the excessive multipath reflections caused by highly reflective surfaces. Multipath reflection caused by the signal bouncing off large objects and metals fixtures results in a duplication of the received signal. There is also the issue of electromagnetic emissions that are generated by heavy equipment, large motors, and generators. These create high levels

of noise that prevents the transmitter and receiver from communicating (Yang et al., 2015). There has been work that characterised radio channel in factory buildings to study the applicability of wireless communication in these settings. Düngen et al. (2019) performed several channel measurements in eleven different industrial sites such as warehouses, manufacturing shops, automation labs, storage areas, production lines and robot cells. The measurements were conducted in the wide-band radio spectrum of 5.8 GHz and the 2.2 GHz region along with some additional measurements using the red optical spectrum. The researchers found that for many industrial applications to meet the demanding packet error rate (PER) requirements, the application of multiple antennas seems to be mandatory. Additionally, the optical experimental measurements indicate that setups with a single transmitter or a single receiver are not feasible solutions for OWC systems in industrial environments. Another benefit of utilising VLC systems is that it is more secure than traditional wireless systems. Security is one of the influencing factors in adopting industrial wireless sensor networks as they are vulnerable to malicious attacks such as eavesdropping, information tampering, denial of service attacks, and interference (Raza et al., 2018; Kim et al., 2010).

3.3 Potential Industrial Applications

This section discusses the potential of VLC applications in industrial environments. The main categories are organised based on work already performed in these areas.

3.3.1 Manufacturing

The use of indoor optical wireless communication in industrial scenarios differs from other indoor environments mostly by requiring reliable connections with moderate data-rates and low-latency at distances of 3-4 m for quick-moving devices (Wilke Berenguer et al., 2018). In addition to robustness against EMI, there are other advantages to using VLC systems in industrial manufacturing cells such as enhanced security, which allows for communication architectures that are low-latency in secure closed-loop systems (Wilke Berenguer et al., 2018; Holfeld et al., 2016). Moreover, the fact that VLC is an unregulated optical frequency means that a fast extension of existing wired industrial networks into hybrid solutions with RF and optical wireless links is possible (Shao et al., 2015).

The use of VLC in flexible manufacturing cells is one of the better-researched areas in the literature. Project OWICELLS (Optical WIreless networks for flexible car manufacturing CELLS) concluded in 2018 and was a collaboration between Fraunhofer Heinrich Hertz Institute and BMW. The project looked into the applicability of VLC systems in manufacturing cells for automobile manufacturing. While the project switched from the use of VLC to IR in its later stages, it is still mentioned here given that the basic characteristics of these two types of OWC are similar, and the fact VLC was used during the earlier stages of the project. The switch to IR chips proved to be faster than white light LEDs as there is a modulation bandwidth limitation when blue phosphor-coated LED chips are used.

As discussed in Chapter 2, there are two ways to produce white-light LED chips with the most common one through the use of a blue LED coated with phosphor due to its low cost and complexity. The production of the white-light is performed through the absorption by a phosphor. This absorption, however, limits the modulation bandwidth (Pathak et al., 2015). This was cited as the reason why the OWICELLS project decided to switch to IR chips (Halper, 2018). The production of white-light LEDs through the mixture of RGB wavelengths can achieve very high data rates as three separate channels can be modulated independently (Chun et al., 2016). Experimentally testing RGB-LEDs in a manufacturing cell could provide some interesting results. In addition, the use of a fourth colour, such as the yellow wavelength, can further increase the capacity (Wang et al., 2015).

Another promising sign on the potential of VLC systems for industrial applications is that these systems are now being made available by Signify. In 2019, Signify released Trulifi Securelink 6013, which is capable of delivering an aggregated physical layer speed of 750 Mbps up to a range of 8 meters (Signify, 2019). The Securelink is designed to establish robust connectivity for machine to machine communications, network to device connectivity or any other connectivity needs thanks to its plug and play design (Signify, 2020).

3.3.2 Mines, Pipelines, Tunnels, and Downhole Applications

In the oil and gas industry, 'downhole applications' generally refer to applications occurring or performed in a well or borehole. The ability to communicate between the surface and downhole instruments is imperative to ensure efficient and reliable production. Commonly used monitoring systems employ wired so-

lutions such as coaxial cables and fibre optics as they provide high data rates and reliable timely solutions. The occurrence of undetectable situations and low data rates are the main factors that restrict the development of wireless communication systems for these types of applications (Li et al., 2014). VLC systems on the other hand, are capable of providing much higher data rates.

Miramirkhani et al. (2018) claimed that the work performed by Li et al. (2014) was not entirely accurate because it assumed an ideal Lambertian source, only considered purely diffuse reflections, and assumed an empty pipeline without considering the effect of the gas. Due to these reasons, a ray tracing-based investigation into the propagation characteristics of the downhole VLC channel was carried out. The considered pipeline in the analysis is used for transporting liquefied natural gas and has a cylindrical shape with a length of 22 meters and a diameter of 1 meter. Results indicate that that the path loss is less severe for white and blue LEDs. It also revealed that a BER of 10^{-6} can be achieved over 22 meters when using pulse amplitude modulation (PAM) up to an order of 8, while the maximum achievable distance is reduced to 19.07 m for 16-PAM.

An experimental investigation of an in-pipe image transmission based on the visible light relay communication (VLRC) technique was presented by Zhao et al. (2019a). Experimental tests were performed in for an empty pipeline and a pipeline that is half-submerged in water. Results show that digital image frame-relay transmission system has some advantages in terms of transmission speed, strong image reconstruction capability, and transmission range. The work by Tokgoz et al. (2019) designed and demonstrated an ACO-OFDM-based VLC system using commercially available LEDs and photodiodes over an underwater pipeline. Experimental results showed that a BER of 10^{-6} can be achievable over a 6.5 m long underwater pipeline channel.

Another underground application that makes use of VLC/VLP systems is in mines, and it is an area that had gained a fair amount of attention. The use of tracking systems in underground mines is generally driven by safety policies due to accidents, and this has led some countries like the U.S. to require mine operators to install an electronic tracking system (Krommenacker et al., 2016). Another use for tracking systems in underground environments is for logistical activities Krommenacker et al. (2016) proposed the use of a VLC-based positioning system based on Cell-ID in underground mines, and reported an accuracy of 0.32 m when there is 5 overlapping cells. Dehghan Firoozabadi et al. (2019) presented a 3D positioning system and reported an average positioning error of 16.4 cm, while an average error of 3.5 cm was achieved when the subjects were close to the LEDs.

Robots have been used for pipeline inspections since it offers more convenient compared with manual inspections especially in hard to reach areas and hazardous locations. To overcome the limited inspection range due to the use of cables, a preliminary study using the VLC technology for gas pipeline inspections was performed by Zhao et al. (2019b). The researchers experimentally tested the application of a wheeled inspection robot for gas pipeline inspections. A VLC system is used to control the robot via pulse-width modulation (PWM) transmitted by a spotlight. The results showed great potential in replacing traditional wireless communications that suffer from electromagnetic interference and low energy efficiency by providing a more stable connection with less attenuation. VLC systems can also contribute to construction work. Céspedes and García Armada (2019) proposed the use of VLC during the construction of tunnels within the framework of Industry 4.0. The authors took into account the illumination requirements and have shown that VLC systems can be considered as a useful solution for providing connectivity in confined environments.

3.3.3 Indoor Positioning for Unmanned and Autonomous Vehicles

Warehouses and distribution centres are strategically important for companies to have a competitive advantage in the market. Warehouse operations generally employ mobile robots, such as automated guided vehicles (AGVs) to transport goods throughout the warehouse (Karaagac et al., 2017). As such, utilising positioning systems with these mobile receivers can play a key role in the realisation of these systems.

Current solutions for indoor positioning in manufacturing and storage facilities usually employ a large set of sensors such as RFID tags, RF-based solutions such as UWB (Li et al., 2019a). The harsh conditions in industrial environments have hindered the adoption of RF-based solutions and proved to be unreliable in these conditions reporting positioning accuracies in the range of meters. Podevijn et al. (2018) performed an experimental performance comparison using four RSS algorithms for indoor localisation between BLE and long range technologies. The tests were performed in a large open industrial environment measuring 69 m $\times$ 69 m and obtained a median accuracy of 15 meters with four BLE beacons. However, it is worth noting that the environment was empty without any objects, which can degrade the system through signal reflections and object movements (Huang et al., 2019). Using unmanned ground vehicles (UGVs) for industrial applications is an area where VLC can contribute to (Bastiaens et al.,

2018; Jarchlo et al., 2019). UGVs are vehicles that operate while in contact with the ground and without an onboard human presence, and when it is automated then it is referred to as AGVs. UGVs in the context of industrial environments can be forklifts, cranes, or ground robots that are usually used to move inventory (Yoon and Bostelman, 2019). One of the current ways used for directing these robots is by using RFIDs that are placed on the ground to function as 'roads' for them to follow by scanning the tags. The use of a VLP system would eliminate the need for additional equipment, reducing operational costs.

There has been some limited work examining VLP for industrial applications. Lam and Little (2019) proposed the use of a specific VLP technique that uses active receivers and fixed low-cost infrastructure for industry 4.0 applications. The authors argued that an infrastructure-based positioning system is the best way forward as a multitude of mobile receivers can utilise the system and position themselves. This would cut the cost and maintain the computational processing at the receiver's side. Bastiaens et al. (2018) employed two different designs to reduce the storage and computational effort for a model-fingerprinting-based RSS VLP system. Simulation models were performed for an AGV and they showed that model-fingerprinting-based RSS positioning only requires modelling less than 1% of the grid points in an elementary positioning cell. A PDOA-based positioning system was experimentally tested in a smart factory area measuring 2.2 m $\times$ 1.8 m $\times$ 2 m (Du et al., 2019). The receiver was mounted on a movable material buffer station and was tracked along a trajectory achieving an average positioning accuracy of approximately 7 cm.

Using UAVs, or drones, for industrial application is another area that is gaining momentum and is being actively pursued as they provide several advantages. Using UAVs in industrial environments has been utilised for a while for different applications (Jordan et al., 2018). It is mainly used by companies to perform visual inspections for a variety of indoor and outdoor settings as it provides a safe and cost-effective way to inspect heights and hard to reach areas as it eliminates the need for manual inspections.

UAVs and micro air vehicles (MAVs) can also be used for warehousing and inventory management/physical stock-taking (Ma et al., 2017). The drone can gather information either by reading RFID tags or by scanning the barcode of the inventory using a mounted camera (Beul et al., 2018; Kwon et al., 2020). The market has already a few companies that provide drones for warehouse management such as Eyesee (eyesee), Infinium Scan (Infinium Robotics), and InventAIRy®(doks). Another envisioned use for drones is material handling in manufacturing environments where drones can pick and drop-off goods to the

Table 3.1: A selection of some of the VLC work performed in different industrial settings.

Ref.	Environment	Application
Berenguer et al. (2017a,b, 2018, 2019)	Manufacturing cell	Communications
Li et al. (2014)	Gas pipeline	Downhole monitoring
Miramirkhani et al. (2018)	Gas pipeline	Downhole monitoring
Tokgoz et al. (2019)	Underwater pipeline	Communications
Krommenacker et al. (2016)	Mines	Positioning
Dehghan Firoozabadi et al. (2019)	Mines	Positioning
Zhao et al. (2019b)	Pipeline	Inspections
Céspedes and García Armada (2019)	Tunnel construction	Communications
Bastiaens et al. (2018)	Factories/Warehouses	AGV positioning
Du et al. (2019)	Smart workshop	AGV positioning

production line (Khosiawan and Nielsen, 2016; Khosiawan et al., 2018). Project UAWorld researchers have successfully implemented the use of drones for manufacturing purposes in a larger than 400 m^2 setting with fifteen indoor satellites to enable accurate positioning (Khosiawan et al., 2016). Main methods for RF-based localisation system for UAVs usually require extensive efforts for measurements mapping (del Carmen Pérez et al., 2019). Utilising VLP systems for drone positioning has the advantage of offering centimetre-level accuracies at a lower cost when compared with using a dedicated system solely for localisation purposes. Encouragingly, Philips Lighting demonstrated an autonomous indoor drone developed by Blue Jay where light fixture transmits a luminaire ID to the drone using VLC (Signify).

A summary of some of the discussed work is shown in Table 3.1. The referenced papers are classified depending on their environments and intended application.

3.4 Unique Challenges

There are some challenges that are unique to industrial environments when it comes to implementing a VLC system. They can generally be divided into these areas:

3.4.1 Greater Link Distances

Most of the applications for VLC systems consider residential applications where the distance between the transmitter and receiver does not exceed a few meters.

In contrast, warehouse and industrial facilities employ high bay lighting fixtures that have longer link distances (Almadani et al., 2018). This can have an impact on the overall path loss (link budget) and can affect the performance of VLC and VLP systems by reducing the SNR and the achievable data rates.

Over the past 20 years, the average rentable area of warehouses in the USA has increased by 60%, and the average size of U.S. warehouses has increased by 143% (CBRE, 2017). The demand for greater areas, that is spearheaded by the e-commerce industry has pushed the average warehouse ceiling height from 25 feet (7.62 m) in the 1990s, to 32.3 feet (9.84 m), with 36 feet (10.97 m) being common, reaching in some cases to 40 feet (12.19 m) (Cushman & Wakefield, 2018). The height is generally dictated by the type of warehouse, for example, bulk warehouses measure 20 to 30-plus feet in newer buildings, whereas the height for regional warehouses generally ranges from 16 to 24 feet (Yap and Circ, 2003).

Considering these values, a look into the feasibility of employing long-range VLC systems deserves an investigation. There has been some work examining long-range VLC systems. The study of mid-range VLC systems is not, however, a commonly researched subject. It is sometimes discussed in V2V communications and outdoor applications but the results cannot be extended to indoor application due to the different design characteristics of the luminaries.

Reported results for long-distance VLC systems have narrowly focused designs, essentially rendering it a free-space optical (FSO) systems. Experimental work performed by Vucic et al. (2009) reported 125 Mbit/s over a distance of 5 m with bit-error-ratios below 2×10^{-3} in a lab setting. The experimental setup used a custom-designed AC amplifier and optics to focus enough light onto the photodiode so that the desired illuminance level can be obtained in front of the receiver.

There are also other byproducts to having higher ceiling heights such as increased intersymbol interference (ISI) and inter-cell interference (ICI) influences Chen et al. (2018). As the luminaires will be placed even higher, this will increase the number of objects they encounter on the way to the receiver, and bigger light-cones would have more instances of overlapping coverage, which can also lead to ICI and co-channel interference (CCI) (Wang and Haas, 2015). This gap can be addressed by testing a VLC/VLP system in an actual industrial setting using commonly-used light fixtures as opposed to lab setups with custom, focused designs.

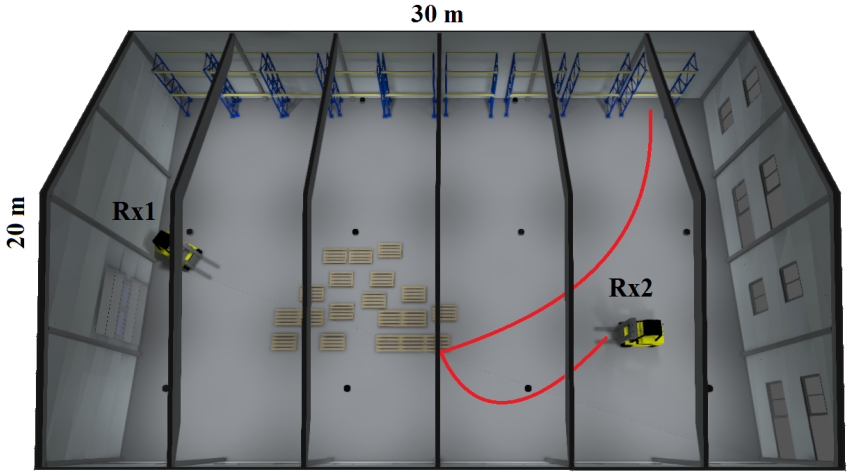

Figure 3.1: Top view of the warehouse demonstrating the locations of the transmitters and receivers, with the red line demonstrating the path for Rx_2. (©2018 IEEE)

3.4.1.1 Analysis of SNR and Link Distance

Compared with conventional ceiling heights, the link distance can be longer in industrial applications so it is important to investigate the relationship between the SNR and link distance. To demonstrate the effect of different ceiling heights on the SNR of the VLC system, a warehouse is considered for an industrial environment as shown in Figure 3.1. The dimensions of the considered warehouse are 30 m $\times$ 20 m and the heights considered will range from 4 to 20 meters. Two receivers, Rx_1 and Rx_2 are considered and placed on top of the forklifts at a height of two meters with a photodiode FOV of 45°.

Two scenarios that utilise a different number of transmitters from different manufacturers are considered here. The first uses OSRAM's 2nd generation compact high bay luminaire with a power of 115 W and 45° semi-angle (OSRAM). They are selected as they are intended for use in the industrial sector and has a recommended mounting height range between 5 to 20 meters. The second scenario uses Philips's coreLine highbay luminaires with a power of 155 W and a semi-angle of 50° (Philips). The system's parameters are summarised in Table 3.2.

3.4.1.1.1 Illumination Results

The minimum illumination requirement for warehouse (Storage rack areas) is 200 lx based on the European standards. To simulate the illumination, DIALux lighting design software is used. The software allows the selection of light fixtures from different light manufacturers to design optimum illumination levels. It

Table 3.2: The main parameters of the system model.

Parameter	Value
Width $\times$ Length	20 m $\times$ 30 m
Height of the Light Fixtures	5.6 m
Walls' Reflectivity	0.86
Floor's Reflectivity	0.34
OSRAM's Semi-Angle	45°
OSRAM's Power	115 W
Philips's Semi-Angle	50°
Philips's Power	155 W
Photodetector's Area	1 cm^2
Receiver's FOV (half angle)	45°
Receiver's Height	2 m
Photdetector's Responsivity	0.54 A/W
Bandwidth	10 MHz

also allows the user to specify the dimensions of an environment and selection of different types of surfaces. The floor material is considered to be fine concrete and has a reflection factor of 34% and all the other walls are painted white with a reflection factor of 86%. These figures are adopted from DIALux. The illumination results for the two different scenarios are shown in Figure 3.2. The first scenario uses twelve OSRAM light fixtures to achieve an average of 240 lx around the entire area as shown in Figure 3.2 (a). The lights offer more consistent coverage and required illumination levels set by the EU standards with a maximum of 323 lx under the lights and around 250 lx for areas between them.

The illumination levels for scenario 2 are shown in Figure 3.2 (b). There are nine Philips CoreLine Highbay luminaires are used to achieve an average illumination level of 241 lx throughout the area. As the Philips lights have a wider beam angle and a stronger output power compared to OSRAM's compact high bay luminaires, see Table 3.2. Scenario 2 on the other hand only requires nine luminaires to achieve the recommended illumination level of 200 lx. The consistency of illumination, however, is better in scenario 1 as it uses twelve light fixtures.

3.4.1.1.2 Link Distance and SNR Results

The SNR is simulated for both receivers with ceiling heights ranging from 4 to 20 meters as shown in Figure 3.3. In Scenario 1, the SNR drops around 12 dB for $Rx1$ and 6 dB for $Rx2$. However, in Scenario 2, the SNR drops around 9 dB in scenario 2 for $Rx1$ and $Rx2$. There are also some fluctuations in the SNR such as at 6.5 meters, this is because as the ceiling height increases, the more lights are within the receiver's field of view. This results in an increase in the total received power. However, because the luminaries are high-powered and

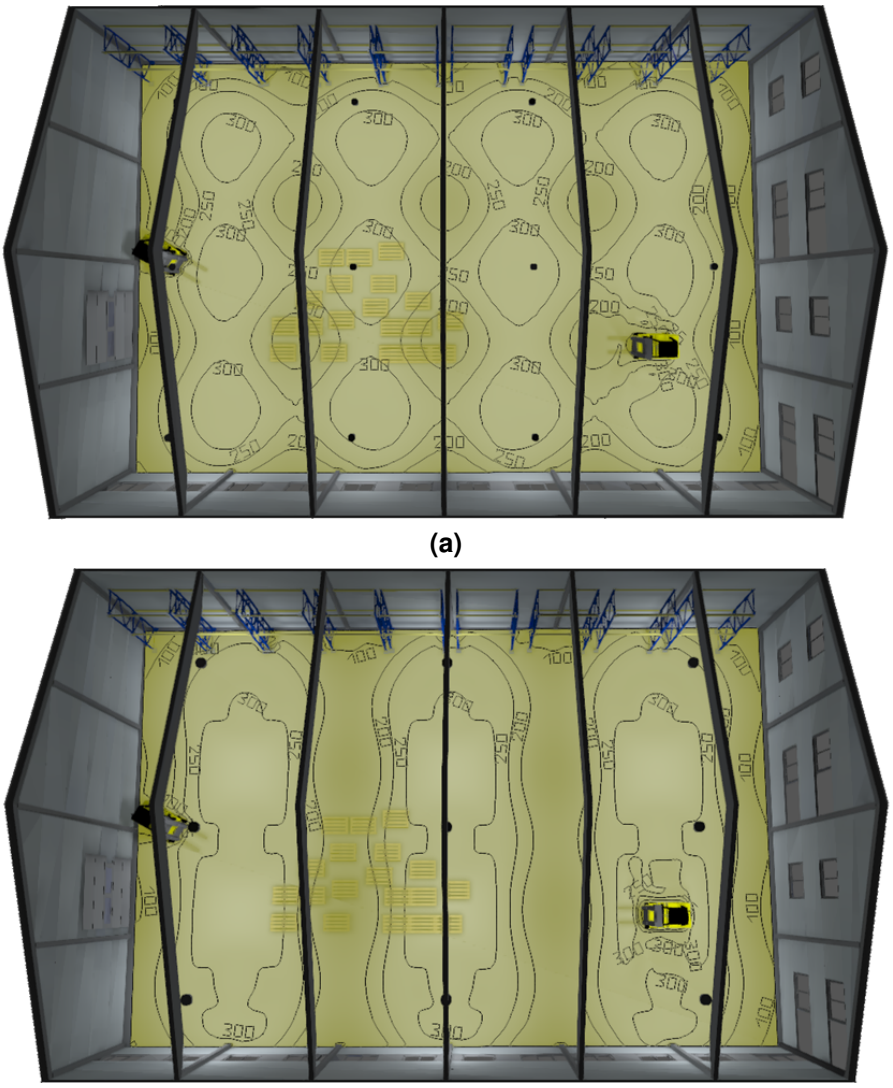

(a)

(b)

Figure 3.2: The illumination results for: (a) Scenario 1 using OSRAM's lights; (b) Scenario 2 using Philips's lights. (©2018 IEEE)

intended to use for large ceiling heights of 5 to 20 meters. The drop in power due to link distances is not as severe as if other non-specialist light fixtures were used.

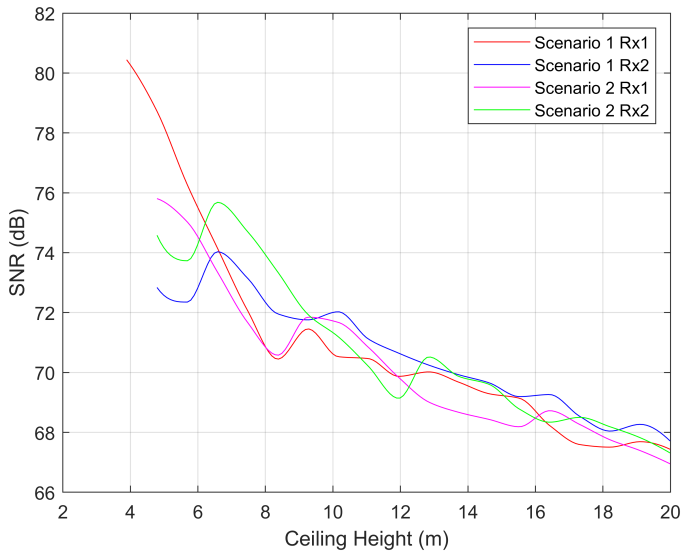

Figure 3.3: The achievable SNR vs ceiling height for the two different scenarios. (©2018 IEEE)

In order to study the signal consistency throughout the warehouse, signal fluctuations due to the receiver's mobility are also simulated for receiver $Rx2$ moving along the highlighted path in Figure 3.1. Figure 3.4 shows the fluctuations in the SNR for the selected path when the ceiling height is set to 5.6 meters. In the first scenario, the signal does not fluctuate greatly compared to the second scenario as the first scenario uses 12 lights while the second scenario uses nine lights. This results in greater uniformity throughout the warehouse. In Scenario 1, the highest SNR value is 76.2 dB and the lowest is 70.2 dB, resulting in a signal difference of 6 dB. In Scenario 2, the maximum SNR is 77 dB and the lowest is 67.2 dB, resulting in a signal difference of around 10 dB. This drop in Scenario 2 is more noticeable because of the lights fixtures are placed more sparsely.

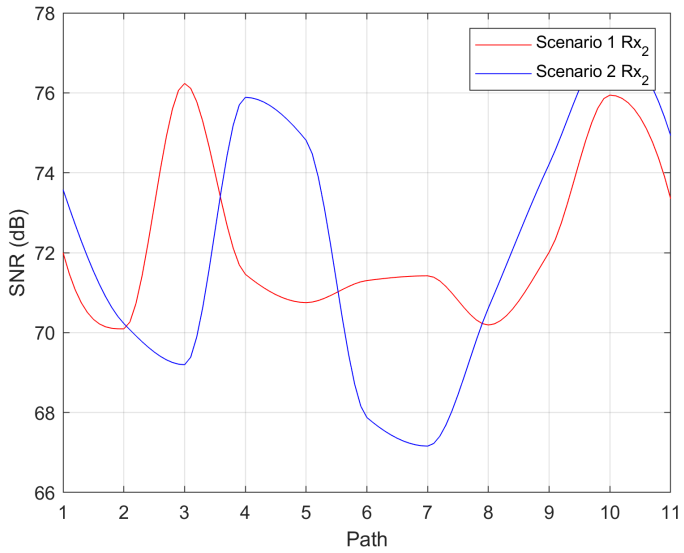

Figure 3.4: SNR signal fluctuation for receiver Rx2 when travelling along the path.

These results highlight point to the importance of having consistent light uniformity to avoid signal fluctuations. The distance results show that high SNR values are achievable due to the high output power of the industrial lights. While the SNR does not suffer greatly from the increase in link distance, it is worth keeping in mind that these results are simulation-based and might not necessarily extend to experimental work.

3.4.2 Indoor Attenuation

The transmission medium for indoor VLC systems is normally considered to be clear air. This assumption is not always true when it comes to some industrial settings. The attenuation contributor depends on the type of industrial environment and they can be oil vapour, water mist, industrial fumes, or coal particles. These particles can affect the VLC signal by causing light signal attenuation due to absorption and scattering. Sources of attenuation can come from water mist as some industrial application requires industrial misting systems, also known as industrial fog systems. They are usually employed for dust or odour suppression, and share a similarity with the naturally occurring fog. Its effect has mainly been discussed by outdoor applications of VLC systems and V2V communications. Other researchers similarly noted that particles in polluted environments, such as industrial environments, could affect the VLC channel (Riurean et al., 2019, 2020).

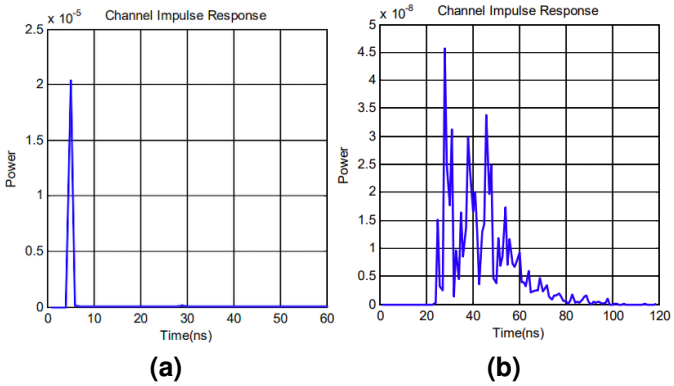

(a) (b)

Figure 3.5: The evaluated manufacturing cell from (Miramirkhani, 2018): (a) Manufacturing cell scenario; (b) Channel impulse response for T6; (c) Channel impulse response for T7. The figures were adopted from (Miramirkhani, 2018).

Research work examining the effect of the attenuation on VLC links mostly examined the effect of fog and rain in outdoor and V2V applications. Elamassie et al. (2018) performed a comprehensive channel modelling study to quantify the effect of rain and fog on V2V applications. They concluded that the presence of fog reduces the achievable link distance up to 26 m. An experimental evaluation of the effects of fog on camera-based VLC for a vehicular setting was performed by Eso et al. (2019) with varying visibility levels due to fog. The results showed a reliable link up to 20 m meteorological visibility for a modulation index (MI) of 0.5 and up to 10 m meteorological visibility for MIs of 1 and 0.75. The link degraded considerably when the meteorological visibility was less than 10 m. However, these results cannot be extended to indoor applications as car headlights are high-powered with narrowly focused designs.

Indoor attenuation also occurs in mine applications. Coal cutters generate large amounts of dust particles that lead to signal attenuation due to absorption and scattering. The effect of coal particles, or coal dust, on VLC optical signals was modelled by Zhai (2015). The authors suggested that coal dust can be considered as a condensation nucleus covered by a thin water vapour layer, based on the fact that coal seam water infusion is used as a dust prevention method for these types of applications.

3.4.3 Severe Multipath Reflections

Considering the effect of multipath reflections is important in intensity-modulated (IM) schemes with direct detection (DD) as it introduces ISI in communication systems. ISI is caused by the arrival of light rays from multiple reflectors to

the receiver. This is especially problematic for industrial applications as industrial environments usually have highly reflective surfaces such as metal fixtures and equipment. There has been some work examining ISI in home and office environments, but only a couple looked into industrial settings. The work by Uysal et al. (2017) performed channel modelling for a manufacturing cell using Zemax® to obtain channel impulse responses (CIRs). Zemax® is an advanced ray-tracing software that allows the user to specify the reflection characteristics of surface materials, specify the light sources, as well as specify the detectors. The simulated manufacturing cell measures 8.03 m $\times$ 9.45 m $\times$ 6.8 m, the robot arm coating material is galvanised steel metal, the floor is considered concrete, the ceiling consists of aluminium metal, and the cell boundaries are Plexiglas. Six commercially available LEDs are constructed in a cube shape and then placed on the head of the robotic arm. Eight test points were placed on the cell boundaries on top of the Plexiglas. The CIR from two receivers (T6 and T7) are shown in Figure 3.5 (a) and (b). A heavily scattered signal is received by T7 caused by non-line-of-sight (NLOS) signals with multipath signals delayed by tens of nanoseconds, which would cause ISI. In contrast, the signal received by the closer receiver (T6) has a clear peak with a single amplitude. The severe time dispersion is also partly due to the fact that multiple LEDs are operated together (Jungnickel et al., 2015).

The performance of a VLC system that suffers from ISI due to multipath reflections can be improved by using OFDM. However, the traditional OFDM commonly used in RF communications cannot be adopted in IM-DD optical communication as the optical signal cannot be complex and negative. This has led to the introduction to many variants of OFDM, such as DC-biased optical OFDM (DCO-OFDM), ACO-OFDM (Armstrong and Schmidt, 2008), Unipolar OFDM (U-OFDM) (Tsonev and Haas, 2014) and flip-OFDM (Fernando et al., 2012).

The use of OFDM in VLC systems has been touted and continues to be, as a much superior method that is robust and capable of delivering high speed when compared with IM-DD schemes (Dimitrov and Haas, 2015; Mossaad et al., 2015; Zhang et al., 2017). However, a growing amount of work in the literature counters this hypothesis (Rajbhandari et al., 2017). Randel et al. (2010) and Wei et al. (2012) reported that IM/DD outperforms DC-OFDM for low ISI LOS signals but not for NLOS signals with high ISI. Analytical results by Vanin (2011) confirmed by brute-force Monte Carlo simulations showed that M-PAM outperforms OFDM with the power gain of 3–3.5 dB at BER of 10^{-3} when 1-4 data bits are transmitted per signal sample. The work by Lian et al. (2019) compared the performance of DCO-, ACO- and U-OFDM with M-PAM for LED-based VLC

systems, where a bandlimited LED with a fixed peak power level and a channel response dominated by the response of the LED were assumed. Numerical results showed that M-PAM offered higher bit rate by 15% compared with the optimised optical OFDM system. However, optical OFDM outperform *M*-PAM in terms of the data rates by 12% for the broadband channel. Theoretical comparisons were performed for an indoor VLC system by Stepniak et al. (2015b) using three different modulation schemes. The authors reported that using PAM with a decision feedback equaliser (DFE) offers the best performance when compared with carrierless amplitude–phase (CAP) with DFE and DMT with bit and power loading. Further experimental comparisons between PAM, CAP, and DMT showed that 2-level PAM and CAP modulations exhibit better immunity to nonlinear distortions compared to their higher level counterparts (Stepniak et al., 2015a). These results illustrate that the use of OFDM, unlike in RF systems, is not always the most optimal modulation scheme for optical communications. Even so, the majority of the highest recorded data rates were achieved using OFDM and its variants (Chun et al., 2019; Chun et al., 2016; Wu et al., 2017).

Multipath reflections have also a degrading effect on the performance of VLP systems (Almadani et al., 2019). The vast majority of papers only consider LOS links when analysing VLP systems. However, this does not provide an accurate evaluation of the VLP system due to the substantial effect of reflections. The impact of multipath reflections has been examined by Gu et al. (2016). Most of the reported positioning errors were below 1 m, while some errors were up to 1.7 m at some locations. This is in contrast when an ideal LOS scenario was considered with sub 1 cm positioning errors. The positioning accuracy when multipath reflections were considered reported a maximum positioning error of 1.85 m, while the maximum positioning error was 23 cm when only the LOS was considered. The work in Tang et al. (2017) reported similar results. Eight different cost metrics for an RSS-based VLP system were evaluated by Plets et al. (2017) under the presence of first-order wall reflections. Multipath reflections had a degrading effect on the performance of the positioning system and the authors reported a nearly linear increase in the positioning error as the wall reflectance coefficient is increased. It should be noted the works in these papers are purely based on simulation but experimental in the literature reported similar effects. Experimental work by Alam et al. (2019) found that the largest positioning errors were caused by in the room were around furniture and near the curtains.

As mentioned previously, OFDM is often employed in VLC systems to mitigate the effect of reflections, The work by Aminikashani et al. (2016) extended this to VLC-based positioning systems. A VLP system utilising OFDM has been

proposed to mitigate the effect of multipath reflections and to provide high data rate transmissions. Reported results achieved a root-mean-square (RMS) error of 0.04 m when OFDM modulation is used while it is 0.43 m when OOK is used. An experimental demonstration of an indoor VLC-based positioning system using OFDMA was presented by Lin et al. (2017) to overcome ICI. Experimental results showed that the proposed method achieved a mean positioning error of 1.68 cm while overcoming the inter-cell interference. The authors noted that the OFDMA-VLC positioning system provides high spectral efficiency with high tolerance against multipath-induced distortion.

Another method to lessen the effect of multipath reflections is the selective selection of only the strongest signals. The method selects the strongest signals, which are usually the closest signals, and excludes the faraway ones that are severely affected by multipath reflections. The use of only the strongest signals has been reported by Gu et al. (2016) and demonstrated that it can reduce the positioning error. The authors also noted that the use of LEDs in a dense layout decreased the effect of multipath reflections. The observation that selecting the strongest signals improved that positioning accuracy has also been reported by Tang et al. (2017).

3.4.4 Multiple Position Estimates

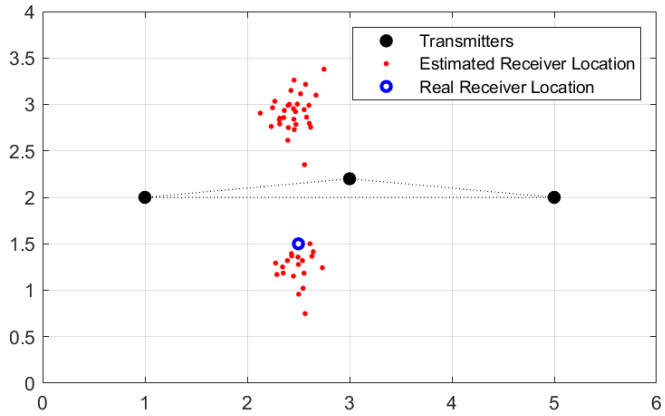

Figure 3.6: A demonstration of the flip-ambiguity effect when the transmitters are placed in a straight or and sometimes even in a semi-straight line. Black denotes the anchor points (LEDs), red denotes the estimated receiver positions, and blue is the real location of the receiver.

With VLP being one of the most promoted areas of VLC, it is important to examine any particulars that can be problematic. Flip-ambiguity in positioning systems occur when the transmitters (anchors) are collinear, or even nearly

collinear (Kannan et al., 2006; Moravek et al., 2012). The placement of the light in a straight line is a design that is generally prevalent in hallways and aisles in warehouses and storage facilities. An example of flip-ambiguity is shown in Figure 3.6. Multiple position estimates were simulated while taking into account fluctuation in the received signal power. The figure shows that the placement of anchors in a collinear fashion causes the positioning algorithm to output possible outcomes on both sides of the room. The presence of noise can also increase the probability of flip ambiguity (Moore et al., 2004).

As discussed previously, this is especially important as it will affect the use of UAVs and UGVs with VLP systems in warehouses and storage facilities. Flip-ambiguity is also relevant in outdoor vehicle VLP systems given the common straight-line placement of streetlights. There is some limited work examining this subject within the general research of positioning systems such as the work by Akcan and Evrendilek (2013), where the authors proposed a heuristic solution that tries to minimise the number of flips in trilateration.

The issue of flip-ambiguity has not been discussed in VLC/VLP systems except for the work by Do and Yoo (2018), where a VLC-based positioning system using LED streetlights has been proposed to be used with a fusion algorithm to solve the problem of collinear LED arrangement. The authors tackle this problem specifically as streetlights are generally placed in a collinear fashion. They further proposed the use of an algorithm that uses two cameras that are placed at different positions in the vehicle to deal with the flip-ambiguity issue. Li et al. (2014) tested a VLP system in different office environments. One of these areas was a corridor with an area of 2 m $\times$ 12 m with five collinear LEDs. Multiple tests were conducted at 60 positions and the authors found that the largest errors were exactly the positions at the two sides of the corridor, suggesting a flip-ambiguity effect. Similarly, Xie et al. (2018) noted that the classic multilateration method cannot be used in a scenario where the LEDs are deployed linearly and proposed the use of their rotating multi-face positioning method to address this problem. Konings et al. (2018) also noted that when luminaires are aligned in a single row, such as in a hallway, then traditional VLP will not function as trilateration schemes will not resolve due to the system only having information from one axis.

The use of lattice-shaped LED layouts also causes multiple position estimates. This issue is not unique to industrial environments but sill occurs in indoor environments. 'Singularities' were investigated by Roa et al. (2007) for indoor positioning systems. The authors highlighted that the regular lattice-shaped configuration on the ceiling is not optimal for location estimation using trilatera-

tion techniques due to the occurring singularities. Alleviating this issue can be done through the use of non-lattice LED configurations. A further look into this issue is discussed in Subsection 4.3.1.

3.4.5 LOS Signal Loss and Blockage

It has been well established that VLC heavily relies on the LOS link, so a clear and uninterrupted path between the transmitter and receiver is imperative. When employing robot arms, a signal loss due to the quick movements of the robot arm is likely to happen. This issue has been well-researched by Fraunhofer Institute for Telecommunications. Experimental work performed by Wilke Berenguer et al. (2018); Berenguer et al. (2017a,b, 2018, 2019) led to the development of an antenna diversity model that consists of placing the receivers around a manufacturing cell to ensure that there will always be a LOS signal. The tests were performed in an industrial environment that is part of BMW's robot testing facility. The cell measures 5 m $\times$ 5.7 m and is surrounded by a metal cage. The measurements were taken along a typical trajectory that has a length of 5 meters, and involved picking up an object Results revealed sudden signal fades up to 20 dB that occur even when the robot arm moves by a few centimetres.

The use of spatial diversity ensures that there is always at least one direct signal connection, meaning that the manufacturing robot arm's process is never interrupted by always having a receiver within the movement range of the robots. This solution may not always be applicable for different uses and layouts especially when considering collaborative robots, colloquially referred to as *cobots*. Robots working alongside humans is one of the key drivers in smart factories and a key concept in Industry 5.0 (Robla-Gómez et al., 2017; Nahavandi, 2019). There could be a risk of the signal being interrupted by an operative if there are several receivers around the robot arms at the same level, something that can be avoided by placing the transmitters/receivers at higher locations or on the ceiling.

3.4.5.1 Dead-Zones in VLP systems

Signal loss is a risk that can also affect VLP systems, especially for receivers such as UAVs as discussed in Subsection 3.3.3. Typically, positioning systems use trilateration or angle-based methods to determine the location of the receiver. This generally requires a signal from three or more spatially distributed

Table 3.3: Simulation parameters.

Parameter	Value
Width $\times$ Length $\times$ Height	25 m $\times$ 15 m $\times$ 8 m
Transmitter's Power	115 W
Number of transmitters	15
Transmitter's separation	5 m
Transmitter's Semi-Angle	45°
Photodetector Area	1 cm^2
Receiver's FOV (half angle)	75° - 80° - 85°

transmitters but the height changes affect the number of transmitters a receiver sees. The loss of a signal from one or more the transmitters due to the signal being outside the FOV of the receiver occurs when the receiver is closer to the light fixtures or ventures to an area outside of the light's beam angle Lam and Little (2018); Almadani et al. (2019b). Additionally, there has been some work that proposed the methods that permit localisation using less than three transmitters by exploiting the angle diversity using multiple receivers (Zhuang et al., 2018).

To demonstrate the occurrence of dead-zones, simulations were carried out in a 20 m $\times$ 15 m $\times$ 8 m warehouse equipped with 15 uniformly distributed light fixtures at the ceiling with a semi-angle of 45°. Three different FOV angles were tested here with a receiver that has an active area of 1 cm^2, and as noted before, the availability of a different number of signals will also be investigated as it differs depending on the localisation system. The system's parameters are summarised in Table 3.3.

Figures 3.7, 3.8, and 3.9 show the 3D coverage area/dead-zones for an aerial receiver with full-FOV values of 150°, 160°, and 170°, respectively. The white area represents the available coverage area while the dark areas are the dead-zone. Dead-zone occurs due to the unavailability of the signals from a second, third, and fourth transmitter LEDs. As can be seen in from figures, there is full room coverage up to a certain height. For a receiver with a full-FOV of 150°, 160°, and 170°, the maximum heights the drone can fly are 5.2 m, 6.2 m and 7.1 m, respectively. Above these heights, the dead-zones start appearing at the corners of the room. The drone can reach a maximum height of 7.1 m, 7.4 m and 7.7 m for the full-FOVs of 150°, 160°, and 170°, respectively, in most parts of the room except at the corners and edges. The results of the coverage simulation are summarised in Table 3.4.

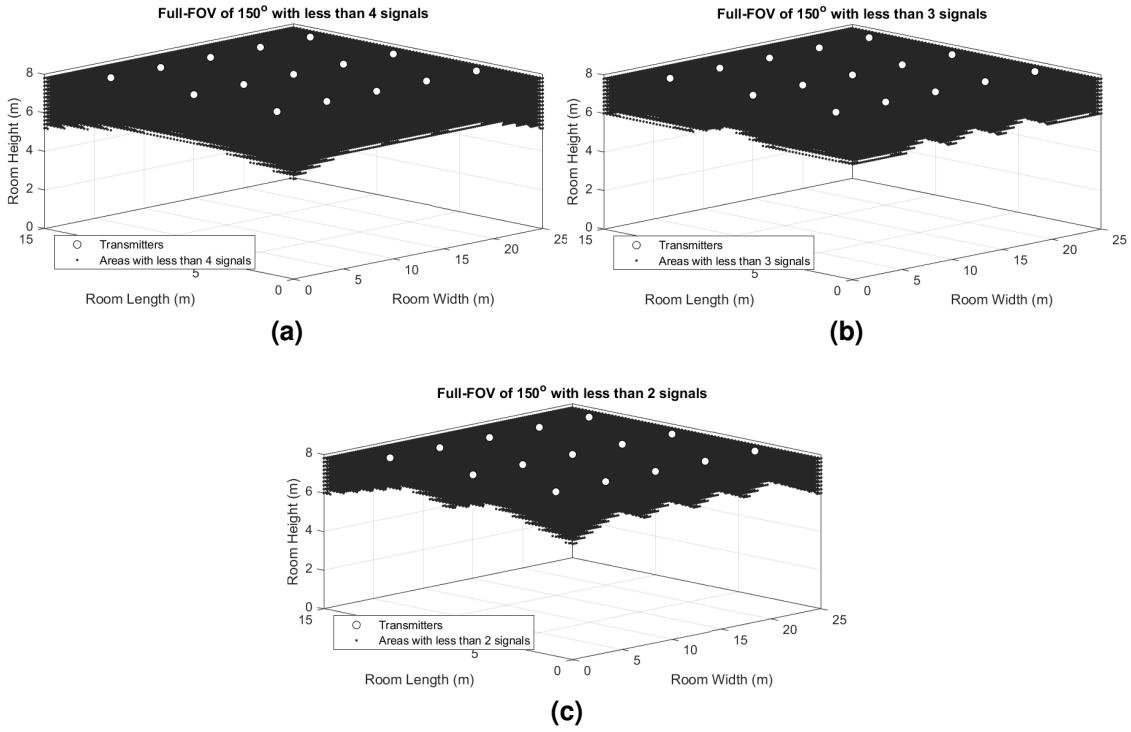

Figure 3.7: Dead-zones for an aerial receiver with a full-FOV of 150° when: (a) there is less than 4 signals; (b) less than 3 signals; (c) less than 2 signals.

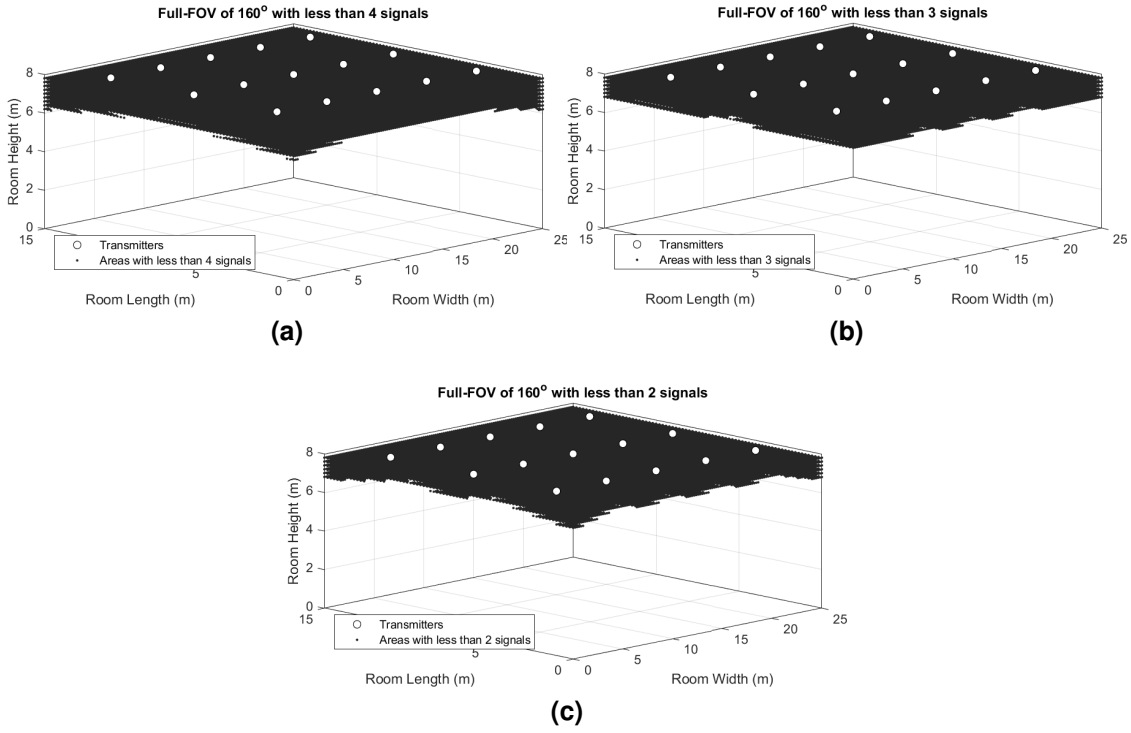

Figure 3.8: Dead-zones for an aerial receiver with a full-FOV of 160° when: (a) there is less than 4 signals; (b) less than 3 signals; (c) less than 2 signals.

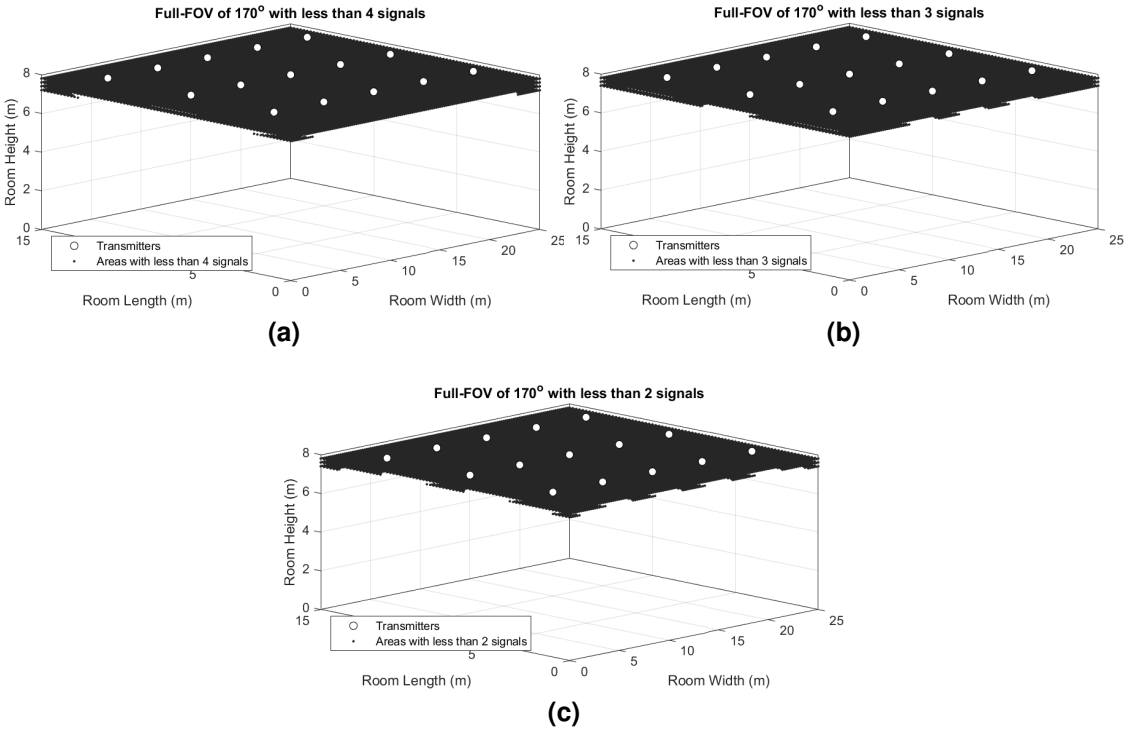

Figure 3.9: Dead-zones for an aerial receiver with a full-FOV of 170° when: (a) there is less than 4 signals; (b) less than 3 signals; (c) less than 2 signals.

Table 3.4: The maximum height a receiver can reach before encountering a dead-zone.

No. of Txs	Location	Receiver's FOV		
		150°	160°	170°
Less than 4	Corners (m)	5.2	6.2	7.1
	Edges (m)	6.0	6.7	7.4
	In-between (m)	7.1	7.4	7.7
Less than 3	Corners (m)	5.9	6.7	7.4
	Edges (m)	6.5	7.0	7.6
	In-between (m)	7.1	7.4	7.7
Less than 2	Corners (m)	5.9	6.7	7.4
	Edges (m)	7.1	7.4	7.7
	In-between (m)	7.4	7.6	7.8

The results clearly indicate the impact of small changes in the FOV on the range of the drone. To enable an aerial receiver to function in these problematic areas, the positioning algorithm can be used with a sensor such as an altimeter or a gyroscope. Mitigating this, in theory, can also be achieved by using a

receiver with a 180° full-FOV. The performance of a 180° FOV receiver that consists of multiple sub-receivers has been studied by Burton et al. (2012) and they have found that the receiver is capable of offering full mobility within a typical home/office environment when compared with a single receiver. Additionally, there has been some limited research examining the use of a fisheye lens that posses an ultra-wide FOV ($\geq$180°). Experiment work by Chen et al. (2015) found that inter-channel interference is alleviated due to the high spatial diversity provided by the fisheye lens-based receiver. The results suggest that the fisheye lens-based imaging receiver is a potential candidate for high-speed VLC applications. The work by Chen et al. (2014) also concluded that fisheye lens-based imaging receiver is a potential candidate for high-performance indoor multiple-input multiple-output (MIMO) VLC applications. However, the use of receivers with an ultra-wide FOV to eliminate dead-zones has not been examined experimentally, nor has the effect of reflections in dead-zones been examined.

3.5 Summary

In this chapter, applications of VLC in industrial settings has been reported and its unique challenges have been examined. The research in this field is still in its early stages. Nevertheless, it demonstrates that there is clearly a place for VLC systems in industrial environments due to the rise of Industry 4.0 and the shortcomings of RF-based systems. The experimental work of a manufacturing cell in collaboration with a car manufacturing company has paved the way for future applications and demonstrated VLC's applicability in real-life industrial applications. The parallel work in VLP systems could also breathe new life into the use of UAVs and UGVs due to the relative simplicity in implementing indoor positioning systems compared with other systems.

Historically, the industrial community has been tentative adopting new technologies. Several factors contribute to this, chiefly, industrial environments have almost no tolerance for downtime. This underscores the importance of having robust communicational links and as such, it should be taken into account for any possible VLC application, even if robustness comes at the expense of high data rates. As with any other technology, experimental work to ensure the system's stability in real-life settings is required before it will be considered by the industry.

In addition, the chapter briefly examined the effect of different ceiling heights on the SNR using two different commercial light fixtures intended for industrial

settings with different beam angles and output powers. Signal fluctuation due to the receiver's mobility was also studied. The results show a 10.4 dB drop in SNR when moving along a selected path under a VLC channel, but a strong signal remains due to the high power of industrial luminaires.

The coverage area for an aerial receiver in an industrial environment was also examined. Dead-zones for positioning algorithms that require the use of two, three, and four transmitters have been simulated for a receiver with different FOV angles. The results demonstrated that the maximum height a drone can reach with a full-FOV of 170° for VLP systems that requires three and four transmitters is 7.7 m, and 7.8 m when requiring two transmitters. The simulations aimed to demonstrate the limitations that flying objects such as drones might encounter based on the receiver's FOV. As mentioned before, this limitation is not exclusive to trilateration methods, as positioning algorithms generally require a certain number of signals to estimate the position.

The discussions in the chapter pointed to a growing potential for mobile receivers in industrial environments. This, however, presents its own sets of challenges such as receiver tilt and an exaggerated effect of multipath reflections. These challenges are examined through simulation in Chapter 4, and experimentally in Chapter 5.

Chapter 4

3D Visible Light Positioning using Received Signal Strength

4.1 Introduction

In this chapter, a novel three-dimensional VLP system using trilateration algorithms with a cost function is proposed and tested for industrial environments. The proposed algorithm uses the received signal strength for estimating the receiver's 3D position without prior knowledge of its height. This reduces the need for additional height sensors used in 3D VLP systems such as a laser or an accelerometer (Lam and Little, 2018; Yasir et al., 2014). The performance of the proposed algorithm in terms of positioning error is evaluated with and without tilting of the receiver, with multipath reflections, and compared by using two different trilateration algorithms. The two compared algorithms are the CMD trilateration algorithm, which is not widely used in the literature, and the widely used linear least squares (LLS) algorithm.

As discussed in Subsection 3.3.3, UAVs are used for different applications such as to perform visual inspections of a variety of indoor and outdoor environments, as they offer a safe and cost-effective way to inspect different heights and hard-to-reach areas, eliminating the need for manual inspections (Jordan et al., 2018). The areas under inspection range from offshore oil rigs, power plants, to facades and buildings. UAVs (or drones) are also used for performing a physical inventory in warehouses. However, the primary challenge is that the drone needs to determine its location in relation to its environment autonomously, which requires control and a positioning system with high accuracy.

Wireless technologies that are currently used for drone localisation are UWB (Benini et al., 2013), ultrasonic (Wu et al., 2017), Bluetooth (Soria et al., 2017), and ZigBee (Ueyama et al., 2014). Almost all of these techniques are sensitive to electromagnetic interference and are based on the highly congested RF spectrum. However, the use of the alternative cost-effective and interference-free technology VLP has not been examined for indoor localisation and tracking of drones. Which is why its examination here is important given the great opportunity provided by the ubiquitous availability of LED lights in homes, offices, and industrial environments.

The majority of existing indoor VLP systems are developed for 2D positioning systems. To have a 3D system, the height of the receiver must be known. Hence, additional sensors are required to estimate the height accurately at the expense of extra hardware and processing power. In the work by Yasir et al. (2014), a 3D positioning system was presented by using the accelerometer and gyroscope to estimate the height. A PSO algorithm was used by Cai et al. (2017) and Zhang et al. (2018). The PSO optimisation algorithm required a minimum of 20 and 40 iterations, respectively, to obtain a final 3D position. Similarly, the use of a modified genetic algorithm showed that 76 iterations were required to obtain a 3D position when four LEDs were used (Chen et al., 2018). A 3D positioning using the RSS and AOA was presented by Yang et al. (2014). However, the proposed algorithm is complex due to the requirement of multiple optical receivers to estimate the AOA. Gu et al. (2014) proposed a method based on previous height estimations, followed by a height adjustment of the location. However, this method was not reliable as the best 2D estimate at the previous height would be different from the actual new height, inducing higher position errors.

Furthermore, the presence of multipath reflections is a major factor in the performance degradation of VLP systems. Gu et al. (2016) analysed the effect of reflections and found that multipath reflections considerably decreased the positioning accuracy, especially around the edges and corners of the room. Tang et al. (2017) reported that the positioning error increased to 1.85 meters when multipath reflections were considered. Another important aspect of drone navigation, and mobile receivers, is the tilt of the receiver, as the drone will not always remain horizontal while flying. Hence, the tilt of a receiver can also affect the positioning accuracy of the VLP system. Experimental results by Jeong et al. (2013) demonstrated a positioning error of 60.4 cm when the receiver was tilted by 30°.

Table 4.1 presents a summary of some of the relevant simulation-based research work. Most of the researched work is in the two-dimensional plane and

Table 4.1: Reported simulation accuracies achieved for VLP systems in the literature using different methods.

Ref.	Method	2D/3D	Area (m)	Accuracy	Notes
Jung et al. (2011)	TDOA	2D	5×5×3	1.8 mm	No noise considered
Naz et al. (2018b)	TDOA	2D	5×5×3	0.13 mm	1 LED w/ multiple PDs arranged circularly
Li et al. (2018)	TDOA-ML	2D	5×5×3	1.66 cm	neural network-based ML method
Trong-Hop Do et al. (2013)	TDOA	2D	5×5×3	3.59 cm	w/ shot, thermal, and reflected light noise
Do and Yoo (2014)	TDOA	2D	5×5×3	3.9 cm	1 ns clock precision
Steendam (2018)	AOA	3D	5×5×2	<10 cm	8 REs with each containing a PD and aperture
Zhang et al. (2018)	RSS / PSO	3D	3×3×4	<3.55 cm	Over multiple iterations
Jung et al. (2013)	RSSR	2D	5×5×3	$\leqslant$3.65 cm	Receiver is on a fixed, known height
Wu et al. (2018)	RSS / DE	3D	4×4×6	0.69 cm	DE algorithm is used to calculate z

a variation in the positioning accuracy can be seen with some work reporting accuracies of less than 1 cm, the rest have accuracies less than 10 cm. Another point worth mentioning is that the area under consideration is generally the popular 5 m $\times$ 5 m $\times$ 3 m room. This further highlight the gap in considering large industrial environments.

The proposed algorithm in this chapter performs a full 3D positioning, while only requiring measured RSS as input without any additional sensors. In the proposed method, the distances for different heights between the LEDs and the drone are obtained using the RSS. Then, the algorithm iterates through different heights and outputs several candidates for the receiver's position using the trilateration algorithms. Finally, the 3D position of the receiver is determined by minimising the cost function to find the receiver's height. This is the first use of the CMD in a VLP system. The performance of the proposed CMD based VLP algorithm is also studied for different tilt angles of the receiver and under the presence of multipath reflections. The positioning error of the CMD algorithm is then compared with the benchmark LLS trilateration algorithm.

The remainder of the chapter is organised as follows. Section 4.2 describes the VLC system model, positioning algorithms along with the cost function, and the NLOS CIR ray-tracing method. Results and discussions are presented in Section 4.3. The summary is presented in Section 4.4.

4.2 Methodology

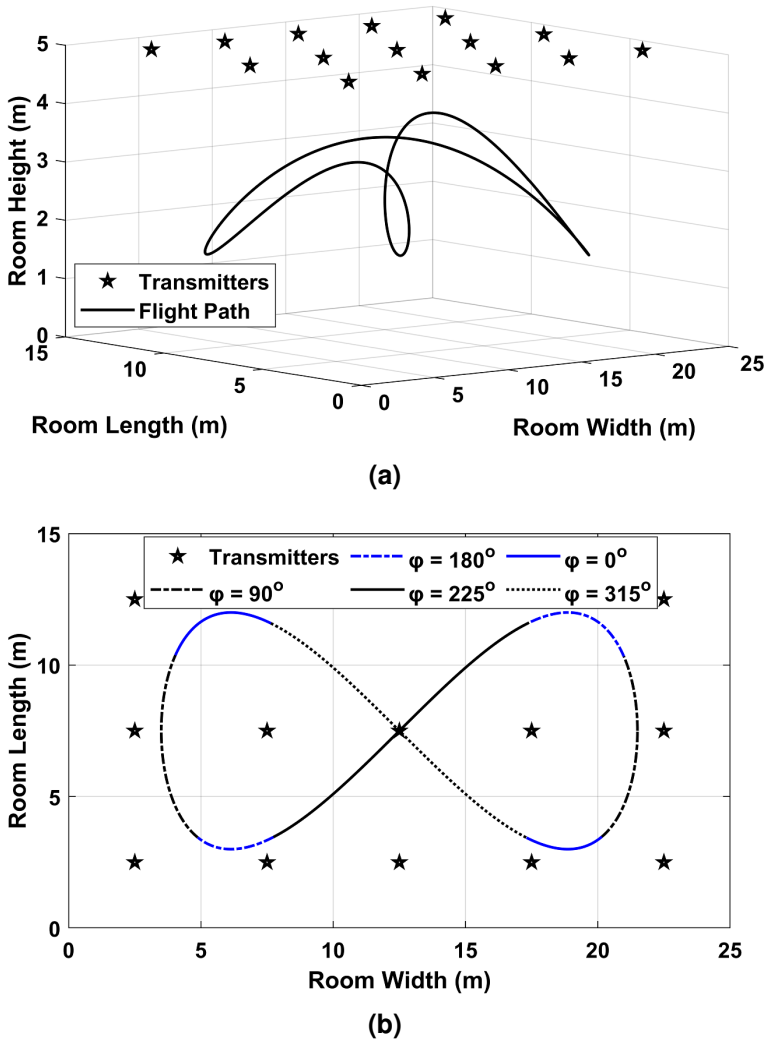

Figure 4.1: (a) The evaluated industrial environment showing the location of the LED light fixtures and the flight path of the drone; (b) a top view of the evaluated environment showing the azimuthal angles (rotation) φ along the entire path of the drone's flight.

4.2.1 VLC System Model

Figure 4.1 (a) shows the considered environment with the flight path of the drone. It is a typical industrial environment measuring 25 m $\times$ 15 m $\times$ 5 m with $N = 15$ uniformly distributed LED-based light fixtures and 5 meters spacing between them. The N LED light fixtures were placed at a fixed height (h_{LED}), with coordinates (x_i, y_i, h_{LED}), where $i = 1 \ldots N$. A receiver with an active area of A_{pd} is located at the unknown location (x, y, z). Other trajectories including rectangular and elliptical were considered for the flight path of the drone. However, after extensive simulations, the infinity (∞) shaped path was selected for further simulation, as shown in Figure 4.1. This is because the selected path covered

multiple heights for the receiver within the proposed industrial environment. Additionally, the (∞) shaped path was also adopted by Beul et al. (2018) for testing their aerial vehicle.

It is assumed that the receiver is able to distinguish signals from different transmitters using time-division multiplexing and that the transmitters are synchronised (Gu et al., 2016). For typical LEDs with Lambertian radiation order m, the received optical power P_{ri} from the i^{th} LED transmitter is given by (Kahn and Barry, 1997):

$$P_{ri} = \begin{cases} P_{ti}\frac{(m+1)A_{pd}}{2\pi d_i^2}\cos^m(\alpha)\cos(\beta), & \beta \leq \psi_{pd} \\ 0, & \beta > \psi_{pd} \end{cases} \tag{4.1}$$

where P_{ti} is the transmitter's power from the i^{th} LED transmitter, d_i is the distance between the i^{th} LED transmitter and the receiver, α is the angle of irradiance, β is the angle of incidence and ψ_{pd} is the FOV of the photodiode receiver, as shown in Figure 4.2 (a). Moreover, by assuming that the N LED transmitters and receiver are horizontally oriented and parallel to each other, then:

$$cos(\alpha) = cos(\beta) = \frac{h_{LED} - z}{d_i} = \frac{h}{d_i} \tag{4.2}$$

where h_{LED} is the height of the LEDs and z is the height of the receiver. $\widehat{d}_i$ can be estimated from the received signal power P_{ri} as (Plets et al., 2017):

$$\widehat{d}_i = \sqrt[m+3]{\frac{(m+1)\,A_{pd}P_t h_i^{m+1}}{2\pi P_{ri}}} \tag{4.3}$$

where h_i is the unknown vertical height difference between LED$_i$ and the receiver. As such, $\widehat{d}_i$ cannot be directly determined from P_{ri} due to the angle-dependent behaviour of the transmitter. This means that some locations have the same received power values P_{ri} at different distances from the transmitter and at different heights. Due to this, a set of estimated distances $\widehat{d}_i$ are generated for different receiver heights z ranging from a minimum height h_{min} and maximum height $h_{max} \leq h_{LED}$ with height increments R_h of 1 mm.

The assumption that the transmitter and receiver planes are parallel to each other might not always hold for a mobile receiver, especially in the case of a moving receiver. In this case, if the receiver tilts, then the angle of incidence is

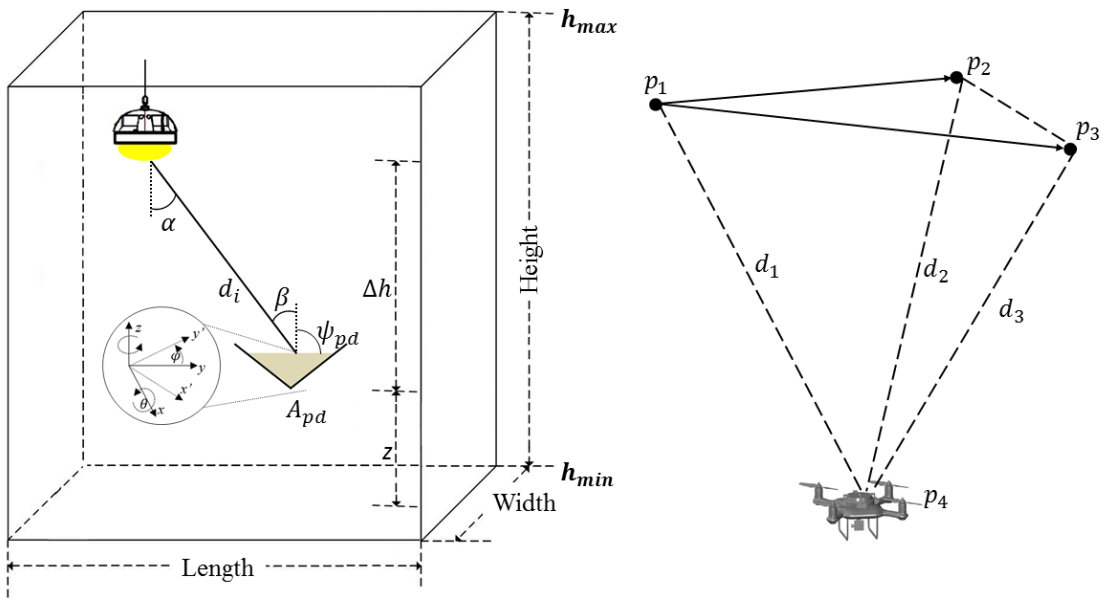

Figure 4.2: (a) The VLP system block diagram; (b) the schematic diagram for the CMD trilateration problem and its parameters.

determined by (Yang et al., 2014):

$$\cos\left(\beta_{tilt}\right) = \frac{(x - x_i)\cos\varphi\,\sin\theta + (y - y_i)\sin\varphi\,\sin\theta + (z - z_i)\cos\theta}{d} \tag{4.4}$$

where $z_i = h_{LED}$ and θ is the receiver's tilting angle, which is the angle difference between the normal vector of the xy-plane and the normal vector of the receiver. φ is the azimuthal rotation angle, which is the angle difference between the x-axis and the orthogonal projection of the receiver's normal vector on the xy-plane.

The received signal in (4.1) can be affected by shot and thermal noises. Artificial lights and sunlight have a direct impact on the shot noise, resulting in a larger background current. It is assumed that there is an indirect sunlight exposure with a background current I_{bg} of 740 µA (Moreira et al., 1997). The shot noise is calculated using (Kahn and Barry, 1997):

$$\sigma^2_{shot} = 2qR_rP_rB + 2qI_{bg}I_2B \tag{4.5}$$

where q is the electronic charge, R_r is the receiver's responsivity, B is the electrical bandwidth, I_{bg} is the background radiation, and I_2 is the noise bandwidth

factor. The thermal noise is given by:

$$\sigma^2_{thermal} = \frac{8\pi\kappa T_k}{G}\eta A_{pd} I_2 B^2 + \frac{16\pi\kappa T_k \Gamma}{g_m}\eta^2 A^2_{pd} I_3 B^3 \tag{4.6}$$

where κ is Boltzmann's constant, T_k is the absolute temperature, G is the open-loop voltage gain, η is the fixed capacitance of the photodetector per unit area, Γ is the FET channel noise factor, g_m is the FET trans-conductance, and I_3 is the noise bandwidth factor. The total noise variance is calculated through the sum of the two noise sources by:

$$\sigma^2_{noise} = \sigma^2_{shot} + \sigma^2_{thermal} \tag{4.7}$$

The noise parameter values have been discussed before and are listed in Table 2.1. After calculating the noise values, the SNR can be calculated using:

$$SNR_i(dB) = 10log_{10}\frac{(R_r P_{ri})^2}{\sigma^2_{noise}} \tag{4.8}$$

The main simulation parameters are summarised in Table 4.2.

Table 4.2: Summary of the system parameters.

Parameter	**Value**
Room Width $\times$ Length $\times$ Height	25 m $\times$ 15 m $\times$ 5 m
Walls' Reflectivity	0.17
Floor's Reflectivity	0.34
Transmitter's Power, P_t	80 W
Transmitter's Semi-Angle, α	45°
Receiver's Height, z	1.5–3.5 m
Photodetector Area, A_{pd}	1 cm^2
Receiver's FOV (Half Angle), ψ_{pd}	80°
Receiver's Responsivity, R_r	0.54 A/W
Background Current, I_{bg}	740 µA
Bandwidth, B	10 MHz

4.2.2 Positioning Algorithms

The positioning is performed by taking into account each set of estimated distances $\widehat{d}_i(i = 1, ..., N)$ using (4.3) for different heights of the receiver. Then, the unknown 3D position is estimated by using the CMD and LLS algorithms and minimising the cost function for the set of heights ranging from a minimum height h_{min} to a maximum height h_{max}.

4.2.2.1 Cayley–Menger Determinant

The proposed method extends the use of the CMD trilateration algorithm by using it with a cost function in VLP systems, which enables the estimation of a receiver's 3D position without prior knowledge of its height. Figure 4.2 (b) shows the position of three transmitters, $p1$, $p2$ and $p3$, with $p4$ being the unknown drone location. The CMD algorithm only requires three transmitters to estimate a location; therefore, the corresponding signals from the three strongest (mostly the nearest) LEDs are taken into account.

The Cayley–Menger bideterminant of two sequences of n points $[p_1, p_2, ..., p_n]$ and $[q_1, q_2, ..., q_n]$ is defined as (Thomas and Ros, 2005):

$$D(p_1, ..., p_n; q_1, ..., q_n) = 2(\frac{-1}{2})^n \begin{vmatrix} 0 & 1 & 1 & 1 & 1 \\ 1 & D(p_1, q_1) & D(p_1, q_2) & \cdots & D(p_1, q_n) \\ 1 & D(p_2, q_1) & D(p_2, q_2) & \cdots & D(p_2, q_n) \\ \vdots & \vdots & \vdots & \ddots & \vdots \\ 1 & D(p_n, q_1) & D(p_n, q_2) & \cdots & D(p_n, q_n) \end{vmatrix} \quad (4.9)$$

where $D(p_i, q_j)$ is the squared distance between points p_i and q_j. When two sequences of points are the same (i.e., $p_i = q_i$), then $D(p_1, ..., p_n;\ q_1, ..., q_n)$ is denoted by $D(p_1, ..., p_n)$ and is simply called CMD (Thomas and Ros, 2005). So (4.9) becomes:

$$D(p_1, p_2, p_3, p_4) = (\frac{1}{8}) \begin{vmatrix} 0 & 1 & 1 & 1 & 1 \\ 1 & 0 & D(p_1, p_2) & D(p_1, p_3) & D(p_1, p_4) \\ 1 & D(p1, p_2) & 0 & D(p_2, p_3) & D(p_2, p_4) \\ 1 & D(p_1, p_3) & D(p_2, p_3) & 0 & D(p_3, p_4) \\ 1 & D(p_1, p_4) & D(p_2, p_4) & D(p_3, p_4) & 0 \end{vmatrix} \quad (4.10)$$

with p_4 is the unknown location of the drone, $D(p_4, p_1)$, $D(p_4, p_2)$ and $D(p_4, p_3)$ are

the distances $\widehat{d_1}$, $\widehat{d_2}$ and $\widehat{d_3}$ that are computed from the RSS for a given receiver height. It is then possible to calculate the unknown position of the receiver (p_4) with respect to three known transmitter coordinates (p_1, p_2, p_3) using (Thomas and Ros, 2005):

$$p_4 = p_1 + k_1 v_1 + k_2 v_2 \pm k_3 (v_1 v_2) \tag{4.11}$$

where $v_1 = p_2 - p_1$, $v_2 = p_3 - p_1$ and the $\pm$ sign accounts for the two mirror symmetric locations with respect to the base plane, but given the impossibility of a receiver being above the light fixtures, one of the possibilities can be ignored. k_1, k_2 and k_3 are given by:

$$k_1 = -\frac{D(p_1, p_2, p_3; p_1, p_3, p_4)}{D(p_1, p_2, p_3)}, k_2 = \frac{D(p_1, p_2, p_3; p_1, p_2, p_4)}{D(p_1, p_2, p_3)}, k_3 = \frac{\sqrt{D(p_1, p_2, p_3, p_4)}}{D(p_1, p_2, p_3)}$$

The CMD algorithm then outputs $(\widehat{x}, \widehat{y}, \widehat{z})$ for each of the generated possible heights Δh, and is then used by the cost function.

4.2.2.2 Linear Least Square

As the correct distances cannot be estimated directly without knowing the receiver's height, 2D trilateration using LLS is performed for each of the generated heights, Δh. The horizontal distance between LED$_i$ and the receiver is given by (Gu et al., 2016):

$$d_i^2(h) = (x_i - x)^2 + (y_i - y)^2 = x^2 - 2xx_i + x_i^2 + y^2 - 2yy_i + y_i^2 \tag{4.12}$$

After eliminating the quadratic terms in x^2 and y^2 by subtracting d_N^2 from d_i^2, $N-1$ equations are obtained ($i = 1 \ldots N-1$):

$$d_i^2(h) - d_N^2(h) = -2x(x_i - x_N) + x_i^2 - x_N^2 - 2y(y_i - y_N) + y_i^2 - y_N^2 \tag{4.13}$$

These equations can be expressed in a matrix form as $b = A\mathbf{x}$, where:

$$b = \frac{1}{2} \begin{bmatrix} d_1^2(h) - x_1^2 - y_1^2 - d_N^2(h) + x_N^2 + y_N^2 \\ d_2^2(h) - x_2^2 - y_2^2 - d_N^2(h) + x_N^2 + y_N^2 \\ \vdots \\ d_{N-1}^2(h) - x_{N-1}^2 - y_{N-1}^2 - d_N^2(h) + x_N^2 + y_N^2 \end{bmatrix} \tag{4.14}$$

$$A = \begin{bmatrix} x_1 - x_N & y_1 - y_N \\ x_2 - x_N & y_2 - y_N \\ \vdots & \vdots \\ x_{N-1} - x_N & y_{N-1} - y_N \end{bmatrix}, \ \mathbf{x} = \begin{bmatrix} x \\ y \end{bmatrix} \tag{4.15}$$

The algorithm then outputs the estimated position $\begin{bmatrix} \widehat{x} \\ \widehat{y} \end{bmatrix}$ for each of the assumed possible heights h using the Moore–Penrose pseudo-inverse of A:

$$\mathbf{x} = (A^T A)^{-1} A^T b \tag{4.16}$$

After that, minimisation is achieved by using (4.17) in order to find the most probable 3D position, as in our previous work in Plets et al. (2019). Algorithm 4.1 summarises the iterative cost function trilateration approach with LLS.

4.2.2.3 Cost function

Once all of the possible receiver locations have been generated using (4.11) and (4.16) for both algorithms for each of the assumed heights between a minimum height (h_{min}), and maximal height with a height interval resolution, the final most probable 3D position of the receiver is found at the minimum of the cost function $C(h)$ as:

$$C(h) = \frac{1}{N} \sum_{i=1}^{N} [\widehat{d}_i(h) - \sqrt{(\widehat{x}(h) - x_i)^2 + (\widehat{y}(h) - y_i)^2 + (\widehat{z}(h) - z_i)^2}]^2 \tag{4.17}$$

where $C(h)$ is the average squared error between the estimated distances $\widehat{d}_i(h)$ using (4.3) and the distances of the estimated location $(\widehat{x}(h), \widehat{y}(h), \widehat{z}(h))$ using (4.11) and (4.16). Given that the generated possible height range is between a certain number of values that can be specified by the user (e.g. the floor (h_{min}) and the ceiling (h_{max})). Algorithm 4.1 details that working of the method. The convergence of the cost function will always occur in the room, even if it is a wrong estimate. It should be noted that the cost function minimisation described above can be used in conjunction with any 2D trilateration algorithm (Plets et al., 2019).

After estimating the position of the unknown receiver, the final estimated position is compared with the actual position of the receiver (x, y, z) to find the

positioning error using:

$$D_{error} = \sqrt{(\widehat{x} - x)^2 + (\widehat{y} - y)^2 + (\widehat{z} - z)^2} \tag{4.18}$$

where $z = h$.

Algorithm 4.1: Iterative cost function trilateration approach with LLS.

Input: measured P_{ri} values, A_{pd}, m, P_t, and LED settings
Output: estimated location $loc_{est}(x, y, z)$

Initialisation: $Cost_{min} = max\_value, loc_{est} = null$
for $(h = h_{min} : R_h : h_{max})$ **do**
  $h = h_{LED} - h$
  calculate $\hat{d}_i(h)$ based on (4.3) for $i = 1 \dots N$
  calculate $[\ \hat{x}(h), \hat{y}(h)\ ]$ based on the insertion of $\hat{d}_i(h)$ in (4.16)
  calculate cost function C(h) of (4.17) and update $Cost_{min}$:
  if $(C(h) < Cost_{min})$ **then**
    $Cost_{min} = C(h); loc_{est} = (\hat{x}(h), \hat{y}(h), h)$
  end
end

4.2.3 Monte Carlo Method for NLOS CIR Calculation

To evaluate the effect of reflections, the ray-tracing Monte Carlo method outlined by Lopez-Hernandez et al. (2000) is adopted. The method propagates rays at random directions that are traced in each Monte Carlo iteration. The first step is creating an empty vector that keeps a record of the received optical power at time instant t, that is initialised with a maximum delay of t_{max}. $\hat{P}_{opt}$ is initialised with a value of 1 and is used to record the optical power loss in the propagation. $\hat{\tau}$ is initialised with a value of zero and is used to record the time that the propagation time for each ray has experienced. By selecting a significant number of light rays, repeating this tracing a large number of times results in a stable CIR result. The ray-tracing Monte Carlo method is summarised in Algorithm 4.2. Multiple rays are generated at each LED position with a distribution probability equal to the emission profile, which is Lambertian is this case. The total emittance power is divided by the total number of rays, then when a ray impinges on a wall or ceiling, the point where it reaches the obstacle is converted in a new optical source and a new ray is generated from that point. This process continues until the time of flight counted from the generation on the emitter reaches the maximum time to simulate (t_{max}). For each ray that bounces from one point to the next, the propagation distance is calculated, and the transmission time t is updated. Also, after every reflection, the power of the ray is reduced by the reflection coefficient

of the surface ρ as:

$$\hat{P}_{opt} = \rho \hat{P}_{opt} \tag{4.19}$$

where ρ is the reflectance coefficient of the surface. Then the power contribution to the CIR optical power vector from the current point is updated from each randomly emitted light ray from the LEDs.

Algorithm 4.2: Ray-tracing CIR simulation with Monte Carlo method. Adapted from Lopez-Hernandez et al. (2000).

Begin
  Generate a new ray $(P_{opt,h}(t) = 0)$
  while $(\hat{\tau} < t_{max})$ **do**
    Propagate ray until any obstacle $(\hat{\tau} \longleftarrow \hat{\tau} + d/c)$
    Reduce power using the reflection coefficient $(\hat{P}_{opt} \longleftarrow \rho \hat{P}_{opt})$
    Calculate the contribution from that point to the receiver
    Generate a light ray from the new point
  end
  Repeat steps 2 and 3 for a number of rays
end

4.2.4 Room Analysis

It is important to check the validity of the selected transmitters and test path before proceeding with any analysis. As such, an illumination simulation is first performed followed by an examination of the dead-zones in the room.

4.2.4.1 Illumination Levels

The minimum illumination requirement for industrial applications and typical workspaces for iron and steelwork with continuous manual labour is 200 lx based on European standards (de Normalisation, Comité Européen, 2002). To ensure that these required illumination levels and coverage are met, simulations were performed using DIALux® lighting design software (DIAL). The software allows the selection of different light fixtures from various light manufacturers for the design of optimum illumination levels. It also allows the selection of different types of surfaces that are made from a range of materials for indoor applications.

Figure 4.3 shows the illumination levels for the proposed industrial environment with a large conveyor belt placed in the middle of the factory floor. OSRAM's PrevaLight High Bay LED based light fixtures with a power of 80 W and

a 45° semi-angle of divergence are used. These luminaires are suitable for industrial applications as they offer high power and wide beam distribution for a consistent coverage area that is typical in industrial environments (Almadani et al., 2018).

The floor material is considered to be fine concrete and has a reflection factor of 34%, and all the walls are red bricks with a reflection factor of 17%. The reflectivity coefficients were adopted from DIALux® software. Simulation results show that an average illumination of 270 lux is achieved around the entire area at the working plane height of 0.8 meters. This verifies that the selected light fixtures meet the minimum required illumination levels specified by the European standards and are suitable for industrial applications.

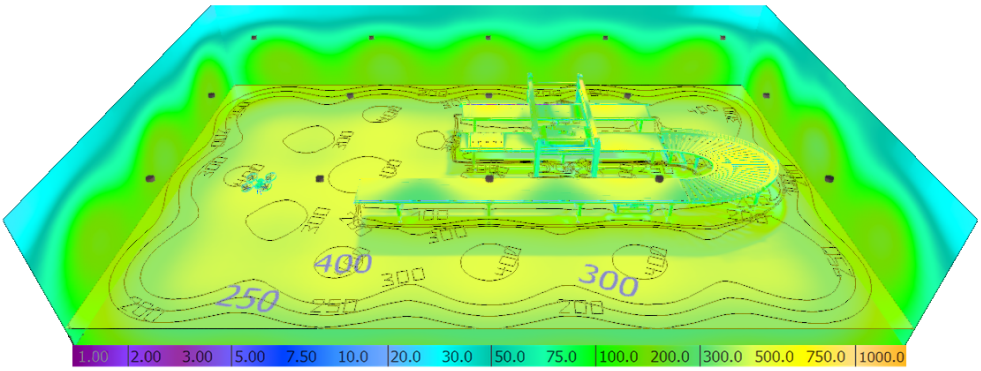

Figure 4.3: Illumination levels for the selected environment under consideration.

4.2.4.2 Dead-Zone Areas

The possibility of the receiver losing a LOS signal that is needed for positioning has been discussed in the previous chapter. To check if the receiver's path would take it into any problematic areas, an examination of the environment shown in Figure 4.1. For the majority of trilateration algorithms, as well the ones used in this chapter, a minimum of three signals are required in order to calculate the receiver's positioning. This requirement was tested for within the room with 10 cm intervals. Figure 4.4 (a) shows a general view of the room where the black areas represent areas that would receive less than three signal. A better side-view od the path's height in relation and the dead-zones is shown in Figure 4.4 (b). The first instance of a dead-zone occurs at a height of 3.7 meters at the corners, while the first instance at the edges of the room occurs at a height of 4 meters. The occurrence of a dead-zone throughout the room is highly dependable on the light layout and whether it is densely or sparsely. Figure 4.4 (c) shows a more concentrated look into the troublesome dead-zone areas. It can be seen that the

areas where an aerial receiver would encounter issues shrink with the height as the receiver will have fewer signals within its sight. Areas in the centre of the room with problematic locations start at a height of 4.1 meters and progressively increases until 4.3 meters, after that the entire plane would have less than three LOS signals. The aerial receiver would not experience any issues as most of the test path travels around the centre, especially as the maximum height the receiver climbs is 3.5 meters.

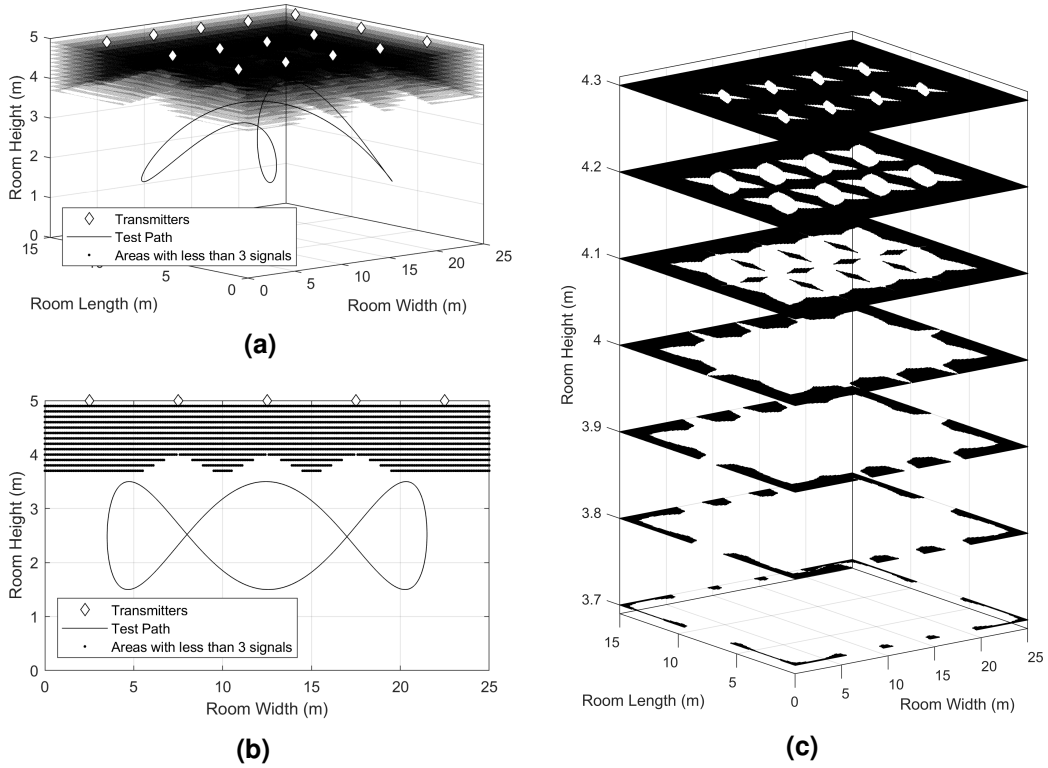

Figure 4.4: (a) A general view of dead-zone areas in the room; (b) A side-view of the dead-zones; (c) a closer look into the maximum heights of the dead-zones.

4.3 Results and Discussion

The performance of the proposed CMD algorithm was evaluated in terms of positioning error for a typical industrial deployment, adhering to the standardised illumination levels, by considering: (i) normal line-of-sight for an untilted receiver, (ii) different tilt angles of the receiver and (iii) multipath reflections.

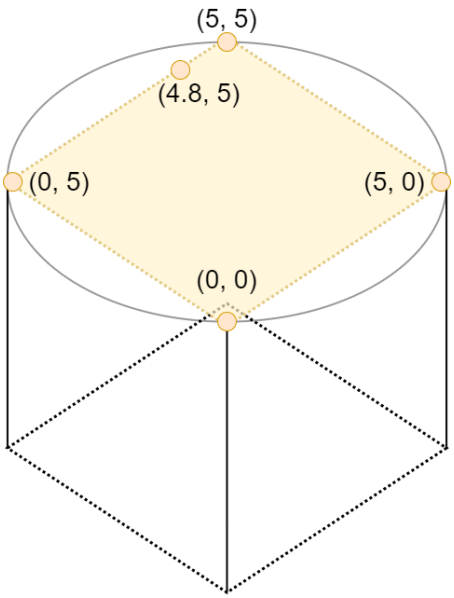

Figure 4.5: The coordinates of the LEDs for the two considered layouts.

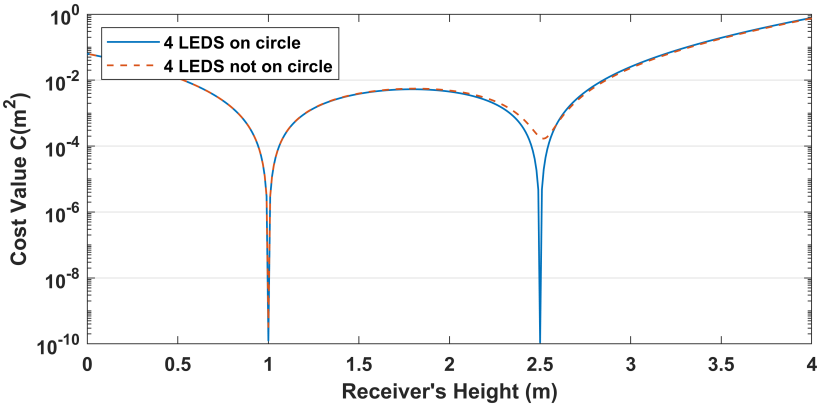

Figure 4.6: Cost function for a receiver placed at (0.5, 2.5, 1).

4.3.1 3D Position Ambiguity in a Square Configuration

The work performed by Plets et al. (2019) showed that location estimations suffer from a possible ambiguity when the four LEDs are mounted in a square shape, or when the fourth LED is located on the circle formed by the other three LEDs, as can be seen in Figure 4.5. To demonstrate this effect, a 5 m $\times$ 5 m $\times$ 5 m room with two different LED configuration is studied here. The first LED layout is arranged in a square-shaped configuration as adopted by many research papers. The second layout is nearly identical except that one of the LEDs is shifted by 0.2 meters, as shown in Figure 4.5. Figure 4.6 shows the cost function when the receiver's location is (0.5, 2.5, 1) with all of the LEDs on the same circle. The results show the cost function's height estimation minimises at a receiver height of 1 m and also at a height of 2.5 m, leading to another 3D location estimation at (1.25, 2.5, 2.5), as shown in Figure 4.7.

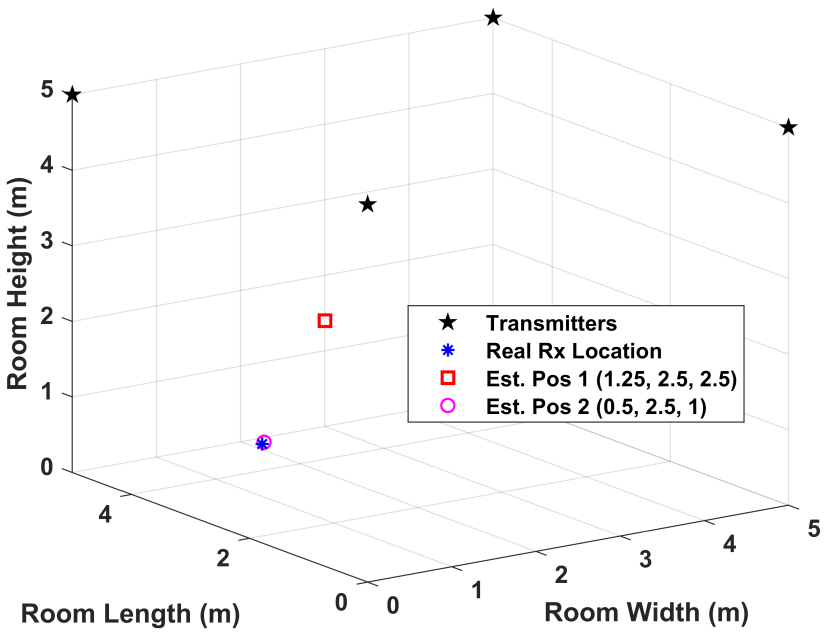

Figure 4.7: A view of the room with the locations of the transmitters the receiver, and the two receiver 3D estimations.

A closer look into the received power from each LED helps in explaining the reason. Due to the radiation pattern's geometrical properties, these two locations (0.5, 2.5, 1) and (1.25, 2.5, 2.5), have exactly the same values of received powers as shown in Figure 4.8. This ambiguity can be resolved through two ways as was examined by Plets et al. (2019), the first is through the use of a fourth LED that is not on the same circle formed by the other LEDs. This has led to the recommendation of a star-shaped layout (or any non-lattice shaped layout) that resolves the ambiguity (Plets et al., 2019). It should be noted that any other non-lattice LED layout would also work as it would make each measurement point in the room unique without a duplicate. To demonstrate this, the simulation was repeated with the four LEDs not on the same circle. Figure 4.6 shows the cost function becoming a zero only at a height of 1 m, resolving the ambiguity. The second method that resolves the ambiguity issue is by substituting one of the LEDs with another LED that has different characteristics than the other three, such as different m values. However, an LED configuration with different m values for different LEDs is not preferred given lighting conditions. Additionally, the inclusion of more than four LEDs resolves the ambiguity as well.

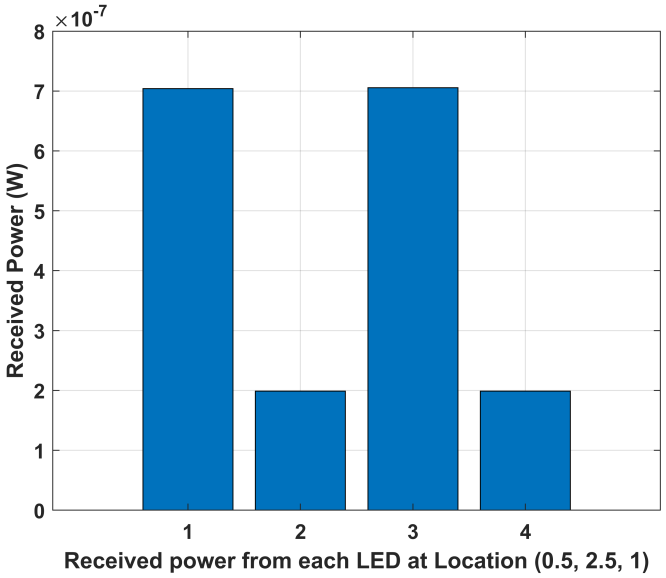

Figure 4.8: The received power from each LED by the receiver located at (0.5, 2.5, 1).

To further illustrate this point, a measurement point was taken every 10 cm in the room and compared with the other test points in the room. Figure 4.9 (a) demonstrates a 3D view of the grid measurement points, duplicated points are in red and every duplicated point has an equivalent identical match with the same received signal power from each LED at different coordinates.

The lattice layout of LEDs is the most used and preferred design due to its uniformity in providing illumination. It is also the most widely used design in VLP literature along with the commonly adopted room design of 5 m $\times$ 5 m $\times$ 3 m. However, lattice-shaped LED layouts suffer from ambiguities, or singularities, due to some measurement points having identical measurements elsewhere in the room. Since the received power equation is dependent on 'incidence angle', this means that there are locations at different coordinates (at different heights) that lead to the same received power measurements. Figure 4.9 (b) shows a top view of the duplicated points and it can be observed that each quadrant is essentially mirrored due to the symmetry of the LED layout. These simulations demonstrate that regular lattice-shaped LED layouts would be problematic for indoor three-dimensional positioning systems, whether they are fingerprinting VLP systems or trilateration-based.

This issue has not been previously looked into for VLP systems but has been investigated for indoor positioning systems in general by Roa et al. (2007). The authors highlighted that the regular lattice-shaped configuration on the ceiling is not optimal for location estimation using trilateration techniques due to the occurring singularities. To avoid any duplicity, then a non-lattice shaped LED configu-

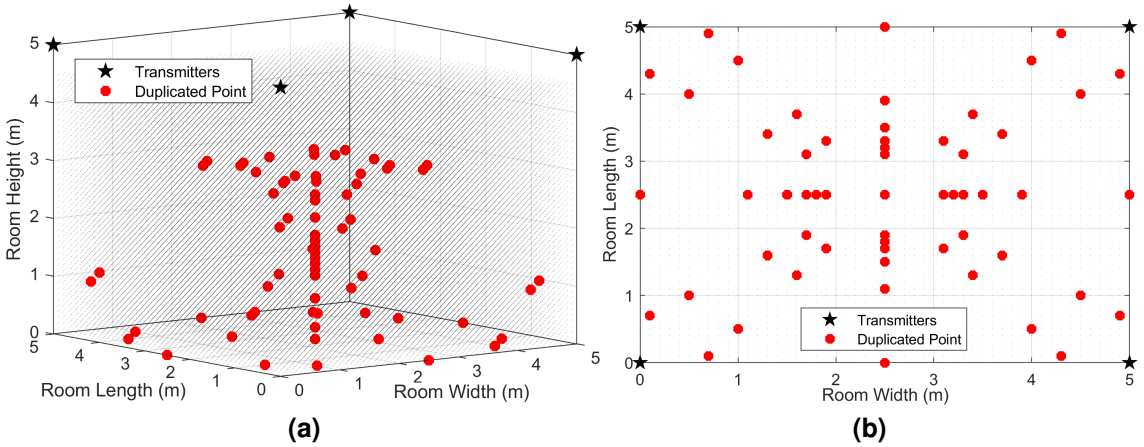

Figure 4.9: (a) A view of the duplicated points in the room; (b) A top view demonstrating the duplicated points.

ration would be used. The number of duplicated in this simulation is dependant on the rounding of decimal points of the received power (rounded to 4 decimal points here) and it increases if less than 4 decimal points are used. Moreover, simulations do not have signal fluctuations unlike experimental implementations. Fluctuations of the received power would induce even more duplicate points. The experimental work by Lv et al. (2017) had measurements with a fluctuation amplitude reaching up to 38% of the average.

In this chapter's simulation analysis, the ambiguity problem does not arise due to the number of LEDs used to cover the large industrial area. However, it is something that should be taken into consideration due to the standard design of rooms with LEDs arranged in a lattice-shaped layout. The issue does arise in the experimental part of the thesis, Chapter 5, in which the performance of the 3D VLP system is performed in a room with 'Square' and 'Star' layouts. To mitigate any position ambiguities, then any layout of the transmitters that would make every single point in the room unique would be sufficient to alleviate this issue.

4.3.2 Positioning Accuracy for Line-of-Sight Reception with an Untilted Receiver

The performance of the algorithm was first evaluated to investigate the effect of tilt on the height estimation using the RSS and the cost function for a position when the receiver was at (10, 6, 2). Figure 4.10 shows the value of the cost function as a function of the receiver's height with and without the effect of tilt for

both the CMD and LLS algorithms.

The result shows that without tilt, the cost function minimised at h = 2 m for CMD and LLS, i.e., the estimated height of the receiver and the actual height were the same. This verified that the estimated height was very precise due to the high SNR values (>34 dB) using (4.8. However, for a tilt angle, $\theta = 5^{\circ}$, the estimated height was 1.82 m when the CMD algorithm was used and 1.89 m when using the LLS algorithm. This shows the adverse effect of tilt on the estimation of height h using RSS.

The flight path shown in Figure 4.1 is considered here. The path consists of 500 points and goes around a manufacturing setting. The selected path takes the drone around most of the room with varying heights ranging from 1.5 to 3.5 meters. The estimated SNR values for the selected flight path ranged from a maximum of 82.8 dB to 19.2 dB when the drone was at (12.5, 7.5, 3.5), which was directly under the LED light fixture in the centre of the room; see Figure 4.1 (b). Note that these high SNR values for VLP were due to the high power LEDs and the adherence to the minimum illumination constraint (Fath and Haas, 2013; Al-Kinani et al., 2017; Zeng et al., 2008).

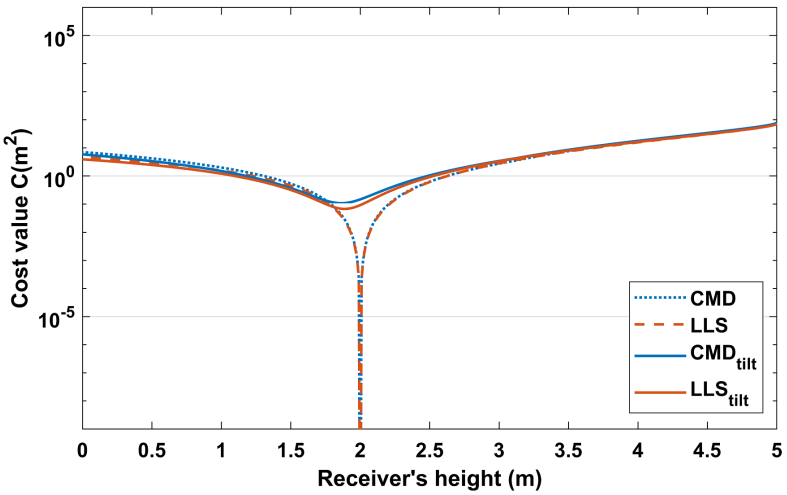

Figure 4.10: Cost function showing the minimum at the receiver height when the receivers are parallel and tilted at an angle of $\theta = 5^{\circ}$.

Figure 4.11 shows the cumulative distribution function (CDF) of the positioning errors for the 500 points. The positioning errors along the path were evaluated using (4.18). The results in Figure 4.11 show small positioning errors and high accuracy, which is similar to reported simulation results (Luo et al., 2017). It can be observed that around 80% of the points had a positioning error of less than 0.78 cm for CMD and 0.94 cm for LLS. Half of the errors (50%) using CMD and LLS were below 0.42 cm and 0.52 cm, respectively. Due to the fact that

LLS used all of the received signals including signals from far-away LEDs, SNR values as low as 1.04 dB were measured at some locations. This can introduce higher positioning errors than the CMD algorithm, which requires only three LED transmitters. The CMD outperformed the LLS algorithm by an average of 14%, and the median was improved by 23%. A breakdown of the errors for the three different axes is shown in the inset of Figure 4.11. The majority (57.7%) of the positioning errors using CMD were comprised of vertical error (z-axis), while the x- and y-axis errors were 19.6% and 22.7%, respectively. However, the majority of the error when using the LLS method was mostly horizontal error with 41.6% from the y-axis and 31.2% from the x-axis. Contrarily, the z-axis was the smallest contributor with around 27.2% of the total positioning error.

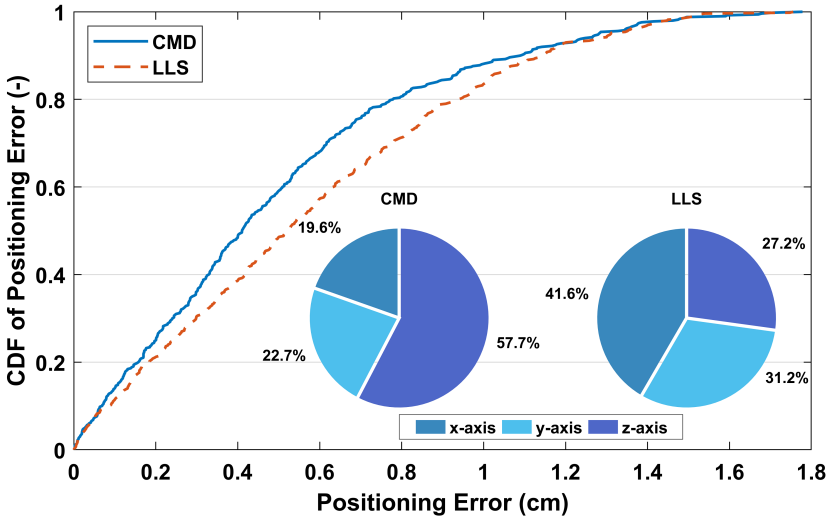

Figure 4.11: The CDF of errors for the flight path for the CMD and LLS algorithms. The inset shows a breakdown of the total positioning error for each axis for CMD and LLS.

4.3.3 The Effect of Tilting

A widespread assumption made in the literature for VLP systems is that the transmitter and receiver are parallel, as assumed in (4.3). However, this assumption does not hold in real-world applications where the moving drone tilts to move forward at different azimuthal angles, as shown in Figure 4.1 (b). Therefore, the effect of tilting was investigated here. The tilt of the drone was set to a forward tilt angle θ with values of 1°, 3° and 5°, and the value of the azimuthal angle φ changed along the path; see Figure 4.1 (b). In this model, the receiver faced the eastern wall when $\varphi = 0°$ and the northern wall when $\varphi = 90°$. Therefore, changing the azimuthal angle during the flight path ensured that the drone was always forward-facing. Noise was not considered here in order to analyse

the effect of tilt and azimuthal angles on the positioning accuracy independently.

Figure 4.12 shows the CDF of the positioning error of the 500 points for the selected path with θ = 1°, 3° and 5° for the proposed CMD algorithm. The performance of the proposed CMD algorithm was also compared with the benchmark LLS algorithm. A clear increase in the positioning error was noticed for all the tilt angles, θ = 1°, 3° and 5°. It was observed that for θ = 1°, the median errors were 6.4 cm and the maximal (95%) errors were 12 cm when CMD was used, while the median errors were 12 cm and the maximal errors were 16.8 cm when LLS was used. Similarly, for θ = 3°, CMD achieved a median error of 18.6 cm and a maximal of 41.3 cm, while LLS had median and maximal errors of 36.4 and 50.6 cm, respectively. For θ = 5°, the median and maximal errors for CMD were 30 and 72.2 cm, and 58.2 and 77.7 cm for LLS. It was also noticed that the CMD algorithm had a few points with errors higher than LLS. The CMD algorithm outperformed the LLS VLP algorithm with a median error difference of 5.6 cm, 17.8 cm and 28.2 cm for θ = 1°, 3° and 5°, respectively.

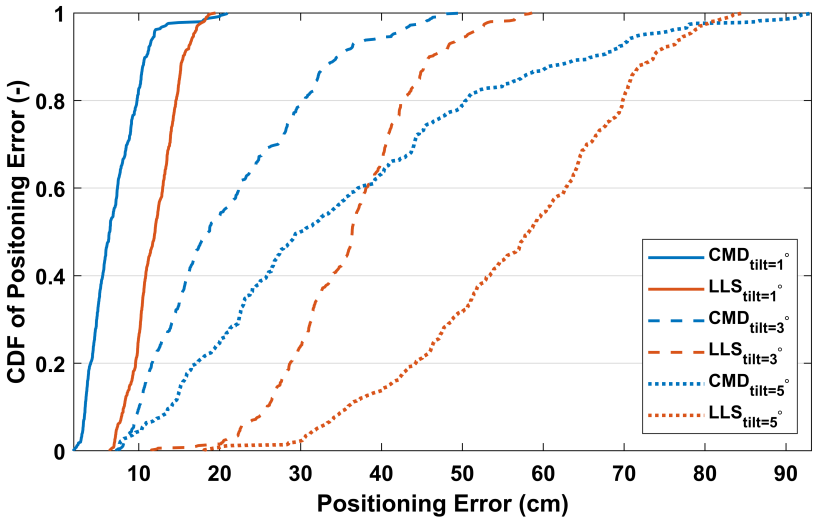

Figure 4.12: CDF of the errors for the flight path for CMD and LLS with tilt, θ values of 1°, 3° and 5°.

It should be noted that the severity of the tilting effect is also dependent on the user, as the operator can adjust the maximum tilt angle when initialising the drone. Additionally, the effect of the receiver tilt could be alleviated by using a compensation method such as the one proposed by Jeong et al. (2013), where the effect of the tilt was compensated using on-board sensors such as a gyroscope that reduced the positioning error from 60.4 cm to 1.62 cm after the compensation. Another method to minimise the effect of tilt is by keeping the drone horizontal and tilting the rotors for movement (Bin Junaid et al., 2018).

4.3.4 Positioning Accuracy with Multipath Reflections

The effect of multipath reflections was also investigated for the proposed CMD algorithm and the LLS algorithm. The position of the receiver was considered at (4,4,1), (7,4,1), (10,4,1) and (13,4,1) in order to test the effect of multipath reflections. The channel impulse response was simulated for the selected positions using the modified Monte Carlo ray-tracing method outlined earlier by Lopez-Hernandez et al. (2000). Up to three reflections were taken into account, as these contained the majority of the signal power (Ma et al., 2017).

To analyse the effect of multipath reflections only, noise was not considered in these simulations. Furthermore, the wall and floor reflectivity coefficients were considered based on the concrete and red brick materials to mimic an indoor industrial environment; see Table 4.2. Figure 4.13 shows the positioning errors for the four specified locations of the receiver with multipath reflections.

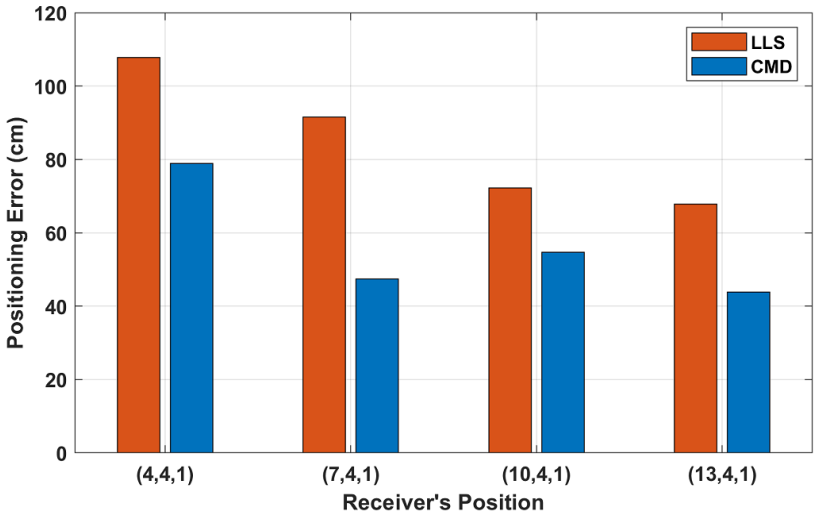

Figure 4.13: The simulated positioning errors due to multipath reflections for selected positions using the CMD and LLS algorithms.

The results show that when the receiver was at (4, 4, 1), and LLS achieved a positioning error of 107 cm, while CMD had an error of 79 cm. When the receiver was at (7,4,1), (10,4,1), and (13,4,1), the positioning error for LLS was 91.53 cm, 72.24 cm and 67.85 cm, respectively, while the CMD achieved a positioning error of 47.36 cm, 54.72 cm and 43.84 cm, respectively. Therefore, the performance of CMD was superior to that of LLS in the presence of multipath reflections. This was due to the fact that LLS used any number of signals that were received by the receiver along with their corresponding reflections, meaning that it had more skewed signals, which had a compounding effect. Hence, the receiver's position estimation was affected by the multipath reflections from those

signals as well, especially given that reflections contribute significantly more to the received power when coming from farther transmitters due to the large room dimensions. However, this effect was less severe in CMD as the algorithm only selected the strongest three signals to find a position. Likewise, a higher positioning error of 170 cm was also reported by Gu et al. (2016) due to multipath reflections even for 2D localisation, albeit for smaller room dimensions.

4.4 Summary

In this chapter, a new and simple algorithm for 3D VLP based on the RSS was proposed and analysed. The proposed method combined the use of a trilateration algorithm with a cost function. Using the cost function coupled with the CMD trilateration algorithm was shown to be more accurate and robust when compared with the widely used LLS algorithm. The algorithm's performance was shown for a receiver travelling a path in a manufacturing environment and the positioning error was simulated with and without the impact of tilt and multipath reflections. The results showed that the proposed CMD VLP algorithm outperformed the LLS algorithm by an average of 14% and a median improvement of 23% without receiver tilt or multipath reflections. When a receiver tilt of 5° was considered, CMD achieved median and maximal errors of 30 and 72.2 cm, while LLS achieved median and maximal errors of 58.2 and 77.7 cm. Furthermore, the effect of multipath reflection was also investigated with the CMD algorithm, achieving an error of 79 cm, while the LLS algorithm achieved an error of 107 cm when the receiver was close to a wall. This shows that the CMD with a cost function algorithm was more accurate than the LLS trilateration method and the use of the cost function could estimate the 3D position of a receiver without prior knowledge of its height.

This chapter verified that the proposed positioning method can determine the three-dimensional location of a receiver without knowledge of its height. While it is possible to incorporate readings from a sensor to localise a receiver. This method is easier to implement than a sensor fusion-based method, rendering it as a more a cost-effective solution. Additionally, a rarely examined trilateration algorithm has been used and demonstrated a higher accuracy than a commonly used trilateration algorithm, but further tests are needed before reaching a conclusion.

While the method has been verified through simulation, experimental work is still needed. Unaccounted parameters might affect the performance of the

proposed method. Moreover, as previously discussed, large disparities exist between reported positioning accuracies obtained through simulation and ones obtained through experimental work. As such, the following chapter tests the method experimentally.

Chapter 5

Demonstration and Evaluation of a 3D Visible Light Positioning System

5.1 Introduction

In order to validate the proposed algorithm from the previous chapter, it is important to test it experimentally to examine its validity. In this chapter, the performance of the proposed 3D VLP system has been experimentally assessed under different scenarios. The algorithm is evaluated for a system under two different LED configurations, with different degrees of receiver tilt, and in the presence of a fully stocked storage rack to examine the effect of multipath reflections on the performance of the VLP system. An examination of previous experimental work in the literature is first presented.

While most of the work presented in the literature examines the performance of VLP systems through simulation, there has been a growing number of experimental work investigating the feasibility and performance of VLP systems. The results from these experiments should not be directly compared as the testing areas vary greatly. Some experiments were conducted in small areas with dimensions of less than two meters, while some were tested in larger areas. Moreover, they vary in several aspects such as the number and type of transmitters, the number of receivers, the used multiplexing techniques, and the degree of prior calibration required.

5.2 Related Work

The work by Guo et al. (2017) proposed a multiple-classifiers fusion localisation framework by using RSS fingerprints. The experiment was performed within a 0.7 m $\times$ 0.7 m area with four LEDs and achieved a median square positioning error of less than 5 cm for the majority of the area. A 3D VLC positioning system based on a modified PSO algorithm was presented and experimentally tested by Cai et al. (2017). The researchers evaluated the system using four LEDs in a cube frame measuring 0.9 m $\times$ 0.9 m$\times$ 1.5 m and achieved an average error of 3.5 cm for a 3D VLP system. Hsu et al. (2018) tested an ML technique with height tolerance was using three LEDs within an area of 1.1 m $\times$ 1 m $\times$ 2.5 m. The result shows that over 80% of the results can be under 5 cm with an improved height tolerance range of 15 cm. Xie et al. (2019) introduced and experimentally tested a VLP method based on median shift (MS) algorithm and unscented Kalman filter (UKF) using image sensors. The test area of their experimental setup was 1.9 m $\times$ 1 m $\times$ 1.9 m and achieved a positioning accuracy of up to 0.42 cm, with an accuracy of 1.41 cm when half of the LED was shielded. The work by Zhang et al. (2019) used an RSS-based VLP system combined with a deep neural network based on the Bayesian Regularisation (BR-DNN) with a sparse diagonal training data set. The method was tested in a 1.8 m $\times$ 1.8 m $\times$ 2.1 m area and achieved a maximum positioning error of 4.58 cm for an even set, and 3.4 cm under a diagonal set of LEDs. A low-complexity TDOA method with an enhanced practical localisation using cross-correlation is reported and achieved a positioning accuracy of 9.2 cm in a 1.2 m $\times$ 1.2 m testbed area (Du et al., 2018). A 2D VLP system using a DPDOA method was experimentally tested by Zhang et al. (2018) and achieved an average RMS positioning error of 1.8 cm and a maximum of 8 cm in a testbed area of 1 m $\times$ 1.2 m $\times$ 2 m. Li et al. (2017) proposed a fusion positioning system based on EKF, which uses an inertial navigation unit to improve the performance of the VLP system. An average positioning error of 33.9 cm was achieved based on RSS alone and 14.5 cm when combined with an EKF.

Three typical office environments were tested by Li et al. (2014). Their proposed method locates the receiver using trilateration/multi-lateration if over three light sources are perceived, along with an optimisation process. If less than three signals are received, then a fusion method is used with an IMU. The achieved 90^{th} percentile positioning errors for the three environments were 0.4 m, 0.7 m, and 0.8 m. When only one transmitter is available, the 90^{th} percentile error increased to 1.1 m. Work by Yasir et al. (2014) proposed the use of the received light intensity with accelerometer measurements to compute distances between

the transmitters and the receiver. An error of less than 25 cm was reported in a 5 m $\times$ 3 m $\times$ 3 m area. A gain difference positioning method based on the angle of arrival and the received signal strength was proposed by Yang et al. (2014). The method uses multiple tilted receivers to calculate the 3D location with reported average error distances of less than 3 cm.

As can be seen, the majority of the experimental work studied the performance of 2D VLP systems and generally required the use of additional hardware or the use of some complex algorithm for 3D localisation. Additionally, most of the experiments analysed the performance in relatively very small areas that are very different from industrial settings. In contrast to some of the previous works by other researchers, this chapter examines a purely RSS-based 3D VLP system in a higher and larger area without the need for an additional receiver or complex algorithms.

Contrarily to some of the previous works by other researchers, this chapter examines a pure RSS-based VLP system in a higher and larger area without the need for an additional receiver or any complex algorithms. The proposed algorithm could be used for VLP-based aerial tracking in industrial warehouses. As discussed in Chapter 3, this is an emerging area where UAVs, or drones, are employed for different sets of application such as stock-taking in warehouses and inspecting hard-to-reach areas (Almadani et al., 2019). The commonly used RF-based technologies generally suffer from electromagnetic interference or unstable RF signals, deeming it unsuitable in providing high accuracy positioning. This is especially the case when the environment undergoes changes, e.g. forklifts or people passing by, storage rack relocation, etc.

5.3 Experimental Setup

The proposed positioning algorithm is tested experimentally in a VLP lab that measures 4 m $\times$ 4 m, with the height of the LEDs at approximately 4.1 m, as shown in Figure 5.1 (a). Black curtains are used as a substitute for walls to ensure that uncontrolled reflections from walls and objects are avoided.

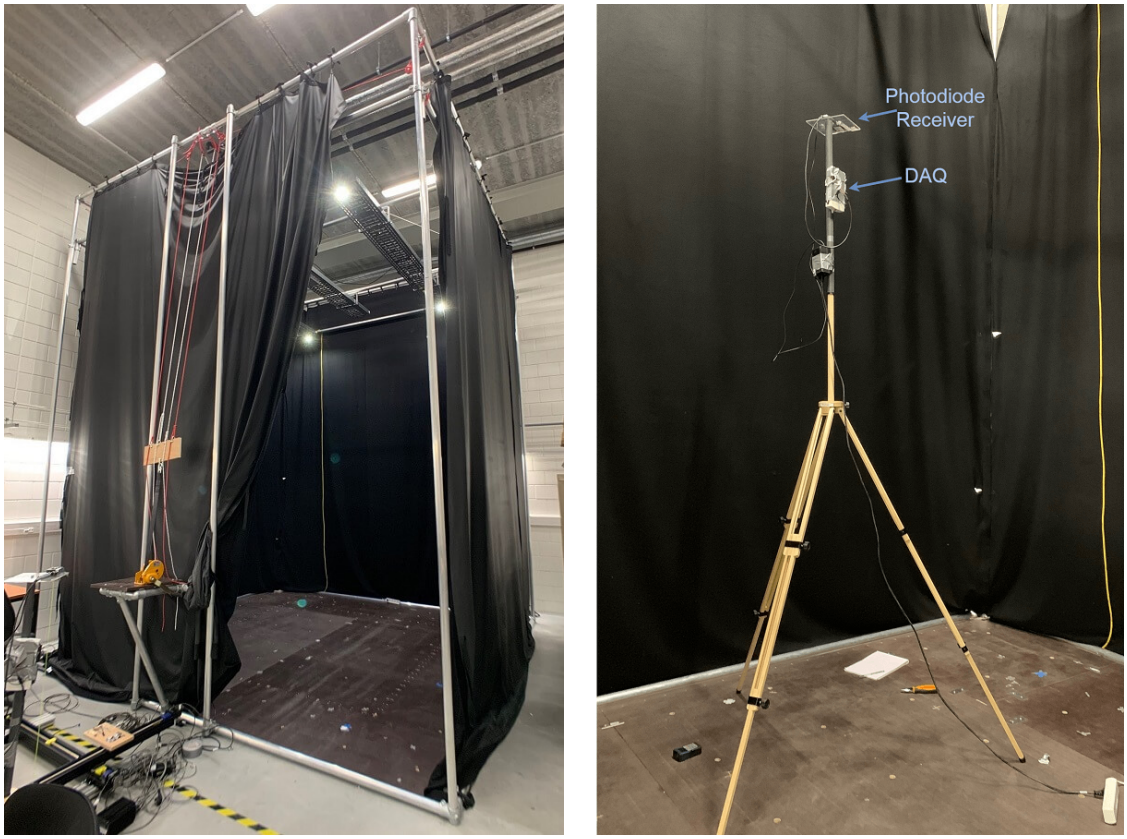

(a) **(b)**

Figure 5.1: (a) The VLP lab experimental setup with black curtains with a view of the LEDs attached to ceiling rails, and (b) a tripod with the receiver mounted on top.

Four BXRE-50C3001-D-24 LEDs, shown in Figure 5.2 (a), are intensity modulated using transmitting pulse trains with a duty cycle of 0.5 with frequencies of 500 Hz, 1 kHz, 2 kHz, and 4 kHz. This ensures that the contributions from the different LEDs can be demultiplexed individually at the receiver's side. The Lambertian order of the LEDs can be seen in Figure 2.2. The actual power of the LEDs can vary from their advertised values by up to 20% as investigated by Plets et al. (2019b). Therefore, a calibration step is performed for each transmitter by collecting one measurement directly under each transmitter ($\alpha = \beta = 0$). Then the estimated transmitted power is calculated using $P_t = \frac{P_r 2\pi d^2}{A_{pd}(m+1)}$ (Plets et al., 2019).

Table 5.1: Summary of the experimental system parameters.

Parameter	Value
Room Width x Length x Height	4 m $\times$ 4 m $\times$ 4.1 m
Transmitters' Power - P_t	13.3 W - 16.6 W - 16.4 W - 16.1 W
Transmitter's semi-angle - α	60°
Receiver's Height Range - z	0.64 - 2.55 m
Photodetector's Area - A_{pd}	13 mm^2
Receiver's Responsivity	0.22 A/W

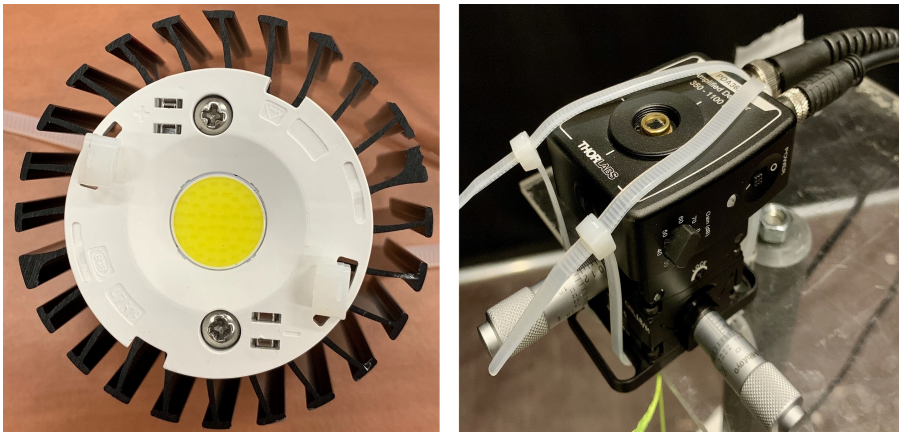

(a) **(b)**

Figure 5.2: (a) The LEDs used in the experiment; (b) The photodiode receiver used in the experiment.

The receiver is a commercial photodiode with an integrated electrical amplifier (PDA36A2 by Thorlabs) that has an active area A_{pd} of 13 mm^2 as shown in Figure 5.2 (b). The photodiode's responsivity was estimated at 0.22 A/W by weighing the photodiode's responsivity spectrum with the LED's spectrum. The receiver is attached to a tripod with a vertical pole that allows adjustment of the receiver's height as shown in Figure 5.1 (b). The data is acquired using National Instrument's USB-6212 for processing. A fast Fourier transform (FFT)-based demodulation is used to extract the received power values for each LED in MATLAB®, as specified in the work by De Lausnay et al. (2015). Table 5.1 shows the main parameters used in the experimental setup and a diagram of the setup is shown in Figure 5.3.

Figure 5.4 shows a path consisting of forty-eight points selected to take the receiver around the room at different heights ranging from 0.64 m to 2.55 m. The black line indicates the travel path, the green square denotes the start point, and red denotes the endpoint. Twenty-five power value readings were collected at each location to reduce the impact of noise.

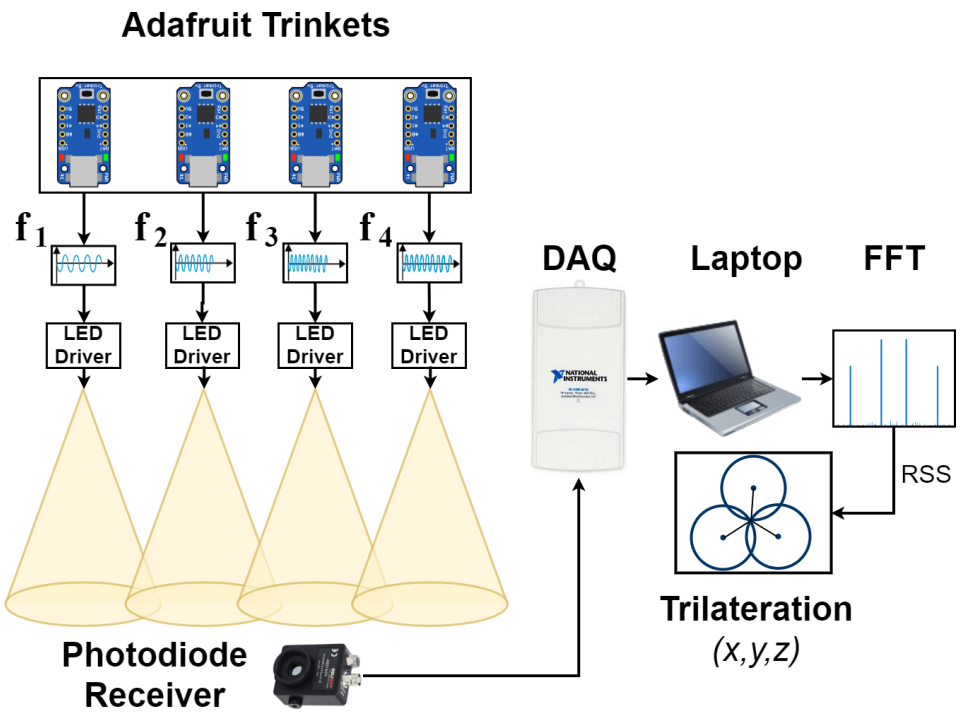

Figure 5.3: An illustration of the experimental setup.

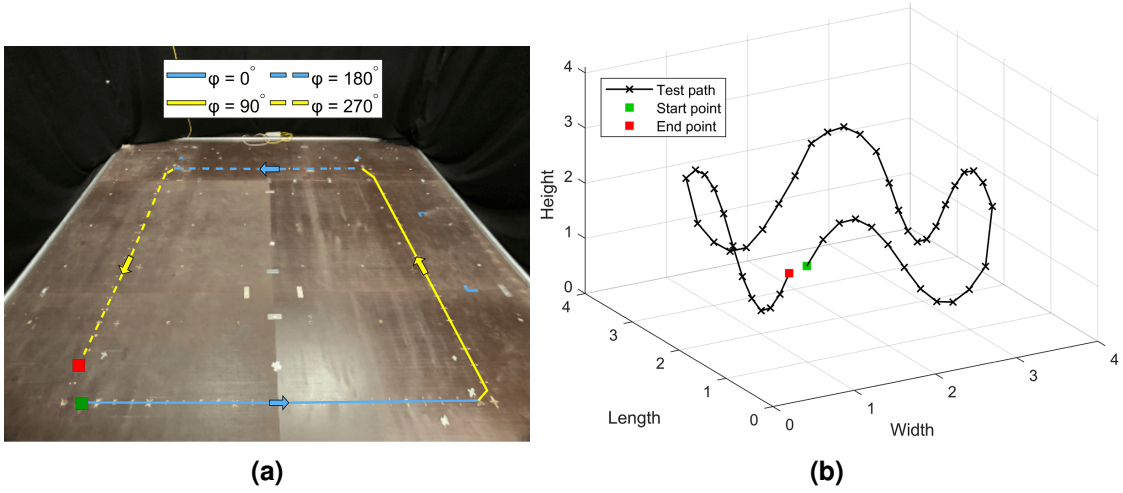

Figure 5.4: (a) The test path shown inside the VLP lab demonstrating the azimuthal orientation φ of the receiver; (b) A 3D view of the path demonstrating the height variations of the receiver along the specified path.

Two LED configurations denoted as 'Square' and 'Star' are used for the evaluation of the VLP as shown in Figure 5.5 (b). The square-shaped is a typical configuration that is adopted by many researchers while the star configuration has a central LED circularly surrounded by the other three LEDs. Previous work by Plets et al. (2019) indicates that a classic configuration with four LEDs mounted in a square-shape is not able to accurately solve the 3D position ambiguity.

Therefore, in order to counter this problem, a star-shaped configuration was proposed. This issue has been illustrated and discussed in Subsection 4.3.1.

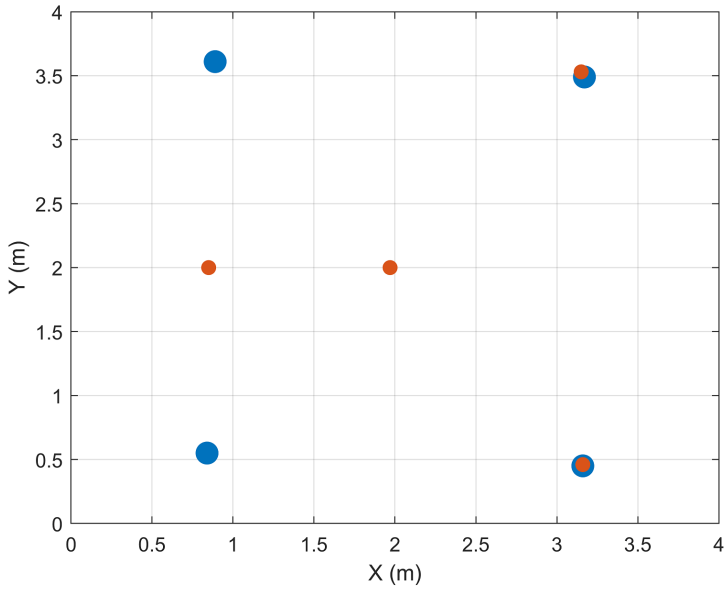

Figure 5.5: Top view of LEDs' locations in the with the blue dots representing the 'Square' configuration and the red dots representing the 'Star' configuration.

The VLC channel model, along with the positioning algorithms and the cost function has been previously presented in Section 4.2.2.

5.4 Results and Discussion

The performance of the algorithms is experimentally evaluated for different parameters in terms of positioning error while considering different realistic factors: (i) different LED configurations, (ii) different receiver tilt angles, and (iii) introduced multipath reflection through the inclusion of a storage rack. Moreover, the results section also examines the performance of the algorithms for a 2D system. In this case, the height of the receiver is assumed to be exactly known through the use of an additional sensor.

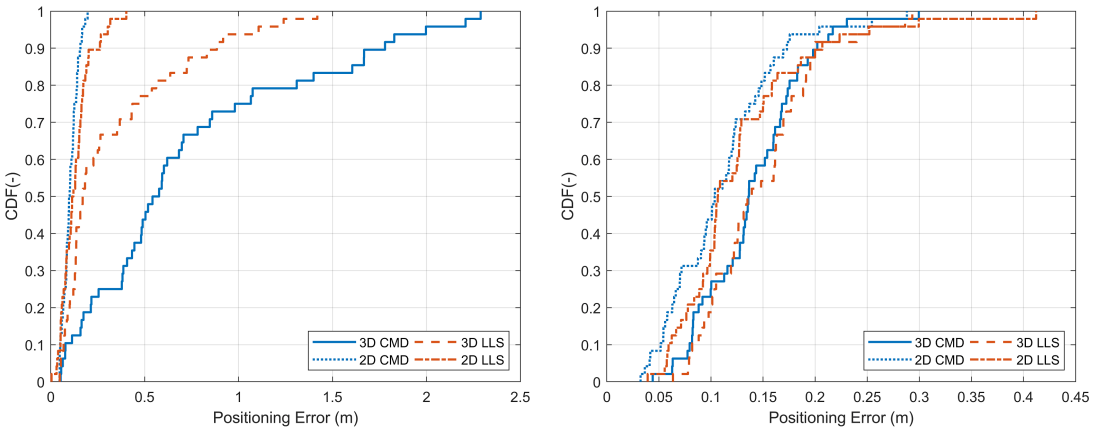

Figure 5.6: The CDF of the 2D and 3D positioning errors for both algorithms with a parallel receiver. (a) Under a square LED configuration; (b) Under a star LED configuration.

5.4.1 Positioning Accuracy for Untilted Receiver

5.4.1.1 Square Configuration

Figure 5.6 (a) shows the CDF using the CMD and LLS algorithms for a 2D and 3D positioning system. The median (p_{50}) and maximal (p_{90}) 2D errors recorded using the LLS algorithm are 11.7 cm and 26.7 cm, while these are 9.9 cm and 15.8 cm using the CMD algorithm. In a 3D system, the measured median error is 17.1 cm and the maximal error is 88.4 cm for the LLS algorithm while the CMD algorithm achieves a median error of 55.9 cm and a maximal error of 177.9 cm. The positioning errors for the 2D estimation are much smaller than the 3D estimation. This is due to the height being known to the receiver, avoiding the need for the cost function and eliminating the 3D positioning ambiguity (Plets et al., 2019). In the case of 2D positioning, the CMD outperforms the LLS algorithms slightly while the LLS algorithm outperforms the CMD algorithm in a 3D system. However, the 3D estimation for both algorithms is unreliable due to the high positioning errors under the square configuration. This is due to the position ambiguity in a square configuration (Plets et al., 2019). The issue arises because some locations in the room have the same received power values as other locations, which occurs due to the radiation pattern's geometrical properties. It should be noted that the positioning error would increase even more if a perfect LED-square layout was used, as the square layout in this experimental setup is slightly skewed.

5.4.1.2 Star Configuration

Figure 5.6 (b) shows the CDF of the positioning errors using the star arrangement of LEDs for both 2D and 3D position estimation. The overall error values have decreased noticeably when compared with the square arrangement as the position ambiguity is not present in the star configuration. The performance of the LLS and CMD algorithms are very similar for the 3D system with the median and maximal errors achieved using the LLS algorithm are 10.6 cm & 24.9 cm, and 10.5 cm & 21.1 cm using the CMD algorithm, respectively. In the case of the 2D system, median and maximal positioning errors of 8 and 25.2 cm were measured using the LLS algorithm and 6.7 cm and 14.6 cm using the CMD algorithm. Note that most of the large errors occurred at heights of more than 2 meters as can be seen in Figure 5.7, which depicts the estimated 3D paths and shows a deviation when the receiver is over 2 meters.

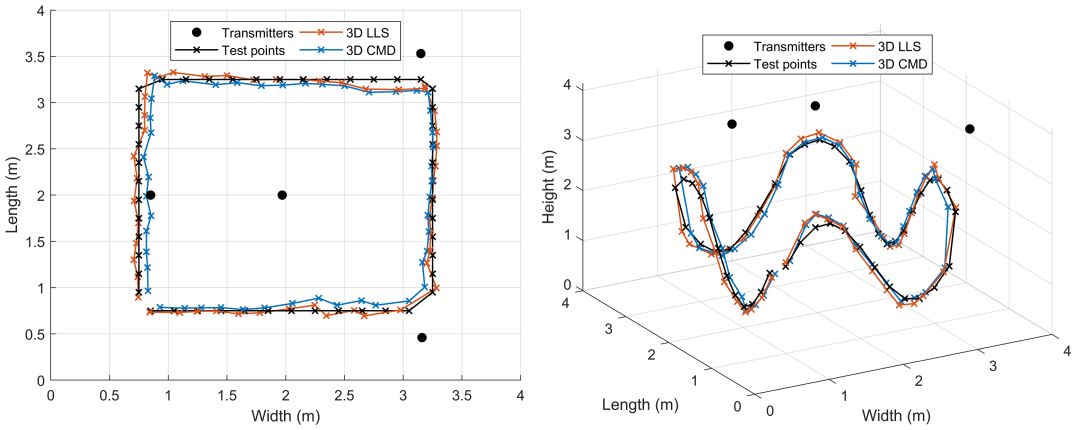

Figure 5.7: An illustration of the estimated paths under a star configuration when the receiver is parallel. (a) A top-view of the test points and the estimated 3D positions using the LLS and CMD algorithms; (b) a 3D view of the test points and the estimated points.

5.4.2 Positioning Accuracy for a tilted receiver

The errors introduced by the receiver tilt are due to the assumption that the transmitters' and receiver's plane and perfectly parallel to each other. This assumption is widely adopted due to its simplicity. However, it is unrealistic as it is almost impossible to achieve perfectly parallel planes in real-life settings, as even a 1° difference can increase the positioning error (Plets et al., 2019a). This is especially important when considering the use of a VLP system with aerial receivers, as they tilt for movement. Therefore, the effect of tilting on the perfor-

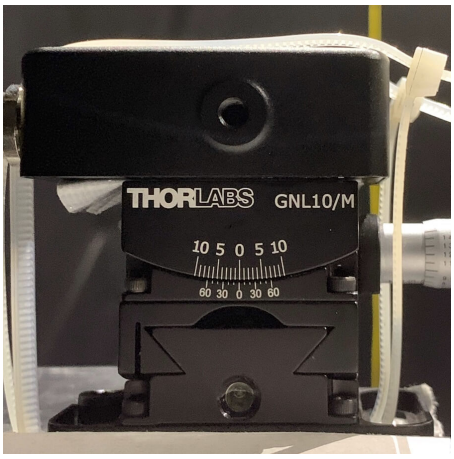

Figure 5.8: A side view of the goniometer used in the experiment.

mance of positioning algorithms is investigated here.

To accurately assess the effect of the receiver's tilt, the receiver is mounted on a Thorlabs GNL10/M[1] goniometer with a range of $\pm 10^{\circ}$ and a precision of 1° as shown in Figure 5.8. investigated.

Two tilt angles of 5° and 10° are considered and investigated. The tilt of the receiver is set to a forward tilt angle, meaning that the receiver is always facing the direction of movement along the path outlined earlier in Section 5.3 and shown in Figure 5.4 (a). The forward tilt is introduced here because drones normally tilt forward to move.

5.4.2.1 Square Configuration

Figure 5.9 (a) shows the CDF of the positioning errors using the square-shaped LED configuration for both 2D and 3D estimation for a receiver tilt angle $\theta = 5^{\circ}$. The measured median and maximal errors using the LLS algorithm were 9.5 cm and 17.8 cm, and it is 8.8 cm and 15.3 cm when the CMD algorithm is used. In a 3D system, the median and maximal errors for 2D using the LLS algorithm are 17.4 and 76.9 cm, while it is 62.9 and 177.5 cm when the CMD algorithm is used. The results show that LLS outperforms the CMD algorithm in a square configuration. Figure 5.9 (c) shows the performance of the system with a receiver tilt of 10°. For a 2D system, the recorded median errors are 19.4 and 15.6 cm for the LLS and CMD algorithms, respectively. The largest errors recorded are when a 3D system was used with a receiver tilt $\theta = 10^{\circ}$ with a median of 27.1 cm using LLS, and 106.7 cm using CMD. These results again

[1] https://www.thorlabs.com/thorproduct.cfm?partnumber=GNL10/M

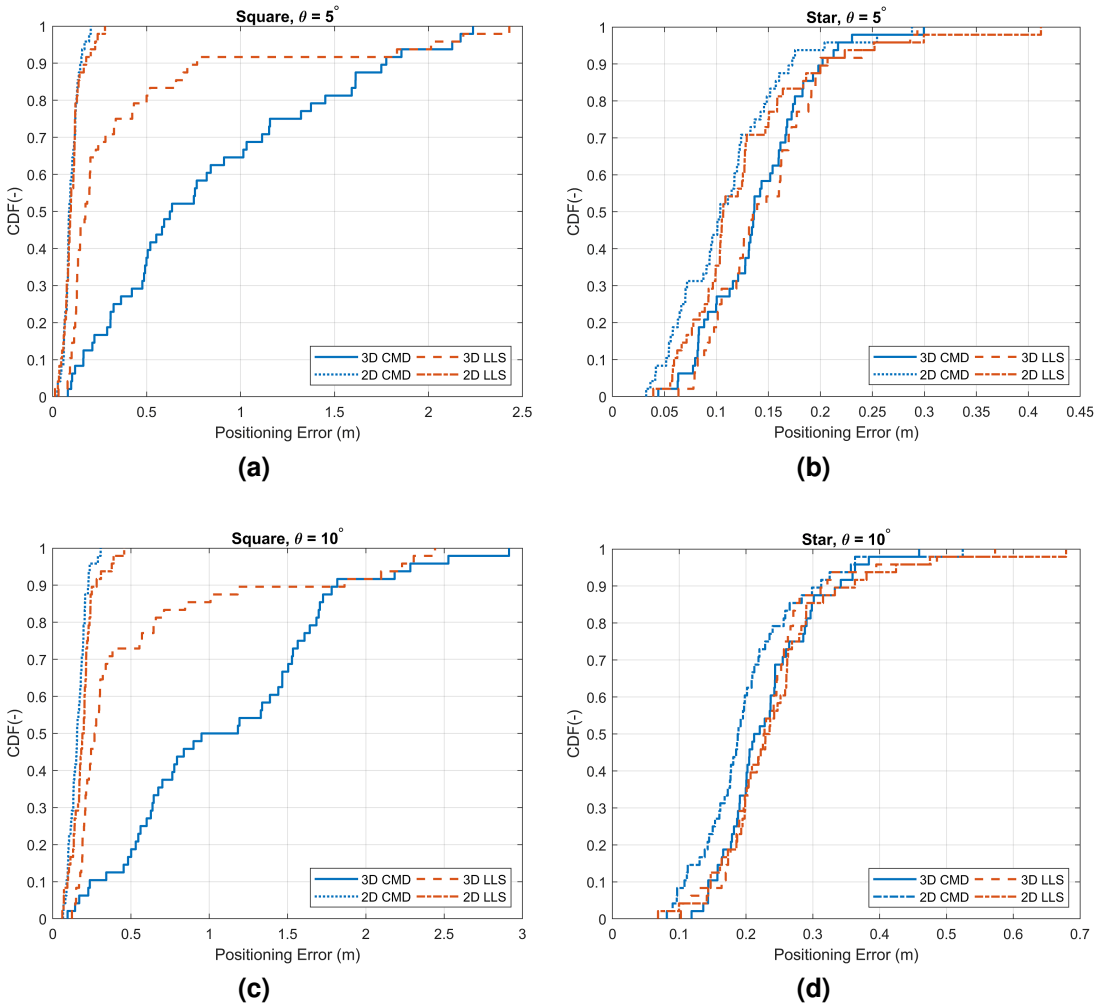

Figure 5.9: The CDF of the 2D and 3D positioning errors for both algorithms with receiver tilt, θ. (a) Square LED configuration with a receiver tilt of 5°; (b) Star LED configuration with a receiver tilt of 5°; (c) Square LED configuration with a receiver tilt of 10°; (d) Star LED configuration with a receiver tilt of 10°.

demonstrate the unreliability of using a square layout when implementing the algorithm. Table 5.2 lists a summary of the obtained accuracies across all tilt angles for the CMD and LLS algorithms under the two LED configurations.

5.4.2.2 Star Configuration

Figure 5.9 (b) shows the CDF of the positioning error for the entire path when the receiver is tilted by $\theta = 5^\circ$ under a star configuration. When the LLS algorithm is used for 3D positioning, the median error is 13.7 cm and the maximal error is 20 cm. In the case of 2D positioning, the median error is 10.7 cm and the maximal error is 20.7 cm, which is slightly better than 3D positioning. When the CMD algorithm is used for 2D positioning, the median and maximal errors

Table 5.2: A summary of the experimentally obtained median and maximal positioning errors for the two LED configurations for 2D and 3D localisation when the receiver has a tilt of 0°, 5°, and 10°.

Positioning Error(cm)	**2D LLS**		**2D CMD**		**3D LLS**		**3D CMD**	
	p_{50}	p_{90}	p_{50}	p_{90}	p_{50}	p_{90}	p_{50}	p_{90}
Square ($\theta = 0°$)	11.7	26.2	9.9	15.8	17.1	88.4	55.9	177.9
Star ($\theta = 0°$)	8	25.2	6.7	14.6	10.6	24.9	10.5	21.1
Square ($\theta = 5°$)	9.5	17.8	8.8	15.3	17.4	76.9	62.9	177.5
Star ($\theta = 5°$)	10.7	20.7	10.4	17.3	13.7	20	13.6	20.2
Square ($\theta = 10°$)	19.4	28.1	15.6	22.8	27.1	186.4	106.7	181.8
Star ($\theta = 10°$)	23.2	36.3	18.8	31.3	22.7	32.2	21.6	34.2

recorded were 10.4 and 17.3 cm, and in the case of 3D positioning, the median and maximal errors are 13.6 and 20.2 cm.

The measured positioning errors with $\theta = 10°$ are shown in Figure 5.9 (d). Median and maximal errors for the 2D system are 23.2 cm and 36.3 cm for the LLS algorithm, while it is 18.8 cm and 31.3 cm for the CMD algorithm, respectively. In a 3D positioning system, the median and maximal errors were 22.7 cm and 32.2 cm when using the LLS algorithm, and 21.6 cm and 34.2 cm using the CMD algorithm.

In can be noticed that some of the errors are higher under a square setting with an untilted receiver than when the receiver is $\theta = 5°$, see Table 5.2. The increase is due to some of the measured samples have large errors that have skewed the maximal errors. Note that, the tilt effect could be alleviated through compensating its value, which can be performed by receivers that are equipped with an IMU/gyroscope (Jeong et al., 2013; Kim et al., 2016) or with algorithms such as simultaneous positioning and orientating (SPAO) (Zhou et al., 2018).

5.4.3 Positioning Accuracy in the Presence of Multipath Reflections

Industrial environments are one of the areas where an indoor positioning system could prove valuable. As discussed previously, UAVs and AGVs can be deployed in warehouses and storage facilities with the help of VLP systems for inventory management applications. In order to replicate an industrial warehouse, a metal storage rack was added to the room as shown in Figure 5.4. The shelf rack, shown in Figure 5.10 (a), is placed at one side of the room along the path and is stocked with different-sized boxes. The height of the storage rack is 2 m and measures 2.36 m when stocked with boxes and has a length of 2.66 m. The

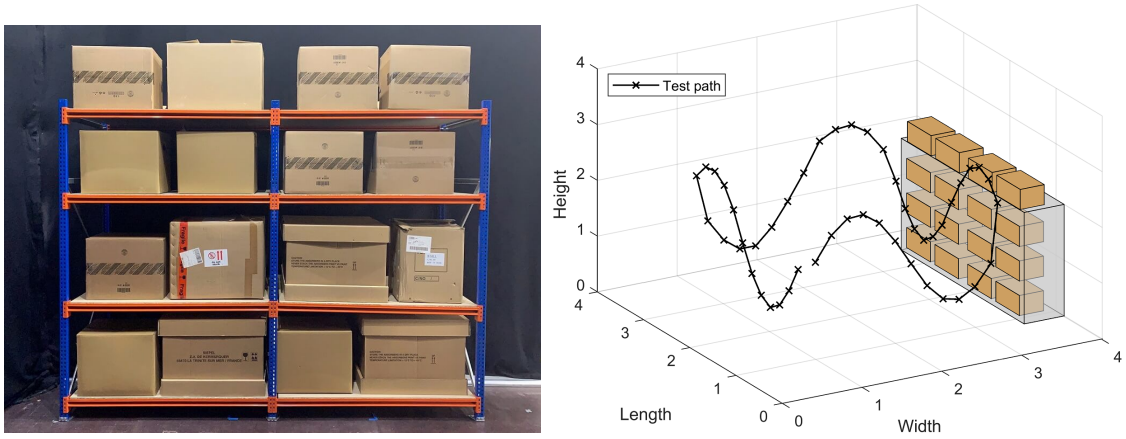

(a) (b)

Figure 5.10: (a) The storage rack stocked with boxes; (b) a 3D view of the storage rack and the test path in relation to the room.

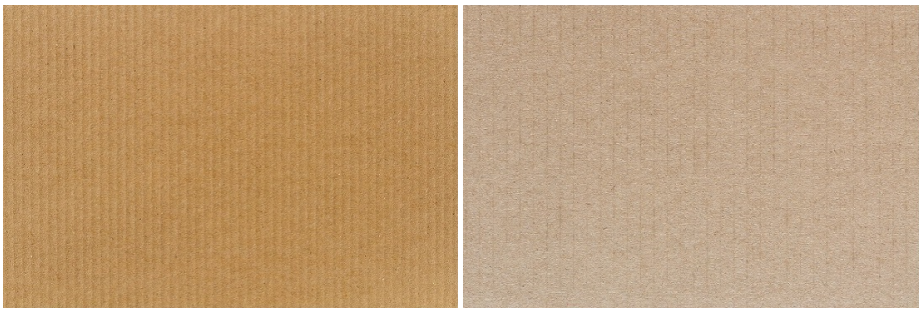

(a) (b)

Figure 5.11: (a) A box surface with 33% reflectivity; (b) with 42% reflectivity.

storage rack is placed 26 cm away from the path test points that runs parallel to it. A 3D illustration of the storage rack and the test points in the room can be seen in Figure 5.10 (b).

Research work has shown that reflections degrade the performance of VLP systems, especially when near highly reflective surfaces such as white painted walls that have a reflectivity of around 70% (Gu et al., 2016). In our case, the reflectivity of the boxes ranges between 33-42% depending on the colour tone of the cardboard as demonstrated in Figure 5.11. These values were obtained using DIALux[2]. The same measurement procedure and scenarios outlined earlier (two LED configurations with 2D and 3D using the CMD and LLS trilateration algorithms) have been repeated, and then the positioning error was calculated.

[2]https://www.dial.de/en/dialux/

5.4.3.1 Untilted Receiver

Figure 5.12 (a) shows the CDF of the positioning errors using a square configuration with the inclusion of the storage rack. In the 2D system, the median and maximal errors using the LLS algorithm are 14.5 cm and 33.4 cm, whereas the CMD algorithm achieves a median and maximal value of 9.3 cm and 16.5 cm using the CMD algorithm. Figure 5.12 (b) shows the CDF of the positioning errors using the LLS and CMD algorithms under a star LED configuration. The median and maximal 2D errors using the LLS algorithm are 8.1 cm and 25.2 cm, whereas a median error of 7.9 cm and a maximal error of 20.1 cm when the CMD algorithm is used. The errors increase slightly in a 3D system with median and maximal errors of 12.2 cm and 26.7 cm using the LLS algorithm. In a 3D system, the CMD algorithm achieved a median and a maximal value of 11.3 cm and 22.7 cm.

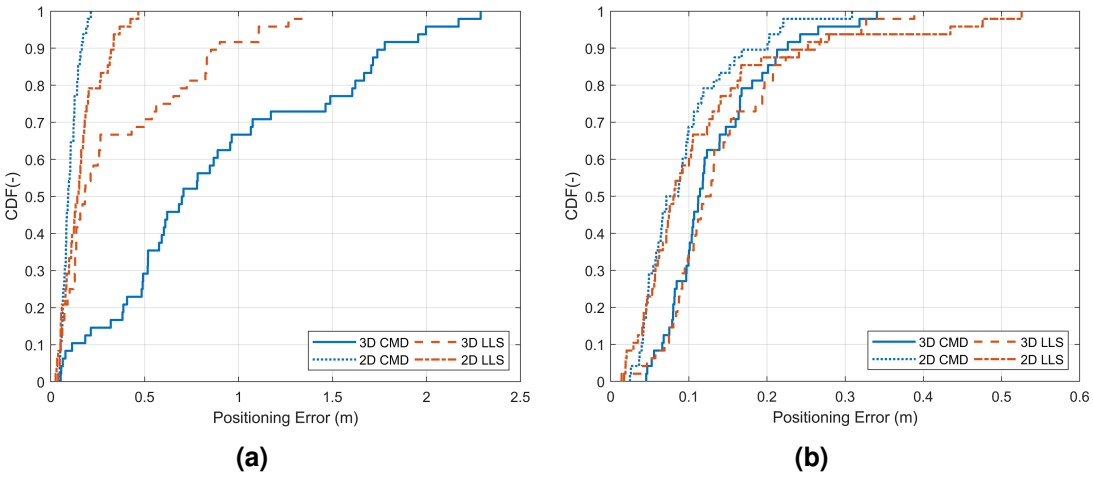

Figure 5.12: The CDF of the 2D and 3D positioning errors for both algorithms when the receiver is tilted and with the inclusion of a storage rack. (a) Square configuration with a receiver tilt of 5°; (b) Star configuration with a receiver tilt of 5°; (c) Square configuration with a tilt of 10°; (d) Star configuration with a receiver tilted 10°.

Figure 5.13 illustrates the estimated paths using the CMD and LLS algorithms. The errors on the right side and top-right side near the storage rack are due to reflections from the boxes and the metal rods. The bottom-right path is not particularly affected as some receiver heights are higher than the storage rack. The detrimental impact of reflections for the points that run parallel to the storage rack can be seen in Figure 5.13 (a).

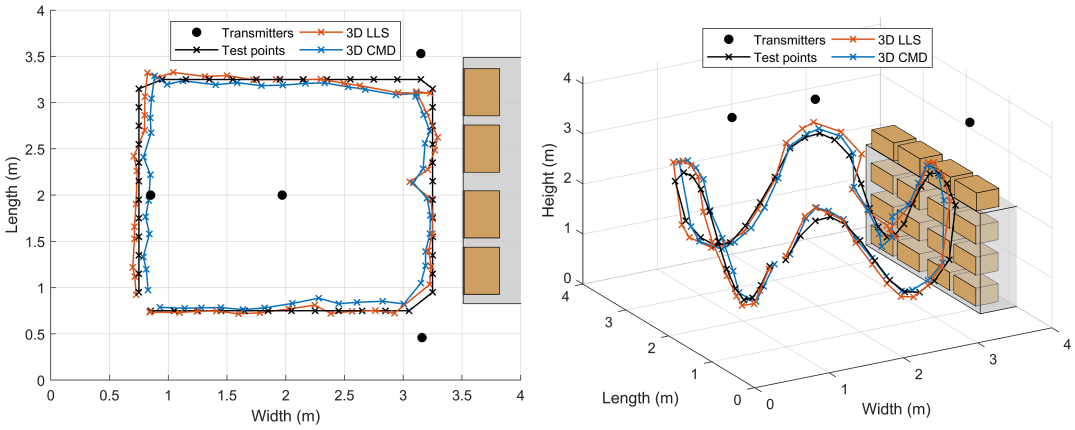

Figure 5.13: (a) A top-view of the test points and the estimated 3D positions using the LLS and CMD algorithms when the receiver is parallel; (b) a 3D view of the test points and the estimated 3D points.

5.4.3.2 Tilted Receiver

Similar to Subsection 5.4.2, the measurements are repeated with the receiver tilted by 5° and 10°. This means that the system/receiver will suffer from both the effects of tilt and multipath reflections. Figure 5.14 shows the CDF of the positioning errors when the receiver is tilted 5° and 10° for both LED configurations. Under a square setting and when the receiver is tilted by 5°, the measured median and maximal 2D errors using the LLS algorithm were 12.6 and 26 cm, whereas it is 9.8 cm and 18.7 cm when the CMD algorithm is used, see Figure 5.14 (a). In the 3D system, the measured median and maximal values are 17.1 cm and 116 cm using the LLS algorithm. Using the CMD algorithm achieved 3D median and maximal values of 79.8 and 171.8 cm. Here, the results show that 70% of the errors in a 3D system using the LLS algorithm are below 22 cm.

In the 2D system when the receiver is tilted by 10°, the LLS algorithm achieved median and maximal errors of 16 and 33 cm. While the CMD algorithm achieved median and maximal values of 12.3 and 24.4 cm. In the 3D system, the LLS algorithm reported a median of 60.7 cm and using the CMD algorithm reported 1.62 m as shown in Figure 5.14 (c). As expected, the errors increase when the tilt is increased to 10°.

Figure 5.14 (b) demonstrates the CDF for a receiver with a tilt of 5° under the star arrangement. Using the LLS algorithm, the achieved 2D median and maximal errors are 11.7 cm and 26.7 cm, whereas they are 10 cm and 21.5 cm when the CMD algorithm is used. For the 3D positioning system, the median error using the LLS algorithm is 13.9 cm, an increase of 13.9% when compared

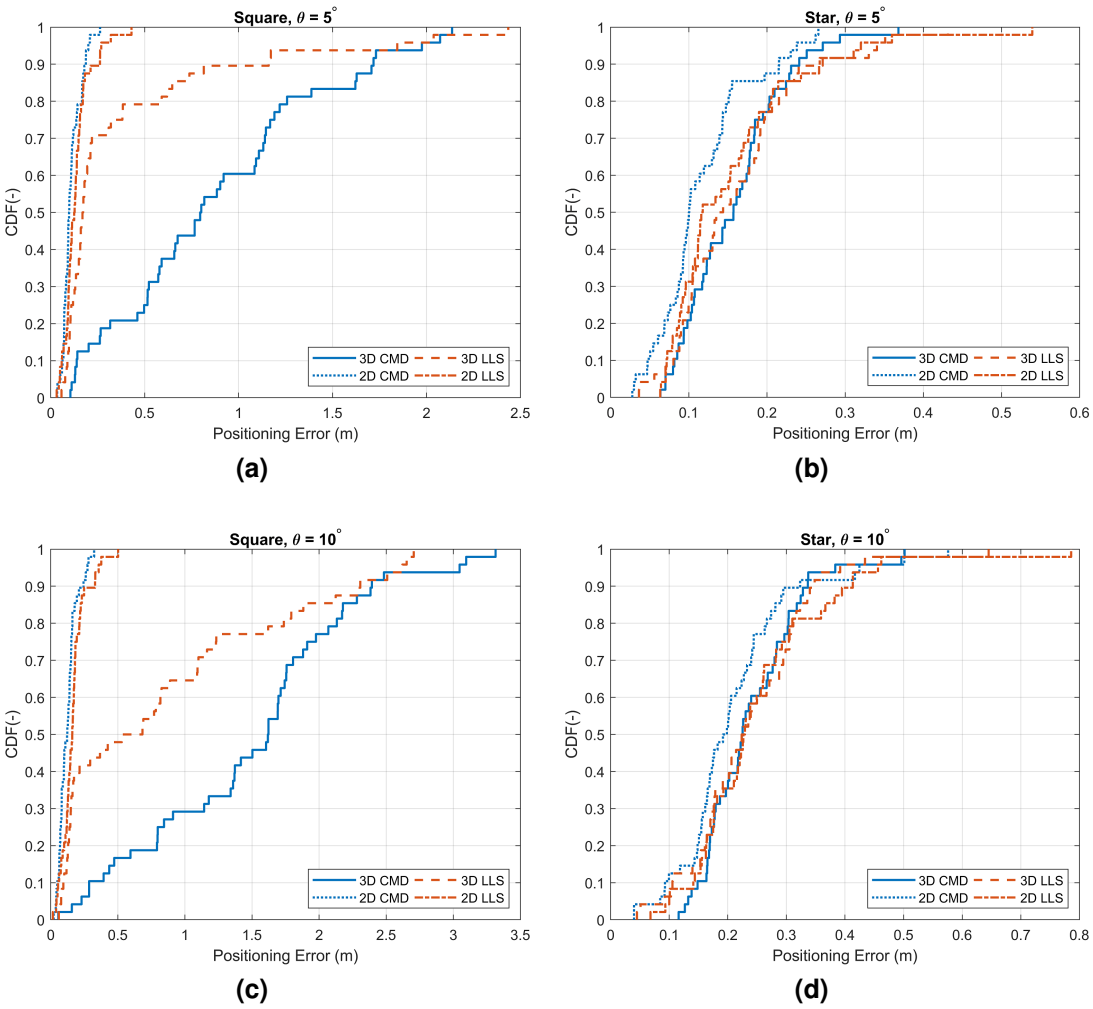

Figure 5.14: CDF of the 2D and 3D positioning errors for both algorithms when the receiver is tilted and with the inclusion of a storage rack. (a) Square configuration with a receiver tilt of 5°; (b) Star configuration with a receiver tilt of 5°; (c) Square configuration with a tilt of 10°; (d) Star configuration with a receiver tilted 10°.

with an untilted receiver. Using the CMD algorithm, the median is 15.7 cm, increasing by 39% to when the receiver was untilted. When the tilt is 5°, the CMD algorithm outperforms the LLS algorithm when it comes to 2D positioning. The results, however, are nearly identical in the 3D positioning system.

When the receiver's tilt is set to 10° under a star arrangement, the performance of the two algorithms in both 2D and 3D positioning system are similar. The median 3D error reported 22.5 cm for both algorithms, see Figure 5.14. Table 5.3 lists a summary of the obtained accuracies across all tilt angles in the presence of the storage rack. Compared to when the receiver was untilted, the errors increased by 84% using the LLS algorithm and doubled when using the CMD algorithm.

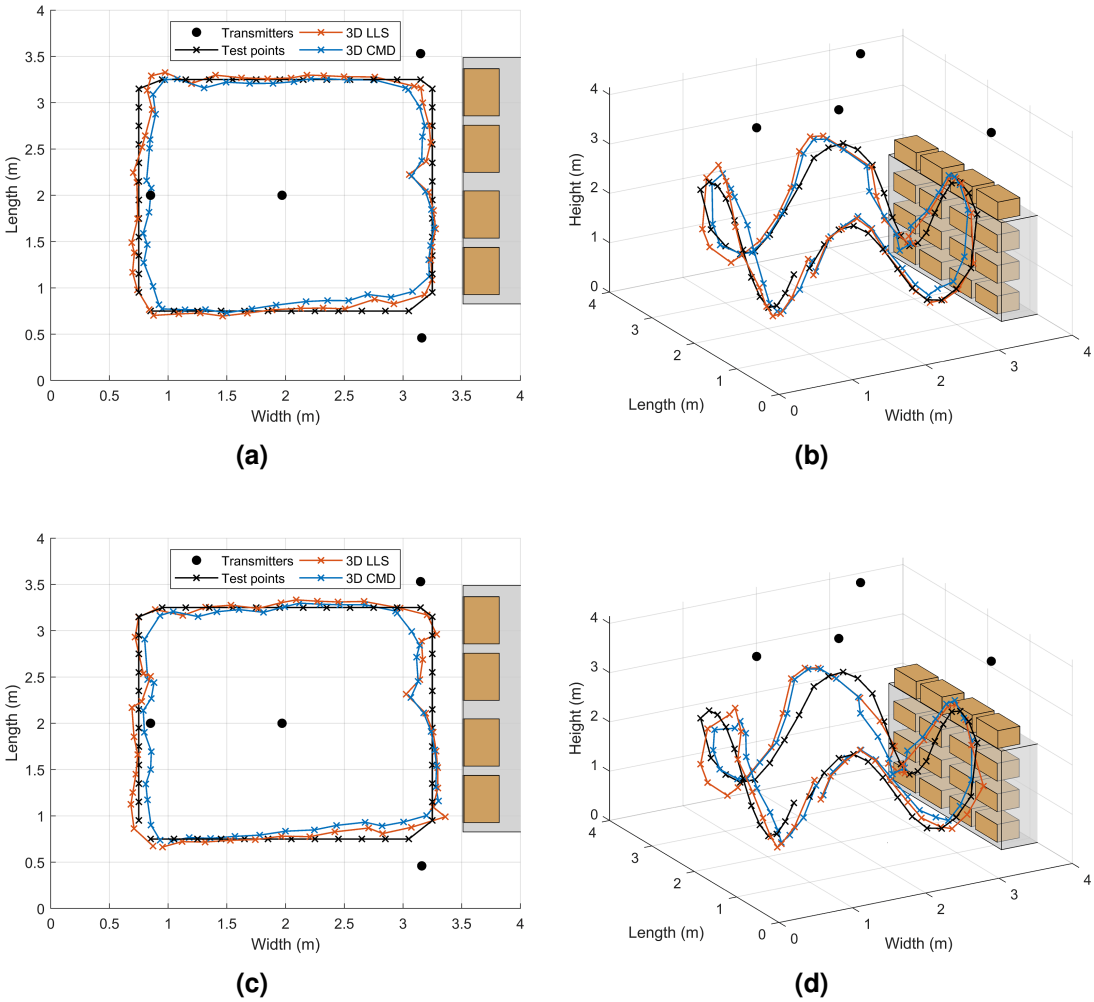

Figure 5.15: An illustration showing the top-view and a general room view of the 3D position estimation with the inclusion of a storage rack and receiver tilt under the star LED configuration. (a) A top-view when the receiver is tilted 5°; (b) when the receiver is tilted 10°; (c) A general view of the room when the receiver is tilted 5°; (d) when the receiver is tilted 10°.

An illustration of the estimated paths can be seen in Figure 5.15, it can be clearly seen that the largest errors occur in the left side of the room while and in the bottom-right of the room as shown in Figure 5.15 (c). Overall, the results do not differ greatly when compared with the results in the absence of the storage rack except for the points that are nearest to the storage rack. These points are examined more closely in the following subsection.

Table 5.3: A summary of the experimentally obtained median and maximal positioning errors for the two LED configurations for 2D and 3D localisation when the receiver has a tilt of 0°, 5°, and 10° in the presence of a storage rack.

Positioning Error (cm)	2D LLS		2D CMD		3D LLS		3D CMD	
	p_{50}	p_{90}	p_{50}	p_{90}	p_{50}	p_{90}	p_{50}	p_{90}
Square ($\theta = 0°$)	14.5	33.4	9.3	16.5	18.2	90	70.2	177.8
Star ($\theta = 0°$)	8.1	25.2	7.9	20.1	12.2	26.7	11.3	22.7
Square ($\theta = 5°$)	12.6	26.2	9.8	18.7	17.1	116	79.8	171.8
Star ($\theta = 5°$)	11.7	26.7	10	21.5	13.9	27.1	15.7	24.1
Square ($\theta = 10°$)	16	33	12.3	24.4	60.7	230.7	162	239.3
Star ($\theta = 10°$)	22.8	41.3	19.5	32.3	22.5	34.8	22.5	33.7

5.4.4 The Impact of Multipath Reflections

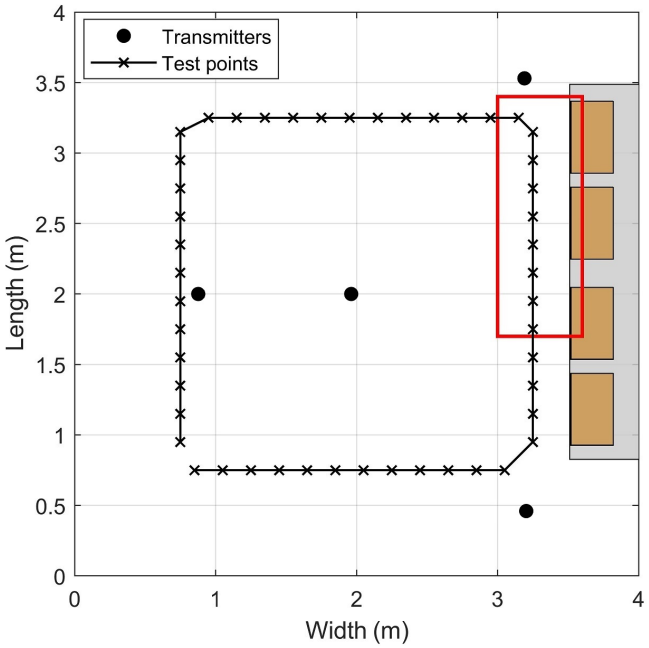

Figure 5.16: A top view of the VLP lab with the area under consideration highlighted in red.

To get a better understanding of the effect of multipath reflections on the performance of VLP systems, the area that is closest to the shelf rack is further examined, as highlighted in red in Figure 5.16. The area that will be investigated consists of nine measurement points with heights ranging from 0.74 to 2.15 m (the shelf rack's height measures 2.36 m when stocked with boxes). Which is why the immediate test points preceding and following the closely examined area with heights greater than 2.36 m will not be examined in this subsection, as they are higher than the shelf rack. A top-view of the estimated 2D and 3D positions within the selected area is shown in Figure 5.17 (a) without the inclusion of a shelf rack and in Figure 5.17 (b) after the shelf rack has been added.

A clear degradation in the 2D and 3D performances for both algorithms can be observed.

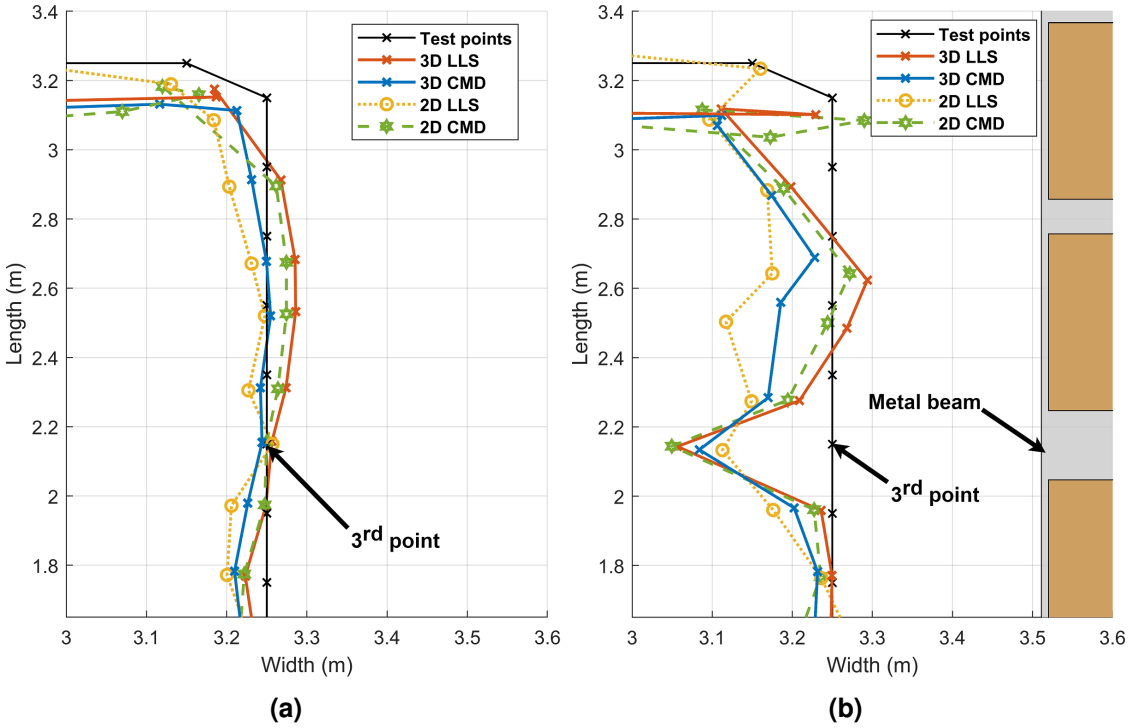

Figure 5.17: The estimated 2D and 3D path for the examined area. (a) without the shelf rack; (b) with the shelf rack. (©2020 IEEE)

For these nine points, the median 2D error achieved using LLS without a shelf rack reported a median of 5.4 cm. When using CMD, the achieved median error was 4.8 cm. The median errors in a 3D system increased slightly to 7.5 cm (a median increase of 39% from 2D) using LLS and 6.6 cm using CMD (an increase of 38% from 2D). Table 5.4 lists the median errors. The impact of reflections nearly doubles the median error.

Table 5.4: A summary of the median errors for the nine highlighted points.

Positioning Error (cm)	2D LLS	2D CMD	3D LLS	3D CMD
Star without shelf	5.4	4.8	7.5	6.6
Star with shelf	12.6	9.1	11.7	12
Percentage increase	133%	90%	56%	82%

Figure 5.18 shows the CDF of the 3D errors for the nine points in a 3D positioning system with and without the shelf rack. After the inclusion of the shelf rack, the reported 3D median error using the LLS algorithm was 11.7 cm and it was 12 cm when the CMD algorithm was used. This translates to a median

increase of 56% for the 3D LLS algorithm and an increase of 82% for the 3D CMD algorithm.

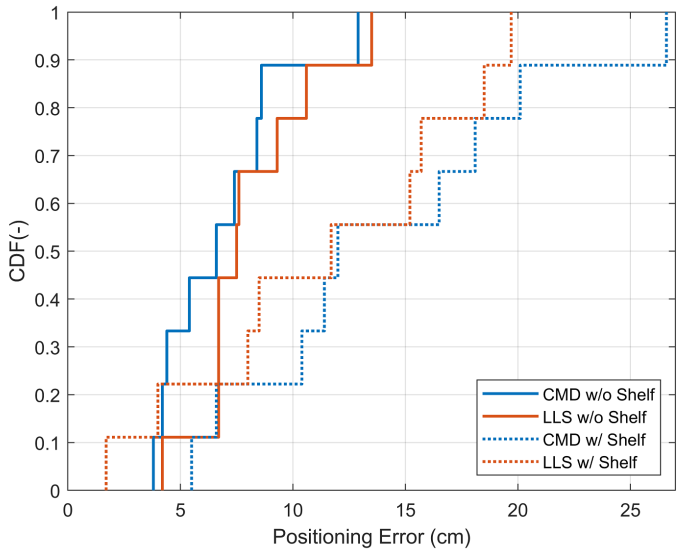

Figure 5.18: CDF of the 3D errors for the nine measured samples with and without the shelf rack.

Without the addition of the shelf rack, the lowest 3D positioning error achieved was 4.2 cm using the LLS algorithm and the highest is 13.5 cm. Using the CMD algorithm achieved a minimum error of 4.2 cm and the highest reported error was 12.9 cm. After the inclusion of a shelf rack, the highest 3D reported error using the LLS algorithm increased to 19.7 cm for the point directly opposite the metal beam (see Figure 5.19 (b)) and the maximum reported error using CMD is 26.6 cm for the same location.

For this particular point (3rd from the bottom as shown in Figure 5.19), the positioning error using the LLS algorithm increased by 13 cm, up from 6.7 cm when the point was calculated prior to adding the shelf rack. Using the CMD algorithm, that specific point reported an error of 26.6 cm, whereas it was 8.6 cm prior to the addition of the storage rack. Reflections are predominant in this specific location due to the location of the middle LED which causes large reflections that impinge perpendicularly on the beam towards the receiver's position. A similar effect can be observed at the points on top (points 7-9).

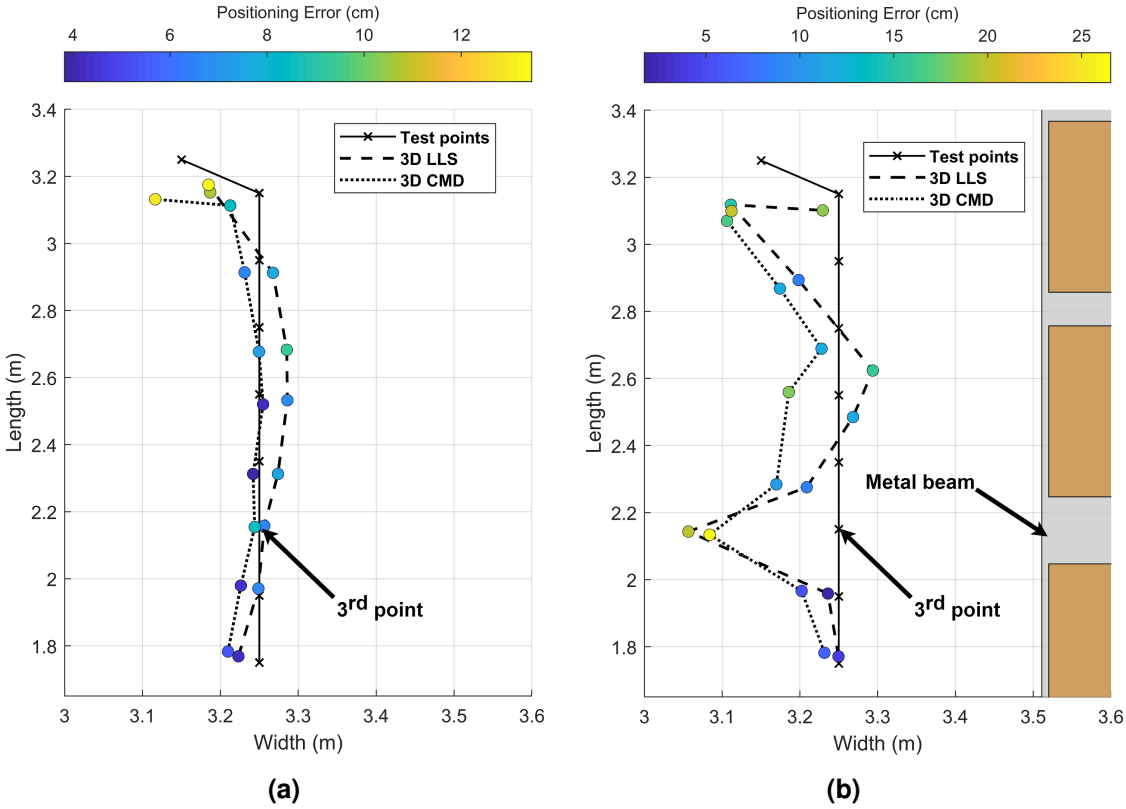

Figure 5.19: Individual 3D errors for the nine points; (a) without the shelf rack; (b) with the shelf rack.

The results show an average increase for both algorithms in terms of the median positioning errors by 79% in 2D systems, and by 69% for 3D systems. The multipath reflections from a metal rod especially worsened the performance of the VLP system demonstrating the degrading effect of multipath reflections on VLP systems and highlights the need to take it into consideration when evaluating a VLP system, an area that is often overlooked in the literature where the assumption of only LOS signals is generally made.

5.5 Discussion

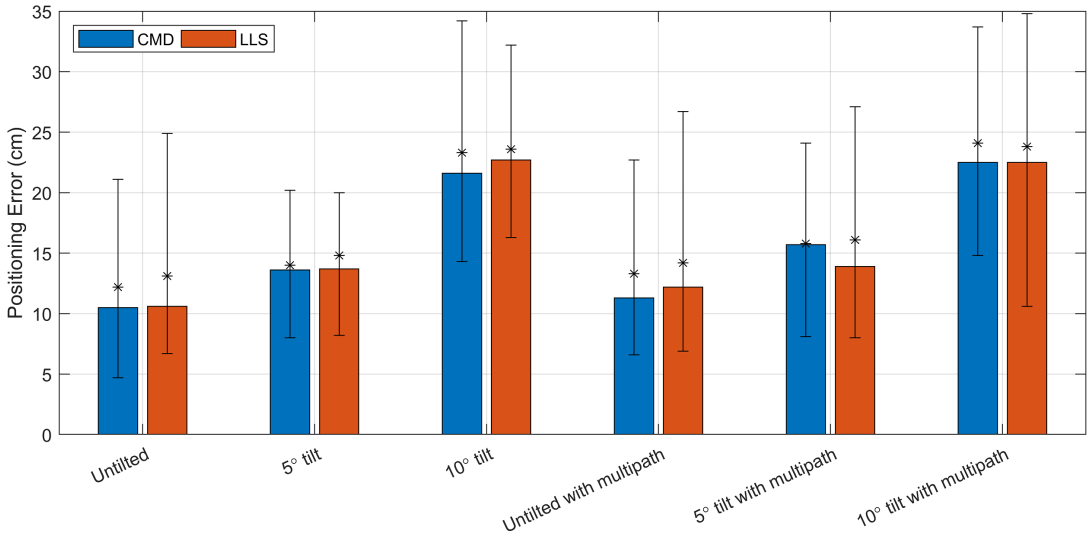

Figure 5.20: The bars show the achieved 3D median errors using the CMD and LLS trilateration algorithms under a star configuration, the error bars show the 10% and 90% quantiles, and the asterisks represent the mean error.

The work in this chapter experimentally evaluated and compared two different VLP trilateration algorithms in a 4 m $\times$ 4 m $\times$ 4.1 m room under two different LED configurations for both 2D and 3D systems. The performances of the algorithms were also examined in the presence of a storage rack to examine the effects of multipath reflections. Our experiments demonstrated the impracticality of using a square-shaped configuration for 3D systems and showed the higher positioning accuracy of a star-shaped configuration.

The results under a star configuration were highly more accurate compared to the square configuration. The 3D median error achieved using LLS and CMD were 10.6 cm and 10.5 cm, respectively. When a tilt of 5° was introduced, the 3D median errors increased slightly to 13.7 cm and 13.6 cm for LLS and CMD, an increase of 29.3% and 29.5%. A tilt of 10° increased the 3D median errors of LLS and CMD to 22.7 cm and 21.6 cm, corresponding to an increase of 114.2% and 106% when compared with a horizontal receiver. From these results, we can conclude that the positioning error increases by around 30% if the receiver is tilted by 5°, and essentially doubles when the receiver is tilted by 10°. Figure 5.20 shows the median errors for all of the considered scenarios under a star arrangement, the error bars show the 10% and 90% quantiles, and the asterisks show the mean error. A slight difference in terms of positioning error between the median and mean can be seen for some of the scenarios.

The effect of multipath reflections on the performance of VLP systems was also examined. A metallic storage rack filled with boxes was added in the evaluated room and tested with a horizontal receiver with a receiver tilt of 5° and 10°. The results for a 3D system under a star configuration reported a median error of 12.2 cm using LLS, an increase of 15% when compared with an empty room. Using the CMD algorithm, the median error was 11.3 cm, which represents an increase of 7.6% compared to its performance in an empty room. The storage rack was 26 cm away from the closest points and the impact of reflections on one particular point increased the positioning error in a 3D system using the LLS algorithm by 13 cm, and by 18 cm using the CMD algorithm. This points out the severity of multipath reflections from metallic structures. As mentioned before, both algorithms in this paper select the three strongest signals to increase the positioning accuracy and lessen the impact of multipath reflections as noted by (Gu et al., 2016; Tang et al., 2017). However, while the impact of reflections may have been reduced, it is still not sufficient enough in limiting the degrading effect of reflections.

The differences in the performances of the algorithms are because they differ mathematically in how they calculate the receiver's position. The CMD method is an analytic procedure, that calculates a point through geometric interrelations (Neuwinger et al., 2009). Whereas the least square method is a numeric procedure that calculates the point at which the distance from three circles intersects. The observation that the CMD trilateration algorithm outperforms the least square quadratic method has also been noted by Lee et al. (2008) when they compared different trilateration algorithms.

It should be noted that some of the errors observed in the experiments could also be caused by other factors. The experimentally adjusted tilt angle can be slightly different from the intended values, the LED having small unknown tilt angles (Plets et al., 2019a), the LED radiation pattern not being perfectly Lambertian, and imperfections in the demultiplexing process.

Table 5.5 provides a summary of the experimental work on indoor VLP systems that were discussed above in Subsection 5.2. The median errors using the CMD trilateration algorithm under a star LED configuration is listed in the table. As discussed earlier, the 3D positioning algorithm uses cost function (CF) while the 2D systems only require the RSS values. It can be seen that relative to the other work, the work in this chapter was performed in a larger area and is capable of achieving low positioning errors.

One point to note here as discussed in Section 2.1.5, is that there is no

agreed-upon metric or procedure in the literature when evaluating of VLP systems. This sometimes results in unfair comparisons between their respective performances. Some researchers use the median, mean, RMS error, a chosen percentile, and sometimes just the lowest achieved error. This subject is of importance and should be addressed by researchers in the future by adopting one of the already available benchmark frameworks that are used by other indoor positioning technologies such as the EvAAL framework (Salvi et al., 2012).

There are other works in VLP systems that similarly does not require previous knowledge of the receiver's height. The work by Yasir et al. (2013) used the accelerometer in mobile devices to determine the AOA of the signal, but the method mathematically complex and pre-calibration step is needed. Work by Lam and Little (2018) made use of a steerable laser positioning at the corner of the room. It only requires the use of one LED but the use of a single laser presents reliability issue in case of signal loss. Wu et al. (2018) proposed a genetic algorithm to determine the receiver's height. However, the algorithm's use of only three signals to reduce the computational complexity lead to unpredictable accidents that the authors refer to as "limitation of the system channel model". In contrast, the method presented in the previous chapter and experimentally tested here are simpler to implement.

Table 5.5: A summary of the discussed experimental work in indoor VLP systems.

Ref.	Method	2D/3D	Test Area (W L H) (m)	Accuracy (cm)	No. of LEDs
Guo et al. (2017)	Fingerprints	2D	$0.7 \times 0.7 \times 1.48$	5	4
Hsu et al. (2018)	RSS w/ ML	3D	$1.1 \times 1 \times 2.5$	3.65	3
Xie et al. (2019)	MS-UKF	2D	$1.9 \times 1 \times 1.9$	0.42	4
Zhang et al. (2019)	RSS w/ BR-DNN	2D	$1.8 \times 1.8 \times 2.1$	4.58	4
Du et al. (2018)	TDOA	2D	$1.2 \times 1.2 \times 2$	9.2	3
Zhang et al. (2018)	DPDOA	2D	$1 \times 1.2 \times 2$	1.8	3
Li et al. (2017)	RSS	2D	$2.5 \times 2.84 \times 2.5$	33.9	7
	RSS-EKF			14.5	
Yasir et al. (2014)	RSS w/ Accelerometer	3D	$5 \times 3 \times 3$	25	3
Yang et al. (2014)	RSS ratio	3D	$2 \times 2 \times 2.5$	3	1 w/ multiple PDs
Cai et al. (2017)	PSO	3D	$0.9 \times 0.9 \times 1.5$	3.492	4
Li et al. (2014)	RSS w/ IMU	3D	5×8	45	5
			2×12	70	
			3.5×6.5	80	
This work	RSS	2D	$4 \times 4 \times 4.1$	6.7	4
	RSS w/ CF	3D		10.5	

5.6 Summary

This chapter experimentally assessed the proposed 3D VLP algorithm from the previous chapter for industrial environments where the availability of RF-based

wireless connectivity is traditionally limited. The presented algorithm can estimate the position of a receiver without requiring previous knowledge of its height. The unknown 3D position of the receiver is calculated by a trilateration algorithm coupled with a cost function and was tested under different scenarios. Two different LED arrangements were considered and the receiver was tilted by different angles to examine the impact of the widespread assumption of having parallel transmitters and receiver planes. These sets of experiments were then also repeated after a fully stocked shelf rack was added in the room. Using the CMD algorithm with a cost function achieved a 3D median experimental accuracy of 10.5 cm in a 4 m $\times$ 4 m $\times$ 4.1 m area with 4 LEDs when the receiver was kept horizontal. Adding receiver tilt of 5°-10° increased the 3D median error to 13.6 and 21.6 cm, respectively. The inclusion of a shelf rack had a degrading effect on the points that runs parallel to it, especially for the points opposite the metal fixtures of the shelf rack. Increasing the average median 3D errors for the LLS and CMD algorithms by 69%.

The presented work highlights the need to take into account the light arrangements as well as the effect of receiver tilt and multipath reflections on the performance of VLP systems. It also extended the use of a trilateration algorithm that is not wildly used into VLP systems. Future work could examine integrating an IMU sensor to compensate for the undesirable effects of tilt. Additional plans could also investigate the performance of the algorithm under a circular LED arrangement as the work by Chow et al. (2015) reported that a circular arrangement offers a slightly higher uniformity than the traditional rectangular LED arrangement.

There is one notable limitation in this work, and almost every other RSS-based localisation system. As mentioned before, trilateration algorithms rely on distance measurements to estimate the receiver's location, these distances are calculated based on the received signal which requires knowledge of the LED transmitters power. Generally, one of the reasons why simulation work report much higher accuracies than experimental work are the assumption that the advertised LED power match real-life measurements. However, and as cited by other work, the advertised powers on the data sheets can vary by up to 20% when measured. As such, experimental RSS-based positioning algorithms in the literature, including this work, usually have a pre-calibration step to adjust the transmitter's power. Promisingly, there has been some work in the literature that can avoid this calibration step (Bastiaens et al., 2020).

Chapter 6

Conclusion and Future Direction

Accurate and realistic experiments that can mimic key characteristics of optical wireless channels play an important factor in designing and testing VLP systems. The work presented in this thesis performed simulation and carried experimental work for VLP applications in industrial settings. The novelty and importance of the research work have been introduced and detailed. This chapter concludes the thesis and then several potential future research directions are outlined.

6.1 Conclusion

Indoor positioning is poised to enable a wide selection of applications and potential in similar ways to outdoor GPS. In order to realise this vision, a robust and cost-effective solution is needed. The research advancements in VLC and VLP systems is indeed demonstrating great potential to be used for indoor localisation. The usage of LEDs for illumination and communicational purposes is appealing as the infrastructure is already ubiquitous.

While an indoor positioning system could be used for different applications, the thesis pays attention to its applicability in industrial environments as this area is not significantly studied in the literature within the context of VLC and VLP systems. Due to the nature of industrial environments, they present a different set of challenges than traditional indoor environments. One of these challenges is the longer link distances. Industrial environments and warehouses have greater heights than typical residential and workplace environments. This was investigated in Chapter 3 to see if a longer link distances do have a significant adverse effect on the VLC signal. By simulating the system model, the results indicate

that given the high output power of luminaires made specifically for industrial settings, the received signal would still have a high SNR.

The use of autonomous robots is one of the most promising areas in industrial environments. The robots are generally classified under two categories, aerial and ground vehicles. This area is expected to grow in the future as we progress further into industrial automation. Methods and technologies that enable the localisation of these receivers are actively researched. Given the great potential and absence of work looking into localising these devices using VLP systems, this topic was chosen for investigation in the thesis.

When it comes to trilateration-based positioning algorithms, a minimum of three independent received signals is generally required. This can pose a risk when it comes to mobile receivers as they might venture into areas where there are less than the minimum required number of signals. This is especially true for aerial receivers. This possibility was looked into in Chapter 3 for a receiver with different FOV angles. The results find that the FOV of the receiver, as well as the semi-angle of the transmitters, are the main factors influencing this limitation. For example, if the receiver has a full FOV angle of 150° and requires four signals in an area with a height of eight meters, then the first dead-zone an aerial receiver would encounter is at 5.2 meters for the corners and 6 meters at the sides of the room. By pointing this issue out, future work should examine the trackability of the receiver when it experiences a signal loss through predictive methods.

Upon examining the literature, it became clear that the limiting factor for extending two-dimensional positioning to three-dimensional positioning is the unknown receiver's height. Extending 2D localisation to 3D would be especially useful for receivers that operate in large open areas with platforms, such as industrial areas. Developing a method that determines the height of the receiver would also be beneficial to aerial receivers. There have been many methods proposed in the literature to address this, mainly using an additional sensor or by integrating another system. These solutions are often complex and costly, so developing a non-complex method that would determine the accurate receiver's height would prove valuable.

After exploring the relevant research and examining the different methods used, the use of a cost function with RSS trilateration-based algorithms has been proposed. The cost function solves the problem of not knowing the receiver's height by iterating through the different possible locations at different heights. The method was simulated and tested in Chapter 4. The work in the chapter also investigated the different issues that arise by using mobile receivers. Mainly,

the existence of receiver tilt and multipath reflections. Surprisingly, the degrading effects of these two factors are largely ignored in the literature even though they have been shown to have a detrimental impact on the accuracy of positioning systems. Moreover, while a large number of the indoor positioning systems are trilateration-based, only one trilateration algorithm seems to be used widely. The work in this thesis also made use of another trilateration algorithm that is barely examined in the literature. Comparing more than one trilateration algorithm would benefit and help researchers by demonstrating the accuracy and performance of different localisation algorithms.

Additionally, one of the observations made upon examining the related research work was the large disparity between reported simulation results and experimental implementations. A large set of work would report low centimetre accuracies, and sometimes even sub-one centimetre positioning errors, then conclude that VLP systems are capable of delivering results much more accurate than other technologies. However, when some of the simulation work was tested experimentally, the accuracies were considerably different from their simulation counterparts. This indicates that there are variables that do not exist when the simulation work is considered caused by multiple factors. Additionally, these variables are considered in the simulation work but do not precisely match reality. For example, the Lambertian emission is assumed perfect in simulation but experimental work demonstrated that this is not the cases. The same case is true when it comes to the transmission power of the LEDs. Simulation work assumes that the value specified in the datasheet by the manufacturer holds true, but experimental measurements demonstrate that the actual and advertised values vary significantly. This discrepancy is strongly influential when it comes to RSS-based positioning systems. Another set of factors are caused by the general prevalent assumption that the transmitters and receiver planes are exactly parallel to each other. Again, this assumption is unrealistic and increases the positioning error in VLP systems significantly.

Due to the reasons outlined above, it is important to examine and validate the proposed method in Chapter 4 experimentally. In Chapter 5, the method was tested in a large testbed under different scenarios. These scenarios aimed to replicate real-life characteristics such as receiver tilt and the presence of a fully stocked shelf rack. The readings were taken when the receiver was tilted by two different angles and with the presence and absence of a shelf rack. Then, these tests were repeated under a different LED layout. The obtained results achieved a median 3D accuracy of 10.5 cm. It was shown the system is capable of delivering comparative accuracies using a technology that is more advantageous than other technologies. The main uses of positioning in industrial environments

are generally intended for mobile robots to perform logistical applications.

The autonomous mobile robot market is rapidly growing (Ghaffarzadeh and Jiao, 2019). When it comes to automated mobile robots, future industrial requirements call for low centimetre accuracies along with object detection mechanisms. Systems that guide AGVs have so far been infrastructure dependent that requires using tags to guide vehicles from one point to another. While these systems are reliable, they are unadaptable and are time-consuming to install. Latest technological advances are moving towards autonomous and infrastructure-independent navigation (Ghaffarzadeh and Jiao, 2019). This sort of navigation has been enabled by progress in SLAM algorithms, which is usually based on lidars, cameras, and the integration of different sensors. The work in the thesis can serve as a guide when designing and implementing positioning systems. The experimental work in Chapter 5 shows that the positioning method can be easily implemented if a straightforward and cost-effective system is required. The tools and requirements to design such as a system are easily implementable.

6.2 Future Direction

This section discusses future work and research directions that can be considered. This includes discussing new potential fields and building on some of the areas identified in our work.

6.2.1 Future Research Work

Given that the work in this thesis examined the performance of a VLP system under different scenarios, additional experimental work is encouraged; especially work that would examine the degrading factors that affect VLP systems. There is still no substantial experimental work that characterises multipath reflections, this is especially important as it has been identified as a major degrading factor on VLP systems. Simulation work has already identified that multipath reflections arising from white painted walls would substantially degrade the accuracy of VLP systems. Additional future work should experimentally examine the performance of VLP systems near white walls and other surfaces. Moreover, work examining the effect of reflections has been using RSS-based methods, it is yet to be seen if the effect of reflections would be more or less severe if other

methods were used

As highlighted by work and in the thesis. The tilt of the receiver introduces errors as the transmitter and receiver planes are almost always assumed parallel. A sensor-fusion experiment to alleviate tilt induced errors with automated vehicles would prove valuable. This is achievable given that nearly all automated vehicles have an onboard IMU unit with a gyroscope that can allow the receiver to compensate for the tilt. Future work would also integrate the readings from an altimeter to have a sensor-fused 3D VLP system for aerial receivers. Combining the use of sensors with a filter has been reported as a method that can decrease the impact of multipath reflections (Li et al., 2019b).

It has been mentioned that the use of OFDM and its many variants in optical communications is one of the ways that mitigates the effect of reflections. There are also other multiplexing techniques that are being proposed for 5G communications that have yet to be widely adapted and researched for VLC systems, such as Filter-Bank multicarrier (FBMC), Universal Filtered multicarrier (UFMC), and Generalised Frequency Division Multiplexing (GFDM). Experimental work utilising these different methods in VLP systems is a largely unexplored area.

Additional work could also examine dead-zones experimentally in a large setting. It would be valuable to identify area limitations in a room for a VLP system with the use of a receiver with a full FOV of 180° to see if that would eliminate dead-zones. Again, while this should work in theory, experimental validation is an important step in paving the way for the technology to be adopted. Investigating this with the use of a filter could be interesting as simulation work found that using EKF helps with the trackability when there are less than three LOS sources (Vatansever et al., 2017). A further challenge that faces indoor positioning systems is the linear placement of transmitters as discussed in Chapter 3. The collinear placement of transmitters is typically found in storage facilities, hallways and corridors. Experimental analysis examining this issue would prove useful.

Bibliography

Abualhoul, M. Y., Marouf, M., Shagdar, O., and Nashashibi, F. (2013). Platooning control using visible light communications: A feasibility study. In *16th International IEEE Conference on Intelligent Transportation Systems (ITSC 2013)*, pages 1535–1540.

Akanegawa, M., Tanaka, Y., and Nakagawa, M. (2001). Basic study on traffic information system using LED traffic lights. *IEEE Transactions on Intelligent Transportation Systems*, 2(4):197–203.

Akcan, H. and Evrendilek, C. (2013). Reducing the number of flips in trilateration with noisy range measurements. In *Proceedings of the 12th International ACM Workshop on Data Engineering for Wireless and Mobile Acess*, MobiDE '13, pages 20–27, New York, NY, USA. ACM.

Akiyama, T., Sugimoto, M., and Hashizume, H. (2017). Time-of-arrival-based smartphone localization using visible light communication. In *2017 International Conference on Indoor Positioning and Indoor Navigation (IPIN)*, pages 1–7.

Al-Kinani, A., Wang, C., Haider, F., Haas, H., Zhang, W., and Cheng, X. (2017). Light and rf dual connectivity for the next generation cellular systems. In *2017 IEEE/CIC International Conference on Communications in China (ICCC)*, pages 1–6.

Alam, F., Faulkner, N., Legg, M., and Demidenko, S. (2019). Indoor visible light positioning using spring-relaxation technique in real-world setting. *IEEE Access*, 7:91347–91359.

Almadani, Y., Ijaz, M., Bastiaens, S., Rajbhandari, S., Joseph, W., and Plets, D. (2019). An experimental analysis of the effect of reflections on the performance of visible light positioning systems in warehouses. In *2019 IEEE 2nd British and Irish Conference on Optics and Photonics (BICOP)*, pages 1–4.

Almadani, Y., Ijaz, M., Joseph, W., Bastiaens, S., Rajbhandari, S., Adebisi, B., and Plets, D. (2019). A novel 3d visible light positioning method using received signal strength for industrial applications. *Electronics*, 8(11).

Almadani, Y., Ijaz, M., Rajbhandari, S., Adebisi, B., and Raza, U. (2018). Application of visible light communication in an industrial environment. In *2018 11th International Symposium on Communication Systems, Networks Digital Signal Processing (CSNDSP)*, pages 1–6.

Almadani, Y., Ijaz, M., Rajbhandari, S., Raza, U., and Adebisi, B. (2019a). Applications of visible light communication for distance estimation: a short survey. In *2019 IEEE Jordan International Joint Conference on Electrical Engineering and Information Technology (JEEIT)*, pages 261–265.

Almadani, Y., Ijaz, M., Rajbhandari, S., Raza, U., and Adebisi, B. (2019b). Deadzones limitation in visible light positioning systems for unmanned aerial vehicles. In *2019 Eleventh International Conference on Ubiquitous and Future Networks (ICUFN)*, pages 419–421.

Amini, C., Taherpour, A., Khattab, T., and Gazor, S. (2016). Theoretical accuracy analysis of indoor visible light communication positioning system based on time-of-arrival. In *2016 IEEE Canadian Conference on Electrical and Computer Engineering (CCECE)*, pages 1–5.

Aminikashani, M., Gu, W., and Kavehrad, M. (2016). Indoor positioning with ofdm visible light communications. In *2016 13th IEEE Annual Consumer Communications Networking Conference (CCNC)*, pages 505–510.

Amsters, R., Demeester, E., Slaets, P., Holm, D., Joly, J., and Stevens, N. (2019). Towards automated calibration of visible light positioning systems. In *2019 International Conference on Indoor Positioning and Indoor Navigation (IPIN)*, pages 1–8.

An, J. and Chung, W. (2016). A novel indoor healthcare with time hopping-based visible light communication. In *2016 IEEE 3rd World Forum on Internet of Things (WF-IoT)*, pages 19–23.

Arafa, A., Dalmiya, S., Klukas, R., and Holzman, J. F. (2015). Angle-of-arrival reception for optical wireless location technology. *Opt. Express*, 23(6):7755–7766.

Armstrong, J. and Schmidt, B. J. C. (2008). Comparison of asymmetrically clipped optical ofdm and dc-biased optical ofdm in awgn. *IEEE Communications Letters*, 12(5):343–345.

Bai, B., Chen, G., Xu, Z., and Fan, Y. (2011). Visible light positioning based on LED traffic light and photodiode. In *2011 IEEE Vehicular Technology Conference (VTC Fall)*, pages 1–5.

Barsocchi, P., Chessa, S., Furfari, F., and Potortì, F. (2013). Evaluating ambient assisted living solutions: The localization competition. *IEEE Pervasive Computing*, 12(4):72–79.

Bastiaens, S., Plets, D., Martens, L., and Joseph, W. (2018). Response adaptive modelling for reducing the storage and computation of rss-based vlp. In *2018 International Conference on Indoor Positioning and Indoor Navigation (IPIN)*, pages 1–8.

Bastiaens, S., Raes, W., Stevens, N., Martens, L., Joseph, W., and Plets, D. (2020). Impact of a photodiode's angular characteristics on rss-based vlp accuracy. *IEEE Access*, 8:83116–83130.

Benini, A., Mancini, A., and Longhi, S. (2013). An imu/uwb/vision-based extended kalman filter for mini-uav localization in indoor environment using 802.15.4a wireless sensor network. *Journal of Intelligent & Robotic Systems*, 70(1):461–476.

Berenguer, P. W., Hellwig, P., Schulz, D., Hilt, J., Kleinpeter, G., Fischer, J. K., and Jungnickel, V. (2018). Real-time optical wireless communication: Field-trial in an industrial production environment. In *2018 European Conference on Optical Communication (ECOC)*, pages 1–3.

Berenguer, P. W., Hellwig, P., Schulz, D., Hilt, J., Kleinpeter, G., Fischer, J. K., and Jungnickel, V. (2019). Real-time optical wireless mobile communication with high physical layer reliability. *Journal of Lightwave Technology*, 37(6):1638–1646.

Berenguer, P. W., Schulz, D., Fischer, J. K., and Jungnickel, V. (2017a). Distributed 8x6 mimo experiments for optical wireless communications. In *2017 European Conference on Optical Communication (ECOC)*, pages 1–3.

Berenguer, P. W., Schulz, D., Fischer, J. K., and Jungnickel, V. (2017b). Optical wireless communications in industrial production environments. In *2017 IEEE Photonics Conference (IPC)*, pages 125–126.

Bergen, M. H., Schaal, F. S., Klukas, R., Cheng, J., and Holzman, J. F. (2018). Toward the implementation of a universal angle-based optical indoor positioning system. *Frontiers of Optoelectronics*, 11(2):116–127.

Beul, M., Droeschel, D., Nieuwenhuisen, M., Quenzel, J., Houben, S., and Behnke, S. (2018). Fast autonomous flight in warehouses for inventory applications. *IEEE Robotics and Automation Letters*, 3(4):3121–3128.

Bin Junaid, A., Diaz De Cerio Sanchez, A., Betancor Bosch, J., Vitzilaios, N., and Zweiri, Y. (2018). Design and implementation of a dual-axis tilting quadcopter. *Robotics*, 7(4).

Binh, P. H. and Hung, N. T. (2016). High-speed visible light communications using znse-based white light emitting diode. *IEEE Photonics Technology Letters*, 28(18):1948–1951.

Burchardt, H., Serafimovski, N., Tsonev, D., Videv, S., and Haas, H. (2014). Vlc: Beyond point-to-point communication. *IEEE Communications Magazine*, 52(7):98–105.

Burke, D. T., Leeb, S. B., Hinman, R. T., Lupton, E. C., Burke, J., Schneider, J. C., Ahangar, B., Simpson, K., and Mayer, E. A. K. (2001). Using Talking Lights to Assist Brain-Injured Patients with Daily Inpatient Therapeutic Schedule. *The Journal of Head Trauma Rehabilitation*, 16(3):284–291.

Burton, A., Le Minh, H., Ghassemlooy, Z., Rajbhandari, S., and Haigh, P. A. (2012). Performance analysis for 180° receiver in visible light communications. In *2012 Fourth International Conference on Communications and Electronics (ICCE)*, pages 48–53.

Béchadergue, B., Chassagne, L., and Guan, H. (2017). A visible light-based system for automotive relative positioning. In *2017 IEEE SENSORS*, pages 1–3.

Béchadergue, B., Chassagne, L., and Guan, H. (2018). Vehicle-to-vehicle visible light phase-shift rangefinder based on the automotive lighting. *IEEE Sensors Journal*, 18(13):5334–5342.

Cahyadi, W. A., Jeong, T., Kim, Y., Chung, Y., and Adiono, T. (2015). Patient monitoring using visible light uplink data transmission. In *2015 International Symposium on Intelligent Signal Processing and Communication Systems (ISPACS)*, pages 431–434.

Cai, Y., Guan, W., Wu, Y., Xie, C., Chen, Y., and Fang, L. (2017). Indoor high precision three-dimensional positioning system based on visible light communication using particle swarm optimization. *IEEE Photonics Journal*, 9(6):1–20.

Cailean, A., Cagneau, B., Chassagne, L., Topsu, S., Alayli, Y., and Blosseville, J. (2012). Visible light communications: Application to cooperation between vehicles and road infrastructures. In *2012 IEEE Intelligent Vehicles Symposium*, pages 1055–1059.

Cailean, A., Cagneau, B., Chassagne, L., Topsu, S., Alayli, Y., and Dimian, M. (2013). Visible light communications cooperative architecture for the intelligent transportation system. In *2013 IEEE 20th Symposium on Communications and Vehicular Technology in the Benelux (SCVT)*, pages 1–5.

Cailean, A. and Dimian, M. (2017). Impact of ieee 802.15.7 standard on visible light communications usage in automotive applications. *IEEE Communications Magazine*, 55(4):169–175.

CBRE (2017). U.s. marketflash | going large: Warehouse sizes increase for modern logistics. https://www.cbre.us/research-and-reports/US-MarketFlash-Going-Large-Warehouse-Sizes-Increase-for-Modern-Logistics. Online; accessed: 09.11.2019.

Chen, C., Zhong, W., Yang, H., Zhang, S., and Du, P. (2018). Reduction of sinr fluctuation in indoor multi-cell vlc systems using optimized angle diversity receiver. *Journal of Lightwave Technology*, 36(17):3603–3610.

Chen, H., Guan, W., Li, S., and Wu, Y. (2018). Indoor high precision three-dimensional positioning system based on visible light communication using modified genetic algorithm. *Optics Communications*, 413:103 – 120.

Chen, T., Liu, L., Tu, B., Zheng, Z., and Hu, W. (2014). High-spatial-diversity imaging receiver using fisheye lens for indoor mimo vlcs. *IEEE Photonics Technology Letters*, 26(22):2260–2263.

Chen, T., Liu, L., Zheng, Z., Song, J., Wu, K., and Hu, W. (2015). Fisheye-lens-based space division multiplexing system for visible light communications. *EURASIP Journal on Wireless Communications and Networking*, 2015(1):237.

Chen, W., Mei, T., Meng, M. Q.-H., Liang, H., Liu, Y., Li, Y., and Li, S. (2008). Localization algorithm based on a spring model (lasm) for large scale wireless sensor networks. *Sensors*, 8(3):1797–1818.

Chow, C. W., Liu, Y., Yeh, C. H., Sung, J. Y., and Liu, Y. L. (2015). A practical in-home illumination consideration to reduce data rate fluctuation in visible light communication. *IEEE Wireless Communications*, 22(2):17–23.

Chun, H., Gomez, A., Quintana, C., Zhang, W., Faulkner, G., and O'Brien, D. (2019). A wide-area coverage 35 gb/s visible light communications link for indoor wireless applications. *Scientific Reports*, 9(1):4952.

Chun, H., Rajbhandari, S., Faulkner, G., Tsonev, D., Xie, E., McKendry, J. J. D., Gu, E., Dawson, M. D., O'Brien, D. C., and Haas, H. (2016). LED based wavelength division multiplexed 10 gb/s visible light communications. *Journal of Lightwave Technology*, 34(13):3047–3052.

Cossu, G., Corsini, R., Khalid, A. M., Balestrino, S., Coppelli, A., Caiti, A., and Ciaramella, E. (2013). Experimental demonstration of high speed underwater visible light communications. In *2013 2nd International Workshop on Optical Wireless Communications (IWOW)*, pages 11–15.

Cox, B., Ottoy, G., and De Strycker, L. (2016). Development of an optoacoustic distance measurement system. In *2016 International Conference on Indoor Positioning and Indoor Navigation (IPIN)*.

Cushman & Wakefield (2018). The evolution of warehouse and distribution center design. http://blog.cushwake.com/industrial/research-spotlight-evolution-warehouse-distribution-center-design.html. Online; accessed: 10.11.2019.

Céspedes, M. M. and García Armada, A. (2019). Characterization of the visible light communications during the construction of tunnels. In *2019 16th International Symposium on Wireless Communication Systems (ISWCS)*, pages 356–360.

Căilean, A. and Dimian, M. (2017). Current challenges for visible light communications usage in vehicle applications: A survey. *IEEE Communications Surveys Tutorials*, 19(4):2681–2703.

Danielis, P., Skodzik, J., Altmann, V., Schweissguth, E. B., Golatowski, F., Timmermann, D., and Schacht, J. (2014). Survey on real-time communication via ethernet in industrial automation environments. In *Proceedings of the 2014 IEEE Emerging Technology and Factory Automation (ETFA)*, pages 1–8.

De Lausnay, S., De Strycker, L., Goemaere, J., Stevens, N., and Nauwelaers, B. (2015). A visible light positioning system using frequency division multiple access with square waves. In *2015 9th International Conference on Signal Processing and Communication Systems (ICSPCS)*, pages 1–7.

de Normalisation, Comité Européen (2002). En 12464-1: Light and lighting-lighting of work places, part 1: Indoor work places. *Comité Européen de Normalisation*.

Dehghan Firoozabadi, A., Azurdia-Meza, C., Soto, I., Seguel, F., Krommenacker, N., Iturralde, D., Charpentier, P., and Zabala-Blanco, D. (2019). A novel frequency domain visible light communication (vlc) three-dimensional trilateration system for localization in underground mining. *Applied Sciences*, 9(7).

del Campo-Jimenez, G., Perandones, J. M., and Lopez-Hernandez, F. J. (2013). A VLC-based beacon location system for mobile applications. In *2013 International Conference on Localization and GNSS (ICL-GNSS)*, pages 1–4.

del Carmen Pérez, M., Gualda, D., Vicente-Ranera, J. D., Villadangos, J. M., and Ureña, J. (2019). Review of uav positioning in indoor environments and new proposal based on us measurements. In *Short Paper Proceedings of the Tenth International Conference on Indoor Positioning and Indoor Navigation - Work-in-Progress Papers (IPIN-WiP 2019) co-located with the Tenth International Conference on Indoor Positioning and Indoor Navigation (IPIN 2019)*.

DIAL. Dialux. Available online: https://www.dial.de/en/dialux/.

Dimitrov, S. and Haas, H. (2015). *Principles of LED light communications: towards networked Li-Fi*. Cambridge University Press.

Do, T. and Yoo, M. (2015). Potentialities and challenges of vlc based outdoor positioning. In *2015 International Conference on Information Networking (ICOIN)*, pages 474–477.

Do, T. and Yoo, M. (2018). Visible light communication based vehicle positioning using LED street light and rolling shutter cmos sensors. *Optics Communications*, 407:112 – 126.

Do, T.-H. and Yoo, M. (2014). Tdoa-based indoor positioning using visible light. *Photonic Network Communications*, 27(2):80–88.

doks. inventairy. https://www.doks-innovation.com/inventairy/?lang=en. Online; accessed: 03.12.2019.

Du, P., Zhang, S., Chen, C., Alphones, A., and Zhong, W. (2018). Demonstration of a low-complexity indoor visible light positioning system using an enhanced tdoa scheme. *IEEE Photonics Journal*, 10(4):1–10.

Du, P., Zhang, S., Zhong, W.-D., Chen, C., Yang, H., Alphones, A., and Zhang, R. (2019). Real-time indoor positioning system for a smart workshop using white LEDs and a phase-difference-of-arrival approach. *Optical Engineering*, 58(8):1 – 7.

Düngen, M., Hansen, T., Croonenbroeck, R., Kays, R., Holfeld, B., Wieruch, D., Berenguer, P. W., Jungnickel, V., Block, D., Meier, U., and Henrik, S. (2019). Channel measurement campaigns for wireless industrial automation. *at - Automatisierungstechnik*, 67(1):7–28.

Elamassie, M., Karbalayghareh, M., Miramirkhani, F., Kizilirmak, R. C., and Uysal, M. (2018). Effect of fog and rain on the performance of vehicular visible light communications. In *2018 IEEE 87th Vehicular Technology Conference (VTC Spring)*, pages 1–6.

Elamassie, M., Miramirkhani, F., and Uysal, M. (2019). Performance characterization of underwater visible light communication. *IEEE Transactions on Communications*, 67(1):543–552.

Eso, E., Burton, A., Hassan, N. B., Abadi, M. M., Ghassemlooy, Z., and Zvanovec, S. (2019). Experimental investigation of the effects of fog on optical camera-based vlc for a vehicular environment. In *2019 15th International Conference on Telecommunications (ConTEL)*, pages 1–5.

eyesee. https://eyesee-drone.com. Online; accessed: 03.12.2019.

Fath, T. and Haas, H. (2013). Performance comparison of mimo techniques for optical wireless communications in indoor environments. *IEEE Transactions on Communications*, 61(2):733–742.

Fernando, N., Hong, Y., and Viterbo, E. (2012). Flip-ofdm for unipolar communication systems. *IEEE Transactions on Communications*, 60(12):3726–3733.

Füchtenhans, M., Grosse, E. H., and Glock, C. H. (2019). Use cases and potentials of smart lighting systems in industrial settings. *IEEE Engineering Management Review*, 47(4):101–107.

Gao, J., Yang, F., and Ma, X. (2017). Indoor positioning system based on visible light communication with gray-coded identification. In *2017 13th International Wireless Communications and Mobile Computing Conference (IWCMC)*, pages 899–903.

Gfeller, F. R. and Bapst, U. (1979). Wireless in-house data communication via diffuse infrared radiation. *Proceedings of the IEEE*, 67(11):1474–1486.

Ghaffarzadeh, D. and Jiao, D. (2019). Mobile robots, autonomous vehicles, and drones in logistics, warehousing, and delivery 2020-2040.

Ghassemlooy, Z., Arnon, S., Uysal, M., Xu, Z., and Cheng, J. (2015). Emerging optical wireless communications-advances and challenges. *IEEE Journal on Selected Areas in Communications*, 33(9):1738–1749.

Ghassemlooy, Z., Popoola, W., and Rajbhandari, S. (2012). *Optical Wireless Communications: System and Channel Modelling with MATLAB®*. CRC Press, Inc., Boca Raton, FL, USA, 1st edition.

Gu, W., Aminikashani, M., Deng, P., and Kavehrad, M. (2016). Impact of multipath reflections on the performance of indoor visible light positioning systems. *Journal of Lightwave Technology*, 34(10):2578–2587.

Gu, W., Zhang, W., Kavehrad, M., and Feng, L. (2014). Three-dimensional light positioning algorithm with filtering techniques for indoor environments. *Optical Engineering*, 53(10):1 – 11.

Guo, X., Shao, S., Ansari, N., and Khreishah, A. (2017). Indoor localization using visible light via fusion of multiple classifiers. *IEEE Photonics Journal*, 9(6):1–16.

Gussen, C., Diniz, P., Campos, M., Martins, W., Costa, F., and Gois, J. (2016). A survey of underwater wireless communication technologies. *Journal of Communication and Information Systems*, 31(1).

Haas, H., Yin, L., Wang, Y., and Chen, C. (2016). What is lifi? *Journal of Lightwave Technology*, 34(6):1533–1544.

Halper, M. (2018). Bmw hopes for smaller li-fi gear on factory floor. https://www.ledsmagazine.com/leds-ssl-design/networks-controls/article/16701672/bmw-hopes-for-smaller-lifi-gear-on-factory-floor. Online; accessed: 15.01.2020.

Hessien, S., Tokgöz, S. C., Anous, N., Boyacı, A., Abdallah, M., and Qaraqe, K. A. (2018). Experimental evaluation of ofdm-based underwater visible light communication system. *IEEE Photonics Journal*, 10(5):1–13.

Hightower, J. and Borriello, G. (2001). Location systems for ubiquitous computing. *Computer*, 34(8):57–66.

Hinman, R. T., Avestruz, A.-T., Lupton, E. C., Livshin, G., Rodriguez, J. I., Leeb, S. B., Clark, C. M., Horvath, K. J., and Volicer, L. (2004). Illumination-based locator assists alzheimer's patients. *IEEE pervasive computing*, 3(2):49–49.

Hinman, R. T., Lupton, E. C., Leeb, S. B., Avestruz, A.-T., Gilmore, R., Paul, D., and Peterson, N. (2003). Using talking lights illumination-based communication networks to enhance word comprehension by people who are deaf or hard of hearing. *American Journal of Audiology*, 12(1):17–22.

Holfeld, B., Wieruch, D., Wirth, T., Thiele, L., Ashraf, S. A., Huschke, J., Aktas, I., and Ansari, J. (2016). Wireless communication for factory automation: an opportunity for lte and 5g systems. *IEEE Communications Magazine*, 54(6):36–43.

Hsu, C., Liu, S., Lu, F., Chow, C., Yeh, C., and Chang, G. (2018). Accurate indoor visible light positioning system utilizing machine learning technique with height tolerance. In *2018 Optical Fiber Communications Conference and Exposition (OFC)*, pages 1–3.

Huang, B., Liu, J., Sun, W., and Yang, F. (2019). A robust indoor positioning method based on bluetooth low energy with separate channel information. *Sensors*, 19(16).

IEEE (2011). Ieee standard for local and metropolitan area networks–part 15.7: Short-range wireless optical communication using visible light. *IEEE Std 802.15.7-2011*, pages 1–309.

IEEE (2019). Ieee standard for local and metropolitan area networks–part 15.7: Short-range optical wireless communications. *IEEE Std 802.15.7-2018 (Revision of IEEE Std 802.15.7-2011)*, pages 1–407.

Infinium Robotics. Infinium scan. https://www.infiniumrobotics.com/infinium-scan/. Online; accessed: 03.01.2020.

ISO (2016). Iso/iec 18305:2016 information technology — real time locating systems — test and evaluation of localization and tracking systems. *International Organization for Standardization*.

Jackson, D. K., Buffaloe, T. K., and Leeb, S. B. (1998). Fiat lux: a fluorescent lamp digital transceiver. *IEEE Transactions on Industry Applications*, 34(3):625–630.

Jang, B. and Kim, H. (2019). Indoor positioning technologies without offline fingerprinting map: A survey. *IEEE Communications Surveys Tutorials*, 21(1):508–525.

Jarchlo, E. A., Kouhini, S. M., Doroud, H., Maierbacher, G., Jung, M., Siessegger, B., Ghassemlooy, Z., Zubow, A., and Caire, G. (2019). Flight: A flexible light communications network architecture for indoor environments. In *2019 15th International Conference on Telecommunications (ConTEL)*, pages 1–6.

Jeong, E., Yang, S., Kim, H., and Han, S. (2013). Tilted receiver angle error compensated indoor positioning system based on visible light communication. *Electronics Letters*, 49(14):890–892.

Jordan, S., Moore, J., Hovet, S., Box, J., Perry, J., Kirsche, K., Lewis, D., and Tse, Z. T. H. (2018). State-of-the-art technologies for uav inspections. *IET Radar, Sonar Navigation*, 12(2):151–164.

Jung, S., Choi, C., Heo, S. H., Lee, S. R., and Park, C. (2013). Received signal strength ratio based optical wireless indoor localization using light emitting diodes for illumination. In *2013 IEEE International Conference on Consumer Electronics (ICCE)*, pages 63–64.

Jung, S., Hann, S., and Park, C. (2011). Tdoa-based optical wireless indoor localization using LED ceiling lamps. *IEEE Transactions on Consumer Electronics*, 57(4):1592–1597.

Jung, S.-Y., Hann, S., Park, S., and Park, C.-S. (2012). Optical wireless indoor positioning system using light emitting diode ceiling lights. *Microwave and Optical Technology Letters*, 54(7):1622–1626.

Jungnickel, V., Uysal, M., Serafimovski, N., Baykas, T., O'Brien, D., Ciaramella, E., Ghassemlooy, Z., Green, R., Haas, H., Haigh, P. A., Gil Jimenez, V. P., Miramirkhani, F., Wolf, M., and Zvanovec, S. (2015). A european view on the next generation optical wireless communication standard. In *2015 IEEE Conference on Standards for Communications and Networking (CSCN)*, pages 106–111.

Kagermann, H., Anderl, R., Gausemeier, J., Schuh, G., Wahlster, W., and Winter, J. (2016). *Industrie 4.0 in a Global Context: Strategies for Cooperating with International Partners (acatech STUDY)*. Herbert Utz Verlag.

Kahn, J. M. and Barry, J. R. (1997). Wireless infrared communications. *Proceedings of the IEEE*, 85(2):265–298.

Kannan, A. A., Guoqiang Mao, and Vucetic, B. (2006). Simulated annealing based wireless sensor network localization with flip ambiguity mitigation. In *2006 IEEE 63rd Vehicular Technology Conference*, volume 2, pages 1022–1026.

Kannan, S. M., Suri, K., Cadavid, J., Barosan, I., v. d. Brand, M., Alferez, M., and Gerard, S. (2017). Towards industry 4.0: Gap analysis between current automotive mes and industry standards using model-based requirement engineering. In *2017 IEEE International Conference on Software Architecture Workshops (ICSAW)*, pages 29–35.

Karaagac, A., Haxhibeqiri, J., Joseph, W., Moerman, I., and Hoebeke, J. (2017). Wireless industrial communication for connected shuttle systems in warehouses. In *2017 IEEE 13th International Workshop on Factory Communication Systems (WFCS)*, pages 1–4.

Keebler, P. and Berger, S. (2011). Managing the use of wireless devices in nuclear power plants. *IN Compliance*, pages 36–51.

Khosiawan, Y. and Nielsen, I. (2016). A system of uav application in indoor environment. *Production & Manufacturing Research*, 4(1):2–22.

Khosiawan, Y., Nielsen, I., Do, N. A. D., and Yahya, B. N. (2016). Concept of indoor 3d-route uav scheduling system. In *Information Systems Architecture and Technology: Proceedings of 36th International Conference on Information Systems Architecture and Technology – ISAT 2015 – Part I*, pages 29–40, Cham. Springer International Publishing.

Khosiawan, Y., Park, Y., Moon, I., Nilakantan, J. M., and Nielsen, I. (2018). Task scheduling system for uav operations in indoor environment. *Neural Computing and Applications*.

Kim, H., Chitti, R. B., and Song, J. (2010). Novel defense mechanism against data flooding attacks in wireless ad hoc networks. *IEEE Transactions on Consumer Electronics*, 56(2):579–582.

Kim, H., Kim, D., Yang, S., Son, Y., and Han, S. (2013a). An indoor visible light communication positioning system using a rf carrier allocation technique. *Journal of Lightwave Technology*, 31(1):134–144.

Kim, J., Yang, S., Son, Y., and Han, S. (2016). High-resolution indoor positioning using light emitting diode visible light and camera image sensor. *IET Optoelectronics*, 10(5):184–192.

Kim, Y., Shin, Y., and Yoo, M. (2013b). Vlc-tdoa using sinusoidal pilot signal. In *2013 International Conference on IT Convergence and Security (ICITCS)*, pages 1–3.

Komine, T. and Nakagawa, M. (2004). Performance evaluation of visible-light wireless communication system using white LED lightings. In *Proceedings. ISCC 2004. Ninth International Symposium on Computers And Communications (IEEE Cat. No.04TH8769)*, volume 1, pages 258–263 Vol.1.

Konings, D., Parr, B., Alam, F., and Lai, E. M. . (2018). Falcon: Fused application of light based positioning coupled with onboard network localization. *IEEE Access*, 6:36155–36167.

Korolija, I., Marjanovic-Halburd, L., Zhang, Y., and Hanby, V. I. (2013). Uk office buildings archetypal model as methodological approach in development of regression models for predicting building energy consumption from heating and cooling demands. *Energy and Buildings*, 60:152 – 162.

Krommenacker, N., Vásquez, O. C., Alfaro, M. D., and Soto, I. (2016). A self-adaptive cell-id positioning system based on visible light communications in underground mines. In *2016 IEEE International Conference on Automatica (ICA-ACCA)*, pages 1–7.

Kwon, W., Park, J. H., Lee, M., Her, J., Kim, S., and Seo, J. (2020). Robust autonomous navigation of unmanned aerial vehicles (uavs) for warehouses' inventory application. *IEEE Robotics and Automation Letters*, 5(1):243–249.

Lam, E. W. and Little, T. D. C. (2018). Refining light-based positioning for indoor smart spaces. In *Proceedings of the 4th ACM MobiHoc Workshop on Experiences with the Design and Implementation of Smart Objects*, SMARTOBJECTS '18, New York, NY, USA. Association for Computing Machinery.

Lam, E. W. and Little, T. D. C. (2018). Resolving height uncertainty in indoor visible light positioning using a steerable laser. In *2018 IEEE International Conference on Communications Workshops (ICC Workshops)*, pages 1–6.

Lam, E. W. and Little, T. D. C. (2019). Visible light positioning for location-based services in industry 4.0. In *2019 16th International Symposium on Wireless Communication Systems (ISWCS)*, pages 345–350.

Le Bas, C., Hoang, T. B., Sahuguede, S., and Julien-Vergonjanne, A. (2017). Lighting fixture communicating in infrared and visible for indoor health monitoring. In *2017 IEEE 19th International Conference on e-Health Networking, Applications and Services (Healthcom)*, pages 1–6.

Lebas, C., Sahuguede, S., Julien-Vergonjanne, A., Combeau, P., and Aveneau, L. (2018). Infrared and visible links for medical body sensor networks. In *2018 Global LIFI Congress (GLC)*, pages 1–6.

Lee, K.-W., Park, J.-B., and Lee, B.-H. (2008). Dynamic localization with hybrid trilateration for mobile robots in intelligent space. *Intelligent Service Robotics*, 1(3):221–235.

Lee, Y. U. and Kavehrad, M. (2012). Two hybrid positioning system design techniques with lighting LEDs and ad-hoc wireless network. *IEEE Transactions on Consumer Electronics*, 58(4):1176–1184.

Leeb, S., Hovorka, G., Lupton, E., Hinman, R., Bentzen, B., Easton, R., and Lashell, L. (2000). Assistive communication systems for disabled individuals using visible lighting. In *15th International Conference on Technology and the Disabled, Northridge, CA*.

Leeb, S. B., Jackson, D. K., Lupton, E. C., and Hovorka, G. B. (2004). Non-flickering illumination based communication. US Patent 6,794,831.

Li, C., Tanghe, E., Plets, D., Suanet, P., Hoebeke, J., Poorter, E. D., and Joseph, W. (2019a). Repos: Relative position estimation of uhf-rfid tags for item-level localization. In *2019 IEEE International Conference on RFID Technology and Applications (RFID-TA)*, pages 357–361.

Li, L., Hu, P., Peng, C., Shen, G., and Zhao, F. (2014). Epsilon: A visible light based positioning system. In *11th USENIX Symposium on Networked Systems Design and Implementation (NSDI 14)*, pages 331–343, Seattle, WA. USENIX Association.

Li, X., Cao, Y., and Chen, C. (2018). Machine learning based high accuracy indoor visible light location algorithm. In *2018 IEEE International Conference on Smart Internet of Things (SmartIoT)*, pages 198–203.

Li, Y., Videv, S., Abdallah, M., Qaraqe, K., Uysal, M., and Haas, H. (2014). Single photon avalanche diode (spad) vlc system and application to downhole monitoring. In *2014 IEEE Global Communications Conference*, pages 2108–2113.

Li, Z., Feng, L., and Yang, A. (2017). Fusion based on visible light positioning and inertial navigation using extended kalman filters. *Sensors*, 17(5).

Li, Z., Yang, W., Xiao, L., Xiong, X., Wang, Z., and Zou, X. (2019b). Integrated wearable indoor positioning system based on visible light positioning and inertial navigation using unscented kalman filter. In *2019 11th International Conference on Wireless Communications and Signal Processing (WCSP)*, pages 1–6.

Lian, J., Noshad, M., and Brandt-Pearce, M. (2019). Comparison of optical ofdm and m-pam for LED-based communication systems. *IEEE Communications Letters*, 23(3):430–433.

Lin, B., Tang, X., Ghassemlooy, Z., Lin, C., and Li, Y. (2017). Experimental demonstration of an indoor vlc positioning system based on ofdma. *IEEE Photonics Journal*, 9(2):1–9.

Lopez-Hernandez, F. J., Perez-Jimenez, R., and Santamaria, A. (2000). Ray-tracing algorithms for fast calculation of the channel impulse response on diffuse IR wireless indoor channels. *Optical Engineering*, 39(10):2775 – 2780.

Lu, Y., Morris, K. C., and Frechette, S. (2016). Current standards landscape for smart manufacturing systems. *National Institute of Standards and Technology, NISTIR*, 8107:39.

Luo, J., Fan, L., and Li, H. (2017). Indoor positioning systems based on visible light communication: State of the art. *IEEE Communications Surveys Tutorials*, 19(4):2871–2893.

Luo, P., Ghassemlooy, Z., Le Minh, H., Bentley, E., Burton, A., and Tang, X. (2014). Fundamental analysis of a car to car visible light communication system. In *2014 9th International Symposium on Communication Systems, Networks Digital Sign (CSNDSP)*, pages 1011–1016.

Lv, H., Feng, L., Yang, A., Guo, P., Huang, H., and Chen, S. (2017). High accuracy vlc indoor positioning system with differential detection. *IEEE Photonics Journal*, 9(3):1–13.

Ma, H., Lampe, L., and Hranilovic, S. (2017). Hybrid visible light and power line communication for indoor multiuser downlink. *IEEE/OSA Journal of Optical Communications and Networking*, 9(8):635–647.

Ma, Y., Selby, N., and Adib, F. (2017). Drone relays for battery-free networks. In *Proceedings of the Conference of the ACM Special Interest Group on Data Communication*, SIGCOMM '17, pages 335–347, New York, NY, USA. ACM.

Maheepala, M., Kouzani, A. Z., and Joordens, M. A. (2020). Light-based indoor positioning systems: A review. *IEEE Sensors Journal*, 20(8):3971–3995.

Matheus, L. E. M., Vieira, A. B., Vieira, L. F. M., Vieira, M. A. M., and Gnawali, O. (2019). Visible light communication: Concepts, applications and challenges. *IEEE Communications Surveys Tutorials*, 21(4):3204–3237.

Mautz, R. (2012). *Indoor positioning technologies*. PhD thesis, ETH Zurich, Zurich.

Mautz, R. and Tilch, S. (2011). Survey of optical indoor positioning systems. In *2011 International Conference on Indoor Positioning and Indoor Navigation*, pages 1–7.

Miramirkhani, F. (2018). *Channel Modeling and Characterization for Visible Light Communications: Indoor, Vehicular and Underwater Channels*. PhD thesis.

Miramirkhani, F. and Uysal, M. (2018). Visible light communication channel modeling for underwater environments with blocking and shadowing. *IEEE Access*, 6:1082–1090.

Miramirkhani, F., Uysal, M., Narmanlioglu, O., Abdallah, M., and Qaraqe, K. (2018). Visible light channel modeling for gas pipelines. *IEEE Photonics Journal*, 10(2):1–10.

Moore, D., Leonard, J., Rus, D., and Teller, S. (2004). Robust distributed network localization with noisy range measurements. In *Proceedings of the 2Nd International Conference on Embedded Networked Sensor Systems*, SenSys '04, pages 50–61, New York, NY, USA. ACM.

Moravek, P., Komosny, D., Simek, M., and Muller, J. (2012). Multilateration and flip ambiguity mitigation in ad-hoc networks. *PRZEGLAD ELEKTROTECHNICZNY*, 88(5B):222–229.

Moreira, A. J., Valadas, R. T., and de Oliveira Duarte, A. (1997). Optical interference produced by artificial light. *Wireless Networks*, 3(2):131–140.

Mossaad, M. S. A., Hranilovic, S., and Lampe, L. (2015). Visible light communications using ofdm and multiple LEDs. *IEEE Transactions on Communications*, 63(11):4304–4313.

Murai, R., Sakai, T., Kawano, H., Matsukawa, Y., Kitano, Y., Honda, Y., and Campbell, K. C. (2012). A novel visible light communication system for enhanced control of autonomous delivery robots in a hospital. In *2012 IEEE/SICE International Symposium on System Integration (SII)*, pages 510–516.

Myoung-geun, M., Su-il, C., Jaehyung, P., and Jin Young, K. (2015). Indoor positioning system using LED lights and a dual image sensor. *J. Opt. Soc. Korea*, 19(6):586–591.

Nah, J. H. Y., Parthiban, R., and Jaward, M. H. (2013). Visible light communications localization using tdoa-based coherent heterodyne detection. In *2013 IEEE 4th International Conference on Photonics (ICP)*, pages 247–249.

Nahavandi, S. (2019). Industry 5.0—a human-centric solution. *Sustainability*, 11(16).

Nakajima, M. and Haruyama, S. (2012). Indoor navigation system for visually impaired people using visible light communication and compensated geomagnetic sensing. In *2012 1st IEEE International Conference on Communications in China (ICCC)*, pages 524–529.

Nakajima, M. and Haruyama, S. (2013). New indoor navigation system for visually impaired people using visible light communication. *EURASIP Journal on Wireless Communications and Networking*, 2013(1):37.

Naz, A., Asif, H. M., Umer, T., and Kim, B. (2018a). Pdoa based indoor positioning using visible light communication. *IEEE Access*, 6:7557–7564.

Naz, A., Hassan, N. U., Pasha, M. A., Asif, H., Jadoon, T. M., and Yuen, C. (2018b). Single LED ceiling lamp based indoor positioning system. In *2018 IEEE 4th World Forum on Internet of Things (WF-IoT)*, pages 682–687.

Neuwinger, B., Witkowski, U., and Rückert, U. (2009). Ad-hoc communication and localization system for mobile robots. In *Advances in Robotics*, pages 220–229, Berlin, Heidelberg. Springer Berlin Heidelberg.

OSRAM. Compact high bay generation 2. https://www.osram.com/cb/products/index.jsp. Online; accessed: 10.01.2020.

Parthiban, R. and Menon, A. (2009). A fuzzy logic algorithm for minimizing error (flame) in wireless sensor networks. In *2009 IEEE/ASME International Conference on Advanced Intelligent Mechatronics*, pages 1435–1440.

Pathak, P. H., Feng, X., Hu, P., and Mohapatra, P. (2015). Visible light communication, networking, and sensing: A survey, potential and challenges. *IEEE Communications Surveys Tutorials*, 17(4):2047–2077.

Peng, Q., Guan, W., Wu, Y., Cai, Y., Xie, C., and Wang, P. (2018). Three-dimensional high-precision indoor positioning strategy using Tabu search based on visible light communication. *Optical Engineering*, 57(1):1 – 11.

Philips. Coreline high-bay g3. http://www.lighting.philips.com/main/prof/indoor-luminaires/high-bay-and-low-bay/high-bay/coreline-highbay. Online; accessed: 10.01.2020.

Plets, D., Almadani, Y., Bastiaens, S., Ijaz, M., Martens, L., and Joseph, W. (2019). Efficient 3d trilateration algorithm for visible light positioning. *Journal of Optics*, 21(5):05LT01.

Plets, D., Bastiaens, S., Ijaz, M., Almadani, Y., Martens, L., Raes, W., Stevens, N., and Joseph, W. (2019). Three-dimensional visible light positioning: an experimental assessment of the importance of the LEDs' locations. In *2019 International Conference on Indoor Positioning and Indoor Navigation (IPIN)*, pages 1–6.

Plets, D., Bastiaens, S., Martens, L., and Joseph, W. (2019a). An analysis of the impact of LED tilt on visible light positioning accuracy. *Electronics*, 8(4).

Plets, D., Bastiaens, S., Martens, L., Joseph, W., and Stevens, N. (2019b). On the impact of LED power uncertainty on the accuracy of 2d and 3d visible light positioning. *Optik*, 195:163027.

Plets, D., Eryildirim, A., Bastiaens, S., Stevens, N., Martens, L., and Joseph, W. (2017). A performance comparison of different cost functions for rss-based visible light positioning under the presence of reflections. In *Proceedings of the 4th ACM Workshop on Visible Light Communication Systems*, VLCS '17, page 37–41, New York, NY, USA. Association for Computing Machinery.

Podevijn, N., Plets, D., Trogh, J., Karaagac, A., Haxhibcqiri, J., Hoebeke, J., Martens, L., Suanet, P., and Joseph, W. (2018). Performance comparison of rss algorithms for indoor localization in large open environments. In *2018 International Conference on Indoor Positioning and Indoor Navigation (IPIN)*, pages 1–6.

Potortì, F., Barsocchi, P., Girolami, M., Torres-Sospedra, J., and Montoliu, R. (2015). Evaluating indoor localization solutions in large environments through competitive benchmarking: The evaal-etri competition. In *2015 International Conference on Indoor Positioning and Indoor Navigation (IPIN)*, pages 1–10.

Priyantha, N. B., Chakraborty, A., and Balakrishnan, H. (2000). The cricket location-support system. In *Proceedings of the 6th Annual International Conference on Mobile Computing and Networking*, MobiCom '00, pages 32–43, New York, NY, USA. ACM.

Qiu, K., Zhang, F., and Liu, M. (2016). Let the light guide us: Vlc-based localization. *IEEE Robotics Automation Magazine*, 23(4):174–183.

Rabadan, J., Guerra, V., Rodríguez, R., Rufo, J., Luna-Rivera, M., and Perez-Jimenez, R. (2017). Hybrid visible light and ultrasound-based sensor for distance estimation. *Sensors*, 17(2).

Rahman, M. S., Haque, M. M., and Ki-Doo Kim (2011). High precision indoor positioning using lighting LED and image sensor. In *14th International Conference on Computer and Information Technology (ICCIT 2011)*, pages 309–314.

Rajagopal, S., Roberts, R. D., and Lim, S. (2012). Ieee 802.15.7 visible light communication: modulation schemes and dimming support. *IEEE Communications Magazine*, 50(3):72–82.

Rajbhandari, S., McKendry, J. J. D., Herrnsdorf, J., Chun, H., Faulkner, G., Haas, H., Watson, I. M., O'Brien, D., and Dawson, M. D. (2017). A review of gallium nitride LEDs for multi-gigabit-per-second visible light data communications. *Semiconductor Science and Technology*, 32(2):023001.

Ramirez-Iniguez, R., Idrus, S. M., and Sun, Z. (2008). *Optical wireless communications: IR for wireless connectivity*. Auerbach Publications.

Randel, S., Breyer, F., Lee, S. C. J., and Walewski, J. W. (2010). Advanced modulation schemes for short-range optical communications. *IEEE Journal of Selected Topics in Quantum Electronics*, 16(5):1280–1289.

Raza, M., Aslam, N., Le-Minh, H., Hussain, S., Cao, Y., and Khan, N. M. (2018). A critical analysis of research potential, challenges, and future directives in industrial wireless sensor networks. *IEEE Communications Surveys Tutorials*, 20(1):39–95.

Remley, C. A., Koepke, G. H., Grosvenor, C. A., Ladbury, J. M., Camell, D. G., Coder, J. B., and Johnk, R. (2008). Nist tests of the wireless environment in automobile manufacturing facilities. Technical report, National Institute of Standards and Technology.

Riurean, S., Leba, M., Ionica, A., Stoicuta, O., and Buioca, C. (2019). Visible light wireless data communication in industrial environments. In *IOP Conference Series: Materials Science and Engineering*, volume 572, page 012095. IOP Publishing.

Riurean, S., Stoicuta, O., Leba, M., Ionica, A., and Rocha, Á. (2020). Underground channel model for visible light wireless communication based on neural networks. In *Trends and Innovations in Information Systems and Technologies*, pages 293–305, Cham. Springer International Publishing.

Roa, J. O., Jiménez, A. R., Seco, F., Prieto, J. C., and Ealo, J. (2007). Optimal placement of sensors for trilateration: Regular lattices vs meta-heuristic solutions. In *Computer Aided Systems Theory – EUROCAST 2007*, pages 780–787, Berlin, Heidelberg. Springer Berlin Heidelberg.

Robla-Gómez, S., Becerra, V. M., Llata, J. R., González-Sarabia, E., Torre-Ferrero, C., and Pérez-Oria, J. (2017). Working together: A review on safe human-robot collaboration in industrial environments. *IEEE Access*, 5:26754–26773.

Sadowski, S. and Spachos, P. (2018). Rssi-based indoor localization with the internet of things. *IEEE Access*, 6:30149–30161.

Salvi, D., Barsocchi, P., Arredondo, M. T., and Ramos, J. P. L. (2012). Evaal, evaluating aal systems through competitive benchmarking, the experience of the 1st competition. In *Evaluating AAL Systems Through Competitive Benchmarking. Indoor Localization and Tracking*, pages 14–25, Berlin, Heidelberg. Springer Berlin Heidelberg.

Sasaki, N., Iijima, N., and Uchiyama, D. (2015). Development of ranging method for inter-vehicle distance using visible light communication and image processing. In *2015 15th International Conference on Control, Automation and Systems (ICCAS)*, pages 666–670.

Schill, F., Zimmer, U. R., and Trumpf, J. (2004). Visible spectrum optical communication and distance sensing for underwater applications. In *In: Proc. of Australasian Conference on Robotics and Automation*.

Seongsu Lee and Sung-Yoon Jung (2012). Location awareness using angle-of-arrival based circular-pd-array for visible light communication. In *2012 18th Asia-Pacific Conference on Communications (APCC)*, pages 480–485.

Sertthin, C., Tsuji, E., Nakagawa, M., Kuwano, S., and Watanabe, K. (2009). A switching estimated receiver position scheme for visible light based indoor positioning system. In *2009 4th International Symposium on Wireless Pervasive Computing*, pages 1–5.

Shao, S., Khreishah, A., Ayyash, M., Rahaim, M. B., Elgala, H., Jungnickel, V., Schulz, D., Little, T. D. C., Hilt, J., and Freund, R. (2015). Design and analysis of a visible-light-communication enhanced wifi system. *IEEE/OSA Journal of Optical Communications and Networking*, 7(10):960–973.

Shi, G., Li, Y., Cheng, W., Dong, L., Yang, J., and Zhang, W. (2019). Accuracy analysis of indoor visible light communication localization system based on received signal strength in non-line-of-sight environments by using least squares method. *Optical Engineering*, 58(5):1 – 11.

Shirehjini, A. A. N., Yassine, A., and Shirmohammadi, S. (2012). An rfid-based position and orientation measurement system for mobile objects in intelligent environments. *IEEE Transactions on Instrumentation and Measurement*, 61(6):1664–1675.

Signify. First autonomous indoor drone by Blue Jay which navigates using VLC technology - Philips Lighting. Online; accessed: 03.12.2019.

Signify (2019). Signify launches trulifi: the world's most reliable, high-speed commercial lifi systems.

Signify (2020). Securelink 6013.

Simona Mirela, R., Antipova, T., Rocha, A., Leba, M., and Ionica, A. (2019). Vlc, occ, ir and lifi reliable optical wireless technologies to be embedded in medical facilities and medical devices. *Journal of Medical Systems*, 43:1–10.

Song, J., Wenbo Ding, Fang Yang, Hui Yang, Wang, J., Xiaofei Wang, and Xun Zhang (2014). Indoor hospital communication systems: An integrated solution

based on power line and visible light communication. In *2014 IEEE Faible Tension Faible Consommation*, pages 1–6.

Soria, P. R., Palomino, A. F., Arrue, B. C., and Ollero, A. (2017). Bluetooth network for micro-uavs for communication network and embedded range only localization. In *2017 International Conference on Unmanned Aircraft Systems (ICUAS)*, pages 747–752.

Steendam, H. (2018). A 3-d positioning algorithm for aoa-based vlp with an aperture-based receiver. *IEEE Journal on Selected Areas in Communications*, 36(1):23–33.

Stepniak, G., Maksymiuk, L., and Siuzdak, J. (2015a). Experimental comparison of pam, cap, and dmt modulations in phosphorescent white LED transmission link. *IEEE Photonics Journal*, 7(3):1–8.

Stepniak, G., Schüppert, M., and Bunge, C. (2015b). Advanced modulation formats in phosphorous LED VLC links and the impact of blue filtering. *Journal of Lightwave Technology*, 33(21):4413–4423.

Sun, X., Zou, Y., Duan, J., and Shi, A. (2015). The positioning accuracy analysis of aoa-based indoor visible light communication system. In *2015 International Conference on Optoelectronics and Microelectronics (ICOM)*, pages 186–190.

Suzuki, A. J. and Mizui, K. (2015). Laser radar and visible light in a bidirectional v2v communication and ranging system. In *2015 IEEE International Conference on Vehicular Electronics and Safety (ICVES)*, pages 19–24.

Tang, W., Zhang, J., Chen, B., Liu, Y., Zuo, Y., Liu, S., and Dai, Y. (2017). Analysis of indoor vlc positioning system with multiple reflections. In *2017 16th International Conference on Optical Communications and Networks (ICOCN)*, pages 1–3.

Thomas, F. and Ros, L. (2005). Revisiting trilateration for robot localization. *IEEE Transactions on Robotics*, 21(1):93–101.

Tokgoz, S. C., Boluda-Ruiz, R., Yarkan, S., and Qaraqe, K. A. (2019). Aco-ofdm transmission over underwater pipeline for vlc-based systems. In *2019 IEEE 30th Annual International Symposium on Personal, Indoor and Mobile Radio Communications (PIMRC)*, pages 1–7.

Torres-Zapata, E., Luna-Rivera, J. M., Perez-Jimenez, R., Guerra, V., Rabadan, J., Rufo, J., and Gutierrez, C. A. (2019). Implementation of a vlc-based indoor localization system. *Transactions on Emerging Telecommunications Technologies*, 30(2):e3498. e3498 ett.3498.

Tram, V. T. B. and Yoo, M. (2018). Vehicle-to-vehicle distance estimation using a low-resolution camera based on visible light communications. *IEEE Access*, 6:4521–4527.

Trong-Hop Do, Junho Hwang, and Myungsik Yoo (2013). Tdoa based indoor visible light positioning systems. In *2013 Fifth International Conference on Ubiquitous and Future Networks (ICUFN)*, pages 456–458.

Tsang, K. F., Gidlund, M., and Åkerberg, J. (2016). Guest editorial industrial wireless networks: Applications, challenges, and future directions. *IEEE Transactions on Industrial Informatics*, 12(2):755–757.

Tsonev, D. and Haas, H. (2014). Avoiding spectral efficiency loss in unipolar ofdm for optical wireless communication. In *2014 IEEE International Conference on Communications (ICC)*, pages 3336–3341.

Ucar, S., Ergen, S. C., and Ozkasap, O. (2016). Security vulnerabilities of ieee 802.11p and visible light communication based platoon. In *2016 IEEE Vehicular Networking Conference (VNC)*, pages 1–4.

Ueyama, J., Freitas, H., Faical, B. S., Filho, G. P. R., Fini, P., Pessin, G., Gomes, P. H., and Villas, L. A. (2014). Exploiting the use of unmanned aerial vehicles to provide resilience in wireless sensor networks. *IEEE Communications Magazine*, 52(12):81–87.

Uysal, M., Miramirkhani, F., Narmanlioglu, O., Baykas, T., and Panayirci, E. (2017). Ieee 802.15.7r1 reference channel models for visible light communications. *IEEE Communications Magazine*, 55(1):212–217.

Vanin, E. (2011). Performance evaluation of intensity modulated optical ofdm system with digital baseband distortion. *Opt. Express*, 19(5):4280–4293.

Vatansever, Z., Brandt-Pearce, M., and Brown, C. L. (2017). Image-sourced fingerprinting for LED-based indoor tracking. In *2017 51st Asilomar Conference on Signals, Systems, and Computers*, pages 903–907.

Vongkulbhisal, J., Chantaramolee, B., Zhao, Y., and Mohammed, W. S. (2012). A fingerprinting-based indoor localization system using intensity modulation of light emitting diodes. *Microwave and Optical Technology Letters*, 54(5):1218–1227.

Vucic, J., Kottke, C., Nerreter, S., Habel, K., Buttner, A., Langer, K. ., and Walewski, J. W. (2009). 125 mbit/s over 5 m wireless distance by use of ook-modulated phosphorescent white LEDs. In *2009 35th European Conference on Optical Communication*, pages 1–2.

Wang, C., Yu, H., and Zhu, Y. (2016). A long distance underwater visible light communication system with single photon avalanche diode. *IEEE Photonics Journal*, 8(5):1–11.

Wang, T. Q., Sekercioglu, Y. A., Neild, A., and Armstrong, J. (2013). Position accuracy of time-of-arrival based ranging using visible light with application in indoor localization systems. *Journal of Lightwave Technology*, 31(20):3302–3308.

Wang, Y. and Haas, H. (2015). Dynamic load balancing with handover in hybrid li-fi and wi-fi networks. *Journal of Lightwave Technology*, 33(22):4671–4682.

Wang, Y., Tao, L., Huang, X., Shi, J., and Chi, N. (2015). 8-gb/s rgby LED-based wdm vlc system employing high-order cap modulation and hybrid post equalizer. *IEEE Photonics Journal*, 7(6):1–7.

Wei, J. L., Ingham, J. D., Cunningham, D. G., Penty, R. V., and White, I. H. (2012). Performance and power dissipation comparisons between 28 gb/s nrz, pam, cap and optical ofdm systems for data communication applications. *Journal of Lightwave Technology*, 30(20):3273–3280.

Wilke Berenguer, P., Schulz, D., Hilt, J., Hellwig, P., Kleinpeter, G., Fischer, J. K., and Jungnickel, V. (2018). Optical wireless mimo experiments in an industrial environment. *IEEE Journal on Selected Areas in Communications*, 36(1):185–193.

Wollschlaeger, M., Sauter, T., and Jasperneite, J. (2017). The future of industrial communication: Automation networks in the era of the internet of things and industry 4.0. *IEEE Industrial Electronics Magazine*, 11(1):17–27.

Wu, D., Zhong, W., Ghassemlooy, Z., and Chen, C. (2016). Short-range visible light ranging and detecting system using illumination light emitting diodes. *IET Optoelectronics*, 10(3):94–99.

Wu, K. J., Gregory, T. S., Moore, J., Hooper, B., Lewis, D., and Tse, Z. T. H. (2017). Development of an indoor guidance system for unmanned aerial vehicles with power industry applications. *IET Radar, Sonar Navigation*, 11(1):212–218.

Wu, T.-C., Chi, Y.-C., Wang, H.-Y., Tsai, C.-T., and Lin, G.-R. (2017). Blue laser diode enables underwater communication at 12.4 gbps. *Scientific Reports*, 7(1):40480.

Wu, Y., Liu, X., Guan, W., Chen, B., Chen, X., and Xie, C. (2018). High-speed 3d indoor localization system based on visible light communication using differential evolution algorithm. *Optics Communications*, 424:177 – 189.

Xie, B., Gong, S., and Tan, G. (2018). Lipro: light-based indoor positioning with rotating handheld devices. *Wireless Networks*, 24(1):49–59.

Xie, Z., Guan, W., Zheng, J., Zhang, X., Chen, S., and Chen, B. (2019). A high-precision, real-time, and robust indoor visible light positioning method based on mean shift algorithm and unscented kalman filter. *Sensors*, 19(5).

Xu, R., Chen, W., Xu, Y., and Ji, S. (2015). A new indoor positioning system architecture using gps signals. *Sensors*, 15(5):10074–10087.

Yang, D., Xu, Y., Wang, H., Zheng, T., Zhang, H., Zhang, H., and Gidlund, M. (2015). Assignment of segmented slots enabling reliable real-time transmission in industrial wireless sensor networks. *IEEE Transactions on Industrial Electronics*, 62(6):3966–3977.

Yang, S., Kim, D., Kim, H., Son, Y., and Han, S. (2012). Indoor positioning system based on visible light using location code. In *2012 Fourth International Conference on Communications and Electronics (ICCE)*, pages 360–363.

Yang, S., Kim, H., Son, Y., and Han, S. (2014). Three-dimensional visible light indoor localization using aoa and rss with multiple optical receivers. *Journal of Lightwave Technology*, 32(14):2480–2485.

Yang, S.-H., Kim, D.-R., Kim, H.-S., Son, Y.-H., and Han, S.-K. (2013). Visible light based high accuracy indoor localization using the extinction ratio distributions of light signals. *Microwave and Optical Technology Letters*, 55(6):1385–1389.

Yap, J. L. and Circ, R. M. (2003). *Guide to classifying industrial property*. Urban Land Institute.

Yasir, M., Ho, S., and Vellambi, B. N. (2013). Indoor localization using visible light and accelerometer. In *2013 IEEE Global Communications Conference (GLOBECOM)*, pages 3341–3346.

Yasir, M., Ho, S., and Vellambi, B. N. (2014). Indoor positioning system using visible light and accelerometer. *Journal of Lightwave Technology*, 32(19):3306–3316.

Ye, S.-H., Kim, Y.-S., Lyou, H.-S., Kim, M.-S., and Lyou, J. (2015). Verification of electromagnetic effects from wireless devices in operating nuclear power plants. *Nuclear Engineering and Technology*, 47(6):729 – 737.

Yoo, J.-H., Jang, J.-S., Kwon, J. K., Kim, H.-C., Song, D.-W., and Jung, S.-Y. (2016). Demonstration of vehicular visible light communication based on LED headlamp. *International Journal of Automotive Technology*, 17(2):347–352.

Yoon, S. and Bostelman, R. (2019). Analysis of automatic through autonomous - unmanned ground vehicles (a-ugvs) towards performance standards. In *2019 IEEE International Symposium on Robotic and Sensors Environments (ROSE)*, pages 1–7.

Zafari, F., Gkelias, A., and Leung, K. K. (2019). A survey of indoor localization systems and technologies. *IEEE Communications Surveys Tutorials*, 21(3):2568–2599.

Zand, P., Chatterjea, S., Ketema, J., and Havinga, P. (2012). A distributed scheduling algorithm for real-time (d-sar) industrial wireless sensor and actuator networks. In *Proceedings of 2012 IEEE 17th International Conference on Emerging Technologies Factory Automation (ETFA 2012)*, pages 1–4.

Zeng, L., O'Brien, D., Le-Minh, H., Lee, K., Jung, D., and Oh, Y. (2008). Improvement of date rate by using equalization in an indoor visible light communication system. In *2008 4th IEEE International Conference on Circuits and Systems for Communications*, pages 678–682.

Zhai, Yanrong;Zhang, S. (2015). Visible light communication channel models and simulation of coal workface energy coupling. *Mathematical Problems in Engineering*.

Zhang, H., Cui, J., Feng, L., Yang, A., Lv, H., Lin, B., and Huang, H. (2019). High-precision indoor visible light positioning using deep neural network based on the bayesian regularization with sparse training point. *IEEE Photonics Journal*, 11(3):1–10.

Zhang, M., Li, F., Guan, W., Wu, Y., Xie, C., Peng, Q., and Liu, X. (2018). A three-dimensional indoor positioning technique based on visible light communication using chaotic particle swarm optimization algorithm. *Optik*, 165:54 – 73.

Zhang, S., Zhong, W., Du, P., and Chen, C. (2018). Experimental demonstration of indoor sub-decimeter accuracy vlp system using differential pdoa. *IEEE Photonics Technology Letters*, 30(19):1703–1706.

Zhang, T., Ghassemlooy, Z., Rajbhandari, S., Popoola, W. O., and Guo, S. (2017). Ofdm-pwm scheme for visible light communications. *Optics Communications*, 385:213 – 218.

Zhang, W., Chowdhury, M. I. S., and Kavehrad, M. (2014). Asynchronous indoor positioning system based on visible light communications. *Optical Engineering*, 53(4):1 – 10.

Zhang, X., Duan, J., Fu, Y., and Shi, A. (2014). Theoretical accuracy analysis of indoor visible light communication positioning system based on received signal strength indicator. *Journal of Lightwave Technology*, 32(21):4180–4186.

Zhao, H. . and Wang, J. . (2019). A novel three-dimensional algorithm based on practical indoor visible light positioning. *IEEE Photonics Journal*, 11(3):1–8.

Zhao, W., Kamezaki, M., Yamaguchi, K., Konno, M., Onuki, A., and Sugano, S. (2019a). A preliminary experimental analysis of in-pipe image transmission based on visible light relay communication. *Sensors*, 19(21).

Zhao, W., Kamezaki, M., Yoshida, K., Yamaguchi, K., Konno, M., Onuki, A., and Sugano, S. (2019b). A coordinated wheeled gas pipeline robot chain system based on visible light relay communication and illuminance assessment. *Sensors*, 19(10).

Zhao, X. and Lin, J. (2016). Maximum likelihood estimation of vehicle position for outdoor image sensor-based visible light positioning system. *Optical Engineering*, 55(4):1 – 8.

Zhou, B., Lau, V., Chen, Q., and Cao, Y. (2018). Simultaneous positioning and orientating for visible light communications: Algorithm design and performance analysis. *IEEE Transactions on Vehicular Technology*, 67(12):11790–11804.

Zhuang, Y., Hua, L., Qi, L., Yang, J., Cao, P., Cao, Y., Wu, Y., Thompson, J., and Haas, H. (2018). A survey of positioning systems using visible LED lights. *IEEE Communications Surveys Tutorials*, 20(3):1963–1988.